



UNIVERSIDAD DE CHILE
FACULTAD DE CIENCIAS FÍSICAS Y MATEMÁTICAS
DEPARTAMENTO DE ASTRONOMÍA

THE TRAMOS PROJECT UPDATED: ENHANCED SAMPLE OF TRANSITING
EXOPLANETS, STRATEGIES, AND ANALYSIS

TESIS PARA OPTAR AL GRADO DE MAGÍSTER EN CIENCIAS MENCIÓN
ASTRONOMÍA

PÍA GABRIELA CORTÉS ZULETA

PROFESOR GUÍA:
PATRICIO ROJO RUBKE

MIEMBROS DE LA COMISIÓN:
CESAR FUENTES GONZALEZ
RICARDO MUÑOZ VIDAL
TOBIAS CORNELIUS HINSE

Este trabajo ha sido parcialmente financiado por Departamento de Postgrado y Postítulo
de la Vicerrectoría de Asuntos Académicos de la Universidad de Chile

SANTIAGO DE CHILE
2019

RESUMEN DE LA TESIS PARA OPTAR AL
GRADO DE: MAGÍSTER EN CIENCIAS
MENCIÓN ASTRONOMÍA
POR: PÍA GABRIELA CORTÉS ZULETA
FECHA: 2019
PROF. GUÍA: PATRICIO ROJO RUBKE

THE TRAMOS PROJECT UPDATED: ENHANCED SAMPLE OF TRANSITING EXOPLANETS, STRATEGIES, AND ANALYSIS

El proyecto Transit Monitoring in the South (TraMoS) busca realizar seguimiento fotométrico de exoplanetas transitantes conocidos. Este proceso provee no sólo información acerca del planeta transitante, sino también sobre la arquitectura del sistema planetario. Desviaciones de la efemeris lineal producida por el movimiento Kepleriano, conocidas como Transit Timing Variations (TTV), sólo se pueden detectar mediante intensivo seguimiento y pueden sugerir la existencia de cuerpos adicionales en el sistema, tales como compañeros planetarios o exolunas.

Esta tesis de magíster recapitula los últimos años del proyecto TraMoS, se seleccionaron nuevos objetivos, se utilizaron nuevas herramientas, y se desarrollaron nuevos análisis. Se estudiaron 27 nuevas curvas de luz de tres Júpiter calientes: WASP-18b, WASP-19b, y WASP-77Ab. Se refinaron sus parámetros físicos y orbitales, y la ecuación de efemeris lineal fue actualizada gracias a la inclusión de datos de transito históricos. Debido a la carencia de variaciones significativas en sus tiempos central de tránsito, la realización de análisis dinámicos puede imponer límites superiores a la masa de perturbadores hipotéticos. Se descartaron cuerpos que poseen masas más grandes que $50 M_{\oplus}$ para WASP-18b, $6 M_{\oplus}$ para WASP-19b, y $10 M_{\oplus}$ para WASP-77Ab. Adicionalmente, se incluyeron datos de TESS para los tres objetivos, lo que apoya que la efemeris lineal es el mejor modelo para los tiempos de tránsito.

Los resultados presentados en esta tesis apoyan la poco frecuente aparición de compañeros en sistemas de Júpites calientes. Estudios futuros podrían evidenciar si estos tipos de planeta sufrieron un proceso de formación diferente por el cual terminan orbitando solos, o si efectivamente poseen compañeros enanos que no se han detectado.

RESUMEN DE LA TESIS PARA OPTAR AL
GRADO DE: MAGÍSTER EN CIENCIAS
MENCIÓN ASTRONOMÍA
BY: PÍA GABRIELA CORTÉS ZULETA
DATE: 2019
SUPERVISOR: PATRICIO ROJO RUBKE

THE TRAMOS PROJECT UPDATED: ENHANCED SAMPLE OF TRANSITING EXOPLANETS, STRATEGIES, AND ANALYSIS

The Transit Monitoring in the South (TraMoS) project aims to perform photometric follow-up in known transiting exoplanets. This process provides not only essential information about the transiting planet but also about their planetary system's architecture. Departures from the linear ephemeris given by Keplerian motion, the so-called Transit Timing Variations (TTV), can only be spotted through extensive follow-up and could suggest the existence of additional bodies in the system, such as planetary companions or exomoons.

This Master thesis recapitulates the last years of the TraMoS project, on which new targets were selected, modern tools were used and new analysis was performed. I studied 27 new light curves of three hot Jupiters: WASP-18b, WASP-19b, and WASP-77Ab. Their orbital and physical parameters were refined, and their linear ephemeris updated thanks to the inclusion of archival transit time data. Given the lack of significant variations in their mid-transit times, dynamical analysis can place upper mass limits in hypothetical perturbers. Bodies with masses greater than $50 M_{\oplus}$ can be discarded for WASP-18b, $6 M_{\oplus}$ for WASP-19b, and $10 M_{\oplus}$ for WASP-77Ab. Furthermore, I included recent TESS data for the three targets, supporting the linear ephemeris as the best fit for their transit times.

The results presented in this thesis support the rare occurrence of companions in hot Jupiter systems. Further studies may confirm if this kind of planet goes through a different formation process ending up orbiting alone on their systems or they have very small and unseen companions.

A Pía y Gustavo, mis padres.

Agradecimientos

Quiero agradecer en primer lugar a mis padres, quienes han sido mi apoyo fundamental tanto emocional como económico todos estos años (desde que nací). Gracias por nunca cortarme las alas, darme la libertad de soñar en grande y recogerme cada vez que me caí (literal y metafóricamente).

También quiero agradecer a mi profe guía, Pato Rojo, por la confianza de pasarme TraMoS y la libertad creativa que tuve para desarrollar este proyecto. Gracias por el apoyo y las enseñanzas estos años, me siento mucho más cerca de ser una astrónoma.

A todas las amigas y amigos que me acompañaron en este largo proceso. La oficina de los Calan-bozos se volvió una zona de comfort para mí y agradezco todos los momentos que pasamos juntos en este inhóspito lugar llamado Calán. A mis amigas de Beauchef, que nos hemos acompañado desde el primer día (casi) del Plan Común y que siempre me dieron ánimos y me apoyaron en los momentos difíciles. A Pierina, mi amiga de la vida, que aunque el universo se encarga de separarnos la amistad sigue intacta como hace catorce (?) años. A las Cazadoras de Estrellas, agredezco haber sido partícipe de este proyecto tan maravilloso que solo me dio alegrías. Sé que seguirán creciendo y motivando a más niñas a ser científicas.

A Matías, por todo tu apoyo y amor incodicional todos estos años. Por ayudarme a pararme cada vez que me caí, darme confianza las veces que ya no creía en mí misma y por escucharme atento con todas mis dudas existenciales. Gracias por ser mi fan número 1 siempre.

A Bibi, la compañera gatuna que apareció en mi vida solo para darme suavidad, ronroneos y tranquilidad.

Contents

List of Tables	vi
List of Figures	vii
1 Introduction	1
1.1 This work	3
2 The Transit Monitoring in the South project	5
2.1 Transiting exoplanets' light curve	6
2.2 Transit Timing Variations	8
3 Analysis and Results of WASP-18b, WASP-19b, and WASP-77Ab	12
3.1 Introduction	13
3.2 Observations and Data Reduction	14
3.3 Light curve and RV analysis	16
3.4 Results and Discussion	18
3.4.1 Transit Parameters and Physical Properties	18
3.4.2 Transit Timing Variations	30
3.4.3 Limits on an Additional Perturber	35
3.4.4 TTV period search	40
3.5 Summary and Conclusions	41
4 TraMoS in the TESS era	47
4.1 WASP-18b	50
4.2 WASP-19b	50
4.3 WASP-77Ab	51
5 Summary and future work	54
Bibliography	56
Appendix	65
A Aperture photometry pipeline	65
A.1 Reduction script of WASP-18, WASP-19 and WASP-77A	66
A.2 Example of output file	72

List of Tables

3.1	Log of Observations	15
3.2	Example photometry of WASP-18, WASP-19 and WASP-77A	17
3.3	System parameter of WASP-18	21
3.4	System parameter of WASP-19	24
3.5	System parameter of WASP-77A	27
3.6	Transit mid-times for WASP-18b	32
3.7	Transit mid-times for WASP-19b	33
3.8	Transit mid-times for WASP-77Ab	35
3.9	Approximate upper mass limits of a putative perturber in various orbital resonances for each system	36

List of Figures

1.1	Mass and orbital period distribution of Exoplanets, and their corresponding discovery methods in color. This plot only shows the exoplanets with measured masses. The transit and radial velocity methods (in orange and blue, respectively) are the most successful techniques to discover extrasolar planets. However, both techniques are still more sensitive to detect Jupiter-mass planets rather than Earth-mass, but the Transit method is more sensitive to short-period planets.	3
2.1	Histogram of the 30 transiting exoplanets with the largest amount of observations within the TraMoS project. The exoplanets WASP-4b and WASP5-b were presented in Hoyer et al. (2012) and Hoyer et al. (2013), respectively. The results from the analysis of WASP-18b, WASP-19b and WASP77-Ab are in Cortés-Zuleta et al. 2019 (submitted, see Chapter 3 for further details). In none of those systems a significant TPV signal was detected.	6
2.2	Geometry of a transiting exoplanet and the observed light curve. Based on the light curve itself it is possible to measure the transit depth ΔF and the orbit's inclination i . The numbers in circle indicate the four contact times: t_1 , t_2 , t_3 and t_4 . Figure from The Handbook of Exoplanets by M. Perryman. . .	8
2.3	Examples of transiting exoplanets and how their light curves differ between them thanks to the physical properties of the exoplanet.	9
2.4	Example of a system with a transiting exoplanet of $1 M_J$ in a 10-day orbit and an Earth-mass perturber planet. The top panel is an Observed minus Computed diagram showing the measured TTV of the Jupiter-mass planet when the perturber has a period of 16.11 days, not in Mean Motion Resonance with the transiting planet. The panel at the bottom shows the TTV of the transiting planet when both are near an interior 2:1 resonance. In this case, the small planet has a period of 19.7 days. The amplification of the TTV signal is by an order of magnitude. Figure generated with the Python package: <code>ttv2fast2furious</code>	11

3.1	Light curves of WASP-18, WASP19 and WASP77 during 8, 9 and 9 different transits, respectively, from the TraMoS project. The fitted best model from EXOFASTv2 is shown as a light blue solid line for WASP-18b, orange for WASP-19b and pink for WASP-77Ab. To the right of each panel are the corresponding residuals of the model. For clarity, both light curves and their residual are offset artificially. The epoch number is indicated above each light curve. The technical information about each observation is listed in Table 3.1.	18
3.2	Radial velocity observations of WASP-18, WASP-19 and WASP-77A from Hellier et al. (2009), Hebb et al. (2010) and Maxted et al. (2013a), respectively. The best fitted model from the joint modeling of RV and light curves with EXOFASTv2 is in solid line color: light blue for WASP-18b, orange for WASP-19b and pink for WASP-77Ab. The residuals of the model are shown at the bottom panel of each figure.	19
3.3	Phased light curv of WASP-18b, WASP-19b and WASP-77Ab transits, from the TraMoS project. The three data set of light curves are fitted simultaneously with RV archival data using EXOFASTv2, in order to estimate the orbital and physical parameters of the system. In the top panel, the light blue solid line is the best fitting model for WASP-18b, and bellow are the residuals in color grey. The same for WASP-19b in color orange at the center panel, and for WASP-77Ab in color pink at the bottom panel.	20
3.4	Observed minus calculated mid-transit times (TTV) for WASP-18b (top), WASP-19b (center) and WASP-77Ab (bottom). The dashed black line corresponds to the proposed linear ephemeris, i.e. zero deviation from the predicted transit time (See Section 3.4.2) computed from our refined orbital period. For that, we considered 19, 59 and 11 transit times of WASP-18b, WASP-19b, and WASP-77Ab, respectively. The grey area corresponds to the error propagation at 1σ , where the quadratic trend looks almost horizontal. The points in color are the TTV from the newly light curves of the TraMoS project (WASP-18b: light blue, WASP-19b: orange, WASP-77Ab: pink) and the black points in the three panels are TTVs measured from previous published transit times. The RMS scatter from the linear ephemeris are 83 seconds for WASP-18b; 75 seconds for WASP-19b, and 121 seconds for WASP-77Ab.	31
3.5	MEGNO ($\langle Y \rangle$) stability map for the WASP-18 system. We over-plot the map with an upper mass of a hypothetical perturbing planet introducing a mid-transit time TTV _{RMS} scatter of 83 s (solid line) as obtained in this study. The stipulated line is the upper mass limit as obtained from the RMS scatter (30.9 m/s) of the radial-velocity curve. For initial conditions resulting in a quasi-periodic (i.e bounded) motion of the system, the $\langle Y \rangle$ value is close to 2.0 (color coded blue). For chaotic (i.e unstable) motion, the $\langle Y \rangle$ is diverging away from 2.0 (color coded red to yellow). Vertical arrows indicate (P_2/P_1) orbital resonances between the perturbing body and the transiting planet. The two planets were assumed to be co-planar, and the perturbing planet's eccentricity was initially set to zero. <i>See electronic version for colors.</i>	38
3.6	Same as Fig. 3.5, but this time for WASP-19 with an TTV _{RMS} of 75 s. The RMS for the radial-velocity measurements was (18.2 m/s). <i>See electronic version for colors.</i>	39

3.7	Same as Fig. 3.5, but this time for WASP-77 with an TTV _{RMS} of 121 s. The RMS for the radial-velocity measurements was (12.0 m/s). <i>See electronic version for colors.</i>	40
3.8	Lomb-Scargle (standard normalized) power vs period for observed TTV residuals of WASP-18 (<i>top panel</i>) and for a simulated set of TTVs randomly drawn from a normal distribution with mean zero and standard deviation of 1.38 minutes (<i>lower panel</i>). See text for more details.	42
3.9	Lomb-Scargle (standard normalized) power vs period for observed TTV residuals of WASP-19 (<i>top panel</i>) and for a simulated set of TTVs randomly drawn from a normal distribution with mean zero and standard deviation of 1.33 minutes (<i>lower panel</i>). See text for more details.	43
3.10	Lomb-Scargle (standard normalized) power vs period for observed TTV residuals of WASP-77 (<i>top panel</i>) and for a simulated set of TTVs randomly drawn from a normal distribution with mean zero and standard deviation of 2.02 minutes (<i>lower panel</i>). See text for more details.	44
4.1	Observed minus calculated (O-C) diagram of the KOI-525b transit times, from the KOINet project. The observations from Kepler are in blue, and two different models were fitted on those data: an orbital decay model is in red, and a periodical TTV model is in green. If only Kepler data is considered, the two models could be plausible. The new ground-based observations (in pink) were essential to confirm the TTV nature of the system, discarding an orbital decay	48
4.2	Match between all the stars with confirmed exoplanets and the TESS targets from Sector 1 to Sector 13. The empty red circles correspond to the star with confirmed exoplanets distributed by its position in the sky, while the filled red circles indicate if the exoplanet has an orbital period of fewer than 27 days, which is the duration of one TESS sector. The black cross indicates which star was already observed by TESS. However, this does not indicate that transit light curves will be provided for sure since the orbital period of the exoplanet needs to be considered. Thus, the first-year mission of TESS will provide for sure transit data of the exoplanets with a filled red circle and a black cross. The zone in the sky within the big black circle corresponds to the Kepler field of view, where the bulk of discovered exoplanets are located.	49
4.3	Observed minus calculated mid-transit times (TTV) for WASP-18b. The dashed black line corresponds to the proposed linear ephemeris, i.e. zero deviation from the predicted transit time computed from our refined orbital period. For that, we considered 63 transit times from the TraMoS project (in light blue), published works and TESS (both in black). The grey area corresponds to the error propagation at 1σ , which follows a imperceptible quadratic trend. The RMS scatter from the linear ephemeris is 47 seconds.	51
4.4	Observed minus calculated mid-transit times (TTV) for WASP-19b. The dashed black line corresponds to the proposed linear ephemeris, i.e. zero deviation from the predicted transit time computed from our refined orbital period. For that, we considered 87 transit times from the TraMoS project (in light blue), published works and TESS (both in black). The grey area corresponds to the error propagation at 1σ , which follows a imperceptible quadratic trend.. The RMS scatter from the linear ephemeris is 65 seconds.	52

4.5 Observed minus calculated mid-transit times (TTV) for WASP-77Ab. The dashed black line corresponds to the proposed linear ephemeris, i.e. zero deviation from the predicted transit time computed from our refined orbital period. For that, we considered 26 transit times from the TraMoS project (in light blue), published works and TESS (both in black). The grey area corresponds to the error propagation at 1σ , which follows a imperceptible quadratic trend. The RMS scatter from the linear ephemeris is 86 seconds.

53

Chapter 1

Introduction

The idea of the existence of planets orbiting other stars different from our Sun has lived in the human imagination for centuries. During the sixteenth century, the Italian philosopher Giordano Bruno suggested¹, for the first time in history, that more planets could be outside the Solar System. More than four hundred years after Bruno's statement, the first exoplanet was confirmed in 1992. Surprisingly, it was not just one exoplanet but three, orbiting the pulsar PSR B1257+12 more than 1000 light-years away from us. Today, more than 4,000 exoplanets are confirmed, and thousands more are waiting for their confirmation.

Having billions of billions of galaxies in the Universe each one with millions of stars, the current number of discovered exoplanets is still very low. Furthermore, the distance at which we can detect exoplanets is limited by our current technology, thus finding a candidate in the closer galaxy – Andromeda – could be considered science fiction. If the Milky Way has *only* around 2×10^{11} stars, how could be the Solar System unique? How could the Earth be the only planet with life on it? Until today, it is still difficult to answer those questions. The Solar System presents a logic structure where the small, rocky planets are closer to the Sun, and the gas giants are located beyond. But no other exoplanetary system has been found having similar features and even not exoplanetary life has been detected yet. Our knowledge about the Solar System challenges the existence of other kinds of planetary architectures with close-in gas giants, for instance, suggesting that there is not a single, universal planetary process formation. Answering such questions makes studying exoplanets a relevant matter nowadays.

The discovery of three exoplanets orbiting the pulsar PSR B1257+12 is still very rare. The technique used to find them is called Pulsar Timing and it consists in measuring the variation of a pulsar's pulsation period due to the presence of a body orbiting it. As pulsars are not very common and we know that planet may be orbiting main-sequence stars – as the Earth and all the Solar System –, they become the principal target on which the hunting of exoplanet is dedicated. Planets are small when compare to their host star, that is why most of the current discovery techniques are focused on observing the effects in the stars, or how what we observed from them changed, caused by the presence of planets.

The most used and successful planet detection techniques are: transits, radial velocity,

¹In the book: *De l'infinito, universo e mondi*, 1584

direct imaging, microlensing and astrometry. Direct imaging is the only technique in which the planet is observed directly but the star needs to be masked in order to only received the thermal emission from the planet. Microlensing is different from all the other discovery techniques because a background star is required to obtain the desired effect: gravitational lensing produced by the star with a planet (multiple lenses). As the primary lens is small – around $1 M_{\odot}$ – the two images produced by the gravitational lensing effect are very close to each other and cannot be resolved with current imaging techniques. The presence of a planet in orbit around the lens star will cause a deviation in the magnification curve of the event. On the other hand, astrometry measurements can be used to discover exoplanets too. With the current high-precision in the position of the stars, even their displacement in the sky can be detected. Similar to the radial velocity technique, through astrometry the displacement of the star due to the gravity of a planet is measured.

The two techniques that have contributed the most to the discovery of extrasolar planets are radial velocity and transits (see Figure 1.1). Each one of these techniques had their own advantages depending on the physical properties of the planetary system. When the orbit of the exoplanet is aligned with the line of sight from Earth, the pass of the planet in front of its host star causes that the star's flux decreases, proportionally to the square of the ratio between the radius of the planet and the star. Thus, the radius ratio between the planet and the star, R_p/R_* can be determined directly using the transit method. On the other hand, the gravity due to the presence of a planet will set the center of mass of the system, in a place different from the star's center. Therefore, the star will move in its own small orbit with a radius proportional to the mass of the planet. In this case, the radial velocity method unveils the planet's minimum mass $M_p \sin i$.

Anyway, the rising research field of exoplanets does not end with their discovery. Performing follow-up and proper characterization of discovered exoplanets are essential to obtain a full list of orbital and planetary parameters. For instance, 39% of the total number of discovered exoplanets have a proper measurement of their masses, and only 17% have their mass and radius computed².

One of the perfect scenarios comes when the two methods, transits and radial velocity, can be used in the same planetary system, allowing to derive essential properties of the planet and its orbit. Combining transits and radial velocity follow-up the whole system can be characterized. From transits we get the orbital inclination, then the real mass can be computed with radial velocity measurements. From transits we get the radius ratio of the system, assuming that the star is previously well characterized, the radius of the planet is derived. Then, as we already have the mass of the planet, the mean density can be estimated. This parameter gives a clue about the possible composition of the planet. Moreover, if the follow-up is performed combining transits with big telescopes, important information about the planet can be unveiled, perhaps even their atmospheric composition and dynamics.

Continued photometric monitoring not only increased the precision of planetary parameters but provides potential information about the planet and its environment. Through the observation of transit events during a long observing baseline, variability in the planetary

²Information obtained from the NASA Exoplanet Archive Database <https://exoplanetarchive.ipac.caltech.edu>

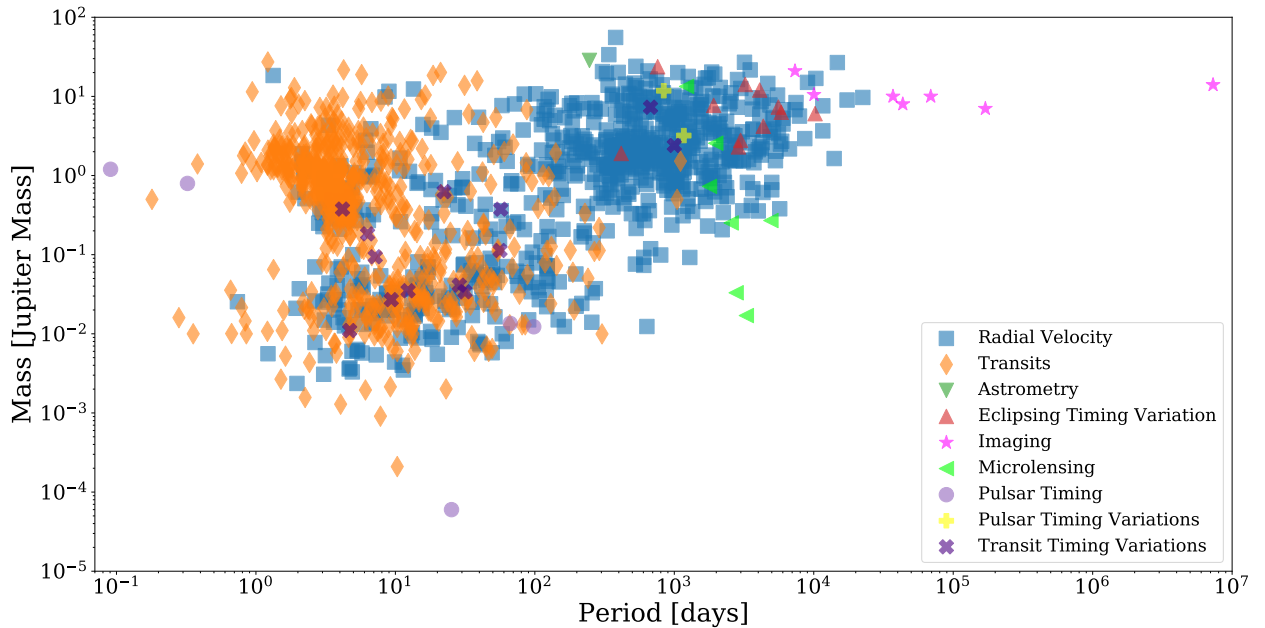


Figure 1.1: Mass and orbital period distribution of Exoplanets, and their corresponding discovery methods in color. This plot only shows the exoplanets with measured masses. The transit and radial velocity methods (in orange and blue, respectively) are the most successful techniques to discover extrasolar planets. However, both techniques are still more sensitive to detect Jupiter-mass planets rather than Earth-mass, but the Transit method is more sensitive to short-period planets.

system can be detected. For instance, the first measurement of two planets gravitationally bounded was made by (Holman et al., 2010), this discovery was made thanks to the continued observations performed by the Kepler mission. This phenomenon is detectable by observing the same transit event multiple times over an extended number of epochs. Any variability in the mid-transit times could be attributed to an additional body. Moreover, variability in transiting exoplanets – specifically in the time of the mid-transit – can be attributed not only to planetary companions, but exomoons(Kipping, 2009a,b), tidal orbital decay(Hoyer et al., 2016a,b), secular orbits changes(Adams and Laughlin, 2006) or relativistic effects (Heyl and Gladman, 2007), among others.

The Transit Monitoring in the South project (TraMoS) aims to detect multi-exoplanetary systems trough the variability in parameters of transiting exoplanets. To achieve this goal, extensive photometric follow-up of transit is being carried on, using one-meter class telescopes located in Chile.

1.1 This work

This thesis is an extension of the Transit Monitoring in the South project (TraMoS, see Chapter 2) started in 2008 by Sergio Hoyer and Patricio Rojo. I selected a new sample of transiting exoplanets, all of them hot Jupiters without any companions detected to date. I analyzed 27 new light curves of the hot Jupiters WASP-18b, WASP-19b, and WASP-77Ab searching for periodic variations in the transit time (TTV) that could suggest the presence

of additional bodies in their systems.

This thesis is organized as follows: Chapter 2 summarizes the TraMoS project, its scientific goals, techniques, and achievements to date. Also, this chapter describes what we can learn from transit exoplanets' light curves and Transit Timing Variations. Chapter 3 shows the analysis and results of the hot Jupiters WASP-18b, WASP-19b, and WASP-77Ab, including their observations and data reduction, light curve and RV analysis, measurements of TTVs and an upper mass limit for possible companions in their systems. Then, Chapter 4 recapitulates the current stage of the TraMoS project on which TESS data is being incorporated. Here, I re-analyze the TTV curves of the previous targets WASP-18b, WASP-19b, and WASP-77Ab with new light curves from TESS. Finally, Chapter 5 contains a summary of this thesis as well as some ideas for future work. The Appendix section includes a brief description of the aperture photometry pipeline utilized, all the Python scripts used to generate each light curve, and an example of the PDF file obtained as a result of the aperture photometry procedure.

Chapter 2

The Transit Monitoring in the South project

The Transit Monitoring in the South (TraMoS) project started in 2008 aiming to perform photometric follow-up of transiting exoplanets using telescopes located in Chile. Through photometric monitoring of transiting events, important information of the planetary system can be obtained, such as the planetary radius, inclination of the orbit, and, in combination with radial velocity data, the planetary mass, among others. Moreover, this kind of analysis allows the detection of variability in the transit's parameters (TPV), if several epochs of the transit event are obtained. The TraMoS project aims, on one hand, to refine the physical and orbital parameters of selected exoplanets systems through photometric follow-up and, on the other, to search for variations in those parameters that could suggest the presence of additional bodies in the system.

To date, almost 400 transit events have been observed of 144 transiting exoplanets (see Figure 2.1). The bulk of the targets in the TraMoS project are hot Jupiters due to its short orbital period and large transit depth. Several facilities were used to perform the photometric follow-up such as the VLT of European Southern Observatory, the SMARTS 0.9 m and 1 m at Cerro Tololo Inter-American Observatory, the Danish 1.54 m at La Silla Observatory, SWOPE and Du Pont telescopes at Las Campanas Observatory and SOAR telescope at Cerro Pachón Observatory, among others. The diameter size of the used telescopes ranges from 0.6 meters to 8 meters. However, in the later stage of the TraMoS project, we built the team expertise using 1 meter-class telescope, for example in the Danish, SWOPE and SMARTS.

The first studies within the TraMoS project were conducted for Segio Hoyer's PhD dissertation (advisor: Patricio Rojo). Current results are summarized as: a possible orbital decay of WASP-43b (Hoyer et al., 2016b) and OGLE-TR-113b (Hoyer et al., 2016a) was ruled out, and no significant TTV signal was detected in WASP-4b (Hoyer et al., 2012) and WASP-5b (Hoyer et al., 2013).

In the following section 2.1, I describe the light curve produced from a transiting exoplanet –the principal target of the TraMoS project – what information about the planet can be obtained from them and how these light curves can give us information about the architecture

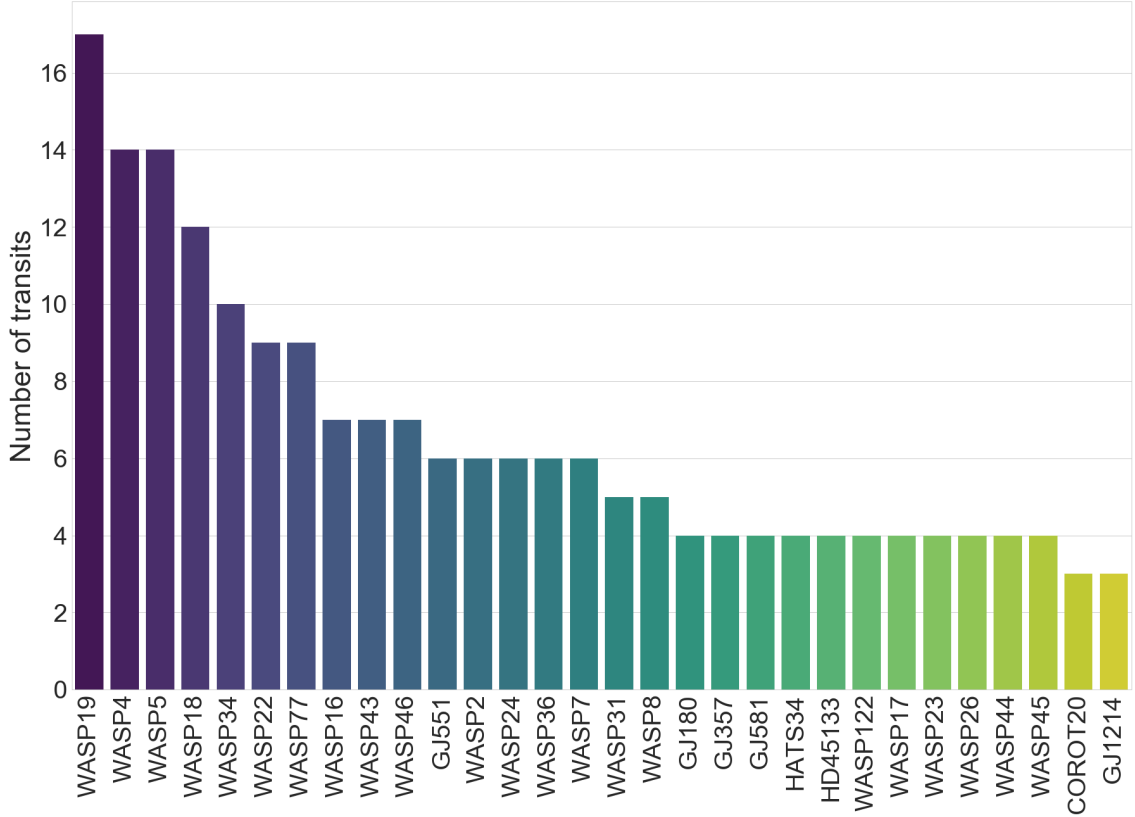


Figure 2.1: Histogram of the 30 transiting exoplanets with the largest amount of observations within the TraMoS project. The exoplanets WASP-4b and WASP5-b were presented in Hoyer et al. (2012) and Hoyer et al. (2013), respectively. The results from the analysis of WASP-18b, WASP-19b and WASP77-Ab are in Cortés-Zuleta et al. 2019 (submitted, see Chapter 3 for further details). In none of those systems a significant TPV signal was detected.

of this kind of systems. Then, in section 2.2, I detail on a specific type of phenomena of transiting exoplanets: the variation of the transit mid-time of its light curve (TTV).

2.1 Transiting exoplanets’ light curve

The light curve produced by a transit event provides important information about the planetary system. For example, it is the only way on which we can derive directly the proportion between the exoplanet and star radius. It can also give information about the impact parameter, and therefore, the inclination of the orbit.

In Figure 2.2 is shown the geometry of a transiting exoplanet. From geometric considerations the transit light curve and the parameters of the planetary system can be described with a few simple relations Seager and Mallén-Ornelas (2003); Winn (2010). When the planet passes in front of its star produced a dimming in its flux called primary transit. The maximum drop during the transit event defines the transit depth ΔF :

$$\Delta F = \left(\frac{R_p}{R_*} \right)^2 \quad (2.1)$$

Where R_p and R_* are the planet and star radius, respectively. The numbers 1, 2, 3 and 4 correspond to the contact times: t_1 , t_2 , t_3 and t_4 (see. Fig. 2.2). The total duration of the transit is $t_T = t_4 - t_1$ and the full duration is $t_F = t_3 - t_2$. The total duration of the transit can be also described considering planetary parameters such as the period P , semi-major axis a and orbital inclination i :

$$t_T = \frac{PR_*}{\pi a} \sqrt{\left(1 + \frac{R_p}{R_*}\right)^2 - \left(\frac{a \cos i}{R_*}\right)} \quad (2.2)$$

The impact parameter b , is the sky-projected distance between the center of the star and the planet at conjunction:

$$b = \frac{a \cos i}{R_*} \left(\frac{1 - e^2}{1 + e \sin \omega} \right) \quad (2.3)$$

Where ω is the argument of pericenter. In the case of circular orbits, the eccentricity e is zero, thus Eq. 2.3 is simplified to:

$$b = \frac{a \cos i}{R_*} \quad (2.4)$$

Depending on the orbital and physical parameters of the exoplanet, the shape of the observed light curve will vary. For example, Figure 2.3 shows how the light curve reflects the configuration of the system. Hot Jupiters are the kind of planet that is relatively easier to detect since their planet-to-star radius ratio is larger, but a smaller planet orbiting a dwarf star could produce a similar ratio of the radius. On the other hand, exoplanets with smaller orbital inclinations will produce shallower drops in the flux, in comparison with planets in the same orbital-plane with the host star.

When modeling the light curve's data, not only the physical parameters of the planet need to be taken into account, but the stars' too. The Limb Darkening effect of the star will change the shape of the observed light curve (during the time period $t_3 - t_2$ in Fig. 2.2), as what we are observing are photons coming from the star itself, especially when carrying-out observations with different filters. The effect of stellar limb-darkening describes the intensity variation across the disk of the star: the star appears brighter at the center and darker closer to the edge (stellar limb). The most general analytic formulae to model a light curve produced by a transiting exoplanet includes the Limb Darkening coefficients (Mandel and Agol, 2002), which can be quadratic or non-quadratic.

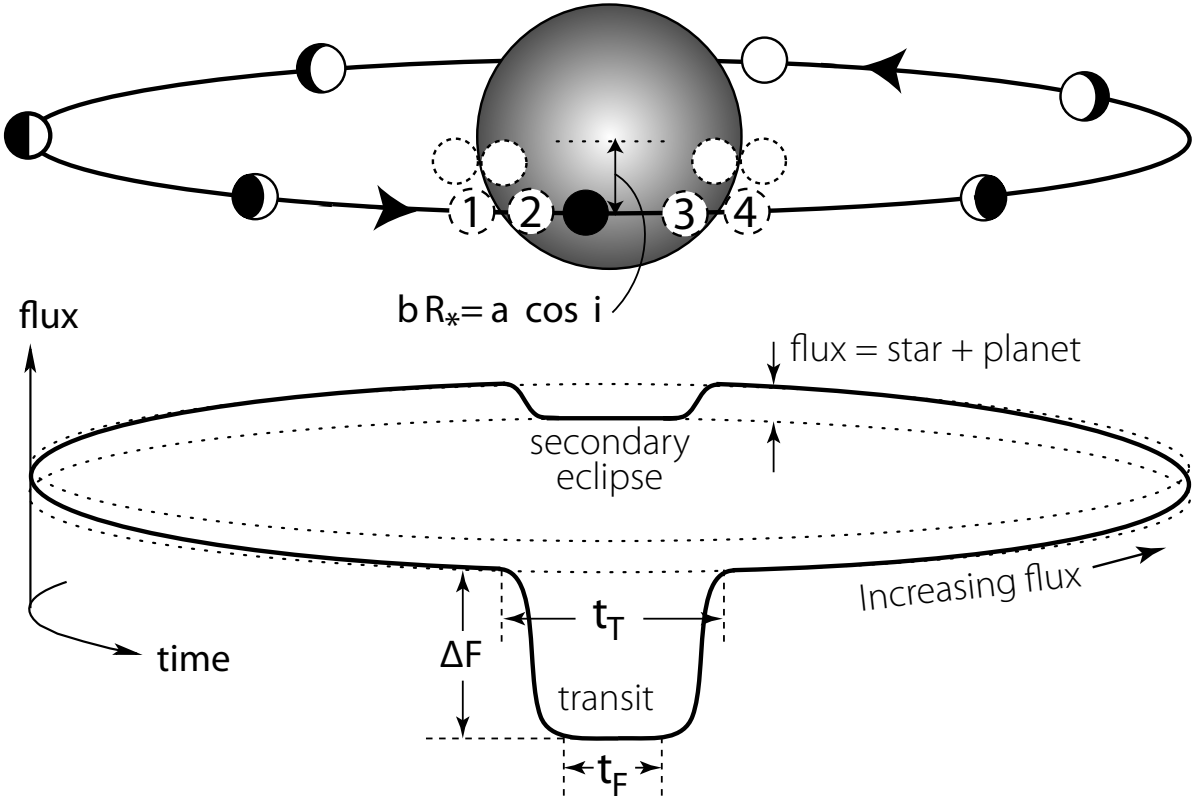


Figure 2.2: Geometry of a transiting exoplanet and the observed light curve. Based on the light curve itself it is possible to measure the transit depth ΔF and the orbit's inclination i . The numbers in circle indicate the four contact times: t_1 , t_2 , t_3 and t_4 . Figure from The Handbook of Exoplanets by M. Perryman.

2.2 Transit Timing Variations

Since the discovery of the first exoplanet, one of the principal questions that arose was: are they alone in their systems? The idea of multi-planetary systems is a consequence of our knowledge about the planetary system where we live in, and until today the Solar System has a larger number of orbiting planets. Besides the Solar System, Kepler-90 has the same number of confirmed exoplanets: eight. Statistically, around 20% of the confirmed exoplanets are part of a multi-planetary system¹, but this number is theoretically larger. Fressin et al. (2013) computed the occurrence of exoplanets through numerical simulation with Kepler data, obtaining that around 52% of the stars should have at least one planet within an 85 days orbit.

The Transit Timing Variations (TTV) technique was first proposed as a way to detect Earth-mass planets in multi-planetary systems due to gravitational interactions with a transiting exoplanet (Holman and Murray, 2005; Agol et al., 2005). However, as mention in Chapter 1, TTVs can be also used to measure tidal interactions between the planet and the

¹Information obtained from the NASA Exoplanet Archive Database <https://exoplanetarchive.ipac.caltech.edu>

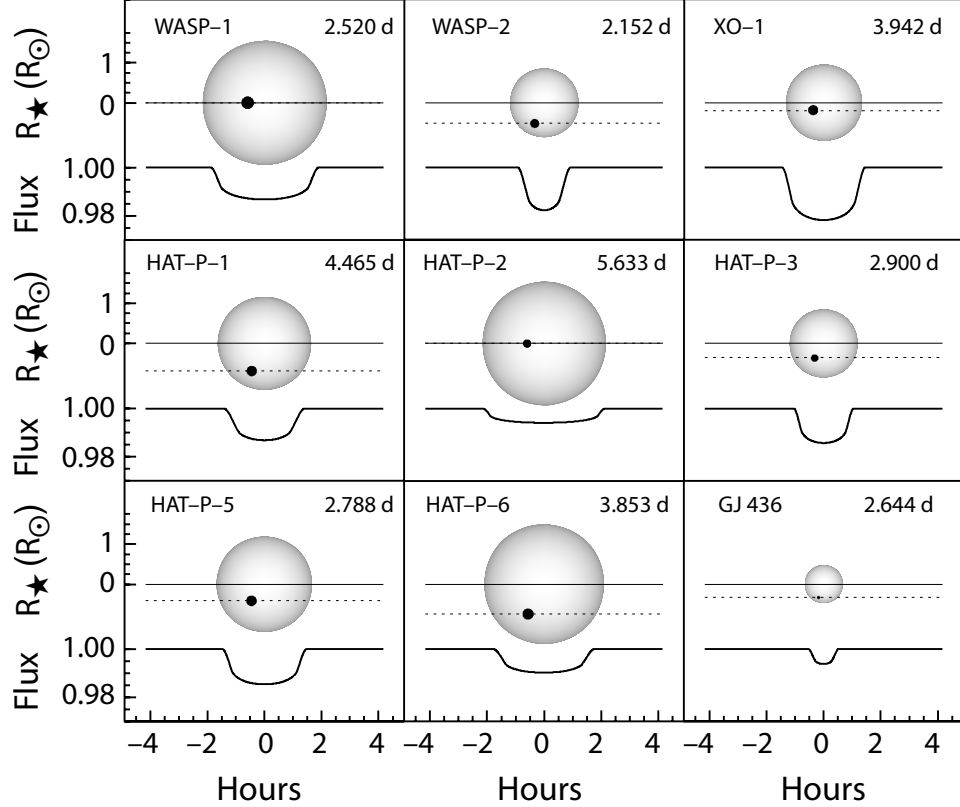


Figure 2.3: Examples of transiting exoplanets and how their light curves differ between them thanks to the physical properties of the exoplanet.

star, such as orbital decays for instance, or to detect exomoons (Kipping, 2009a,b), among others phenomena in the star itself.

For a given light curve of a transiting exoplanet (see Figure 2.2), the transit mid-time T_c (or central time of the transit) is computed as:

$$T_c = \frac{t_4 + t_1}{2} \quad (2.5)$$

A single (non-perturbed) transiting planet will stay in a Keplerian orbit around its host star, producing a transit time strictly periodic. Thus, the transit time T_c follows a linear function in the transit epoch E :

$$T_c(E) = T_0 + E \cdot P \quad (2.6)$$

Where T_0 is a reference transit time, E is the number of epochs since T_0 , and P is the orbital period of the planet. The presence of a second (perturbing) planet produces transits no exactly periodic, hence Eq. 2.6 will not be valid. As the transit times will be no longer a linear function, the time between transits varies. The variation in time produced by the

perturber body depends on the mass and geometry of their orbits. The magnitude of this variation between successive transits of the transiting planet (Holman and Murray, 2005), assuming that the perturber body is in a inner orbit, $a_2 < a_1$, and follows a eccentric orbit with a periastron distance of $a_2(1 - e_2)$, is:

$$\Delta t = \frac{45\pi}{16} \frac{M_2}{M_*} P_1 \alpha_e^3 (1 - \sqrt{2}\alpha_e^{3/2})^{-2} \quad (2.7)$$

Where $\alpha_e = a_1/(a_2(1 - e_2))$ is the ratio of the semi-major axis of the planets, considering a nonzero eccentricity for the perturbing planet ($e_2 \neq 0$).The orbital period of transiting exoplanet is P_1 , while the perturbing planet has a mass M_2 , and orbital period P_2 . The Eq. 2.7 obtains the best results, compared with numerical simulations, when $e_2 > 0.3$.

Assuming that the orbital parameters of the known transiting exoplanet are already derived from its light curve, the orbital parameters and mass of the hypothetical perturber can be estimated numerically (Nesvorný and Morbidelli, 2008a; Nesvorný, 2009), even if the second planet does not transit the star.

The TTV method is an efficient tool to search for additional unseen companions since, to employ this technique, only photometry of the transiting exoplanet during transit events is required. Moreover, this technique enhances its sensitivity when the two bodies in the system are close to Mean Motion Resonances (MMR) (Agol et al., 2005; Steffen and Agol, 2005; Agol and Steffen, 2007) (see Figure 2.4) .

Holman et al. (2010) presented the first multi-planetary system confirmed using the TTV method: two planets orbiting Kepler-9, a Sun-like star. These two Saturn-size planets are in near 2:1 orbital resonance with periods of 38.9 and 19.2 days. To model the dynamical interaction of the system, only 9 transits of Kepler-9b and 6 from Kepler-9c were required. This confirmed the effectiveness of the TTV method to characterize planetary systems with a scarce number of transits.

Since the discovery of Holman et al. (2010), around 20 exoplanets have been discovered and characterized thanks to the measurement of variations on their transit times and the following proper dynamical modeling of the system. Most of them are Kepler systems because of its high duty-cycle, on which it provided years on transits data. Kepler stopped working on 2018, but the Transit Exoplanet Satellite Survey (TESS) is currently delivering its first results with new planetary systems showing TTVs. For example, two exoplanets – possibly one Jupiter and a sub-Saturn like – were recently discovered by Dawson et al. (2019) orbiting TOI-216, in near 2:1 resonance.

To date, only two hot Jupiters have been found to show TTV signals due to the presence of additional companions on their systems: WASP-47b (Becker et al., 2015) and Kepler-730b (Cañas et al., 2019), even though the TTVs was proposed as a technique to search for additional companions of gas giants. The lack of observed companions in hot Jupiter systems could provide crucial information about planetary formation processes. Through the TTV method not only the transiting exoplanet is being studied but the whole planetary system.

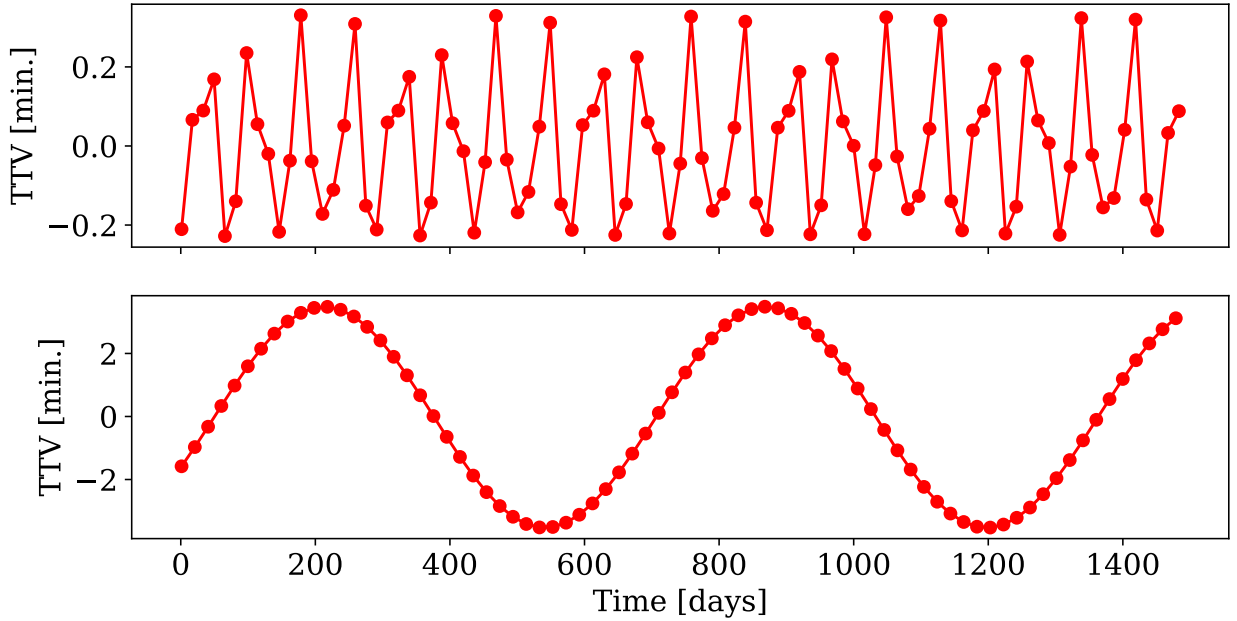


Figure 2.4: Example of a system with a transiting exoplanet of $1 M_J$ in a 10-day orbit and an Earth-mass perturber planet. The top panel is an Observed minus Computed diagram showing the measured TTV of the Jupiter-mass planet when the perturber has a period of 16.11 days, not in Mean Motion Resonance with the transiting planet. The panel at the bottom shows the TTV of the transiting planet when both are near an interior 2:1 resonance. In this case, the small planet has a period of 19.7 days. The amplification of the TTV signal is by an order of magnitude. Figure generated with the Python package: `ttv2fast2furious`.

Steffen et al. (2012b) analyzed Kepler data to constrain the occurrence rate of companions in hot Jupiter systems. In a sample of 63 hot Jupiter candidates, none of them show evidence of possible companions in their system. When comparing with other types of exoplanets, 30% of hot Neptune candidates may have companions and 10% of warm Jupiter candidates. This could suggest that hot Jupiter may have different formation processes on which smaller companions are not allowed in their system: probably they are ejected through planet-planet scatter during migration. TTV studies could provide important clues about formation processes and dynamical evolution, and their mass and period dependency.

Chapter 3

Analysis and Results of WASP-18b, WASP-19b, and WASP-77Ab

TraMoS V: Updated ephemeris and transit timing variations of the hot Jupiters WASP-18b, WASP-19b and WASP-77Ab¹

PÍA CORTÉS-ZULETA^{1,2}, PATRICIO ROJO¹, SONGHU WANG^{2,5}, TOBIAS C. HINSE³, SERGIO HOYER⁴, BASTIAN SANHUEZA¹, PATRICIO CORREA-AMARO¹, JULIO ALBORNOZ¹

¹ Departamento de Astronomía, Universidad de Chile, Camino El Observatorio 1515, Las Condes, Santiago, Chile

² Department of Astronomy, Yale University, New Haven, CT 06511, USA

³ Chungnam National University, Department of Astronomy and Space Science, 34134 Daejeon, Republic of Korea

⁴ Aix Marseille Univ, CNRS, CNES, LAM, Marseille, France

⁵ 51 Pegasi b Fellow

Abstract

We present 22 new transit observations for the exoplanets WASP-18b, WASP-19b, and WASP-77Ab, from the Transit Monitoring in the South (*TraMoS*) project. We simultaneously model our newly collected transit light curves, as well as archival photometry and radial velocity data to obtain refined physical and orbital parameters. We did not find significant TTV_{RMS}² variations larger than 83, 75, and 121 seconds for WASP-18b, WASP-19b, and WASP-77Ab, respectively. Dynamical simulations were carried out to constrain the masses

¹Based on paper submitted to A&A on July 9, 2019.

²RMS: root-mean-square

of a possible perturber. The observed RMS could be produced by a perturber body with an upper limit mass of 5 and $7 M_{\oplus}$ in 1:2 and 3:1 resonance, and $25 M_{\oplus}$ in 2:1 resonance for WASP-18b. In the case of WASP-19b, companions with masses up to 0.9, 2 and $6 M_{\oplus}$, in 2:1, 3:1, and 5:3 resonances, reproduce the RMS. In this system, we also discard a hypothetical perturber of $500 M_{\oplus}$ in 1:3 resonance, because of the mass limit from RV variations. For WASP-77Ab a planet with masses between $1 - 7 M_{\oplus}$ in 1:2, 1:3, 2:1, 2:3, 3:1, 3:5, 5:3 resonances could reproduce the observed RMS in the TTVs. Finally, using a Lomb-Scargle period search we find no evidence of a periodic trend on our TTV data for the three exoplanets.

3.1 Introduction

High-precision long-term transit follow-ups provide tremendous opportunities in improving our understanding of exoplanets, leading to obtain more accurate measurements of planetary radius, especially those detected with ground-based transit surveys (e.g., HATNet and HATSouth, Bakos 2012; SuperWASP, Pollacco et al. 2006; KELT, Pepper et al. 2007; TRES, Alonso et al. 2007, CSTAR, Wang et al. 2014). With improved photometry, we can refine planetary orbital ephemeris (Wang et al., 2018b), which is vital to schedule future transit-related observations, such as Rossiter-McLaughlin effect measurement (Nutzman et al., 2011; Sanchis-Ojeda and Winn, 2011; Sanchis-Ojeda et al., 2013; Wang et al., 2018a) and transmission spectrum follow-up (Mancini et al., 2016a; Mackebrandt et al., 2017).

Long-term photometric follow-up also provides a unique chance to study the variations of the orbital periods. A recent study shows the apparent orbital decay in the WASP-12 system (Patra et al., 2017), which intrigues a series of theoretical studies (Millholland and Laughlin, 2018; Weinberg et al., 2017) to discuss the potential mechanisms. The transit follow-up also plays an important role in exoplanet system which shows interesting Transit Timing Variations (TTV) (Ballard et al., 2011; Ford et al., 2012; Steffen et al., 2012a; Fabrycky et al., 2012; Mancini et al., 2016b; Wang et al., 2017a; Wu et al., 2018).

Ballard (2018) predicted that around 5% of planets discovered by TESS (Ricker, 2014) will show TTVs. Transit follow-up of these targets is very critical, because most of them will only be monitored for ~ 27 days, whereas the typical TTV period is around years.

Furthermore, extended TTV studies are crucial to confirm or rule out exoplanetary systems, in cases where space-based observations will not cover the long-time scales required to characterize them (von Essen et al., 2018). Thus, combining ground and space-based observations will be crucial.

The TTV method (Miralda-Escudé, 2002; Agol et al., 2005; Holman and Murray, 2005) also provides a powerful tool to detect additional low-mass planets in hot Jupiter systems, which is usually hard to find by using other techniques (Steffen et al., 2012b). Many efforts have been devoted to this field (Pál et al., 2011; Hoyer et al., 2012, 2013; Szabó et al., 2013), but so far only two hot Jupiters have been found to accompany with additional close-in planets (WASP-47: Becker et al. (2015), and Kepler-730: Cañas et al. (2019)). The accurate occurrence rate of the ‘WASP-47-like’ system is still unknown.

To refine orbital parameters of currently known exoplanets, and to search for additional planets by using TTV method, we organized the Transit Monitoring in the South hemisphere (TraMoS) project (Hoyer et al., 2011) since 2008. We uses one-meter class telescopes in the north of Chile to conduct high-precision long-term transit follow-up.

Following the previous efforts from the TraMoS project, in this work, we present new light curves of three hot Jupiters: WASP-18b, WASP-19b, WASP-77Ab. Combining our new light curves, and archival photometric and radial velocity data sets, we refined the orbital and physical parameters of the systems, and constrained the upper mass limit of potential additional planetary companions.

WASP-18b is a transiting hot Jupiter discovered by Hellier et al. (2009) within the WASP-South transit survey (Pollacco et al., 2006). It is an extremely close-in planet orbiting a F6 type star with a period of 0.94 days. Regarding its physical properties, WASP-18b is about ten times more massive than Jupiter with approximately the same radius ($M_P = 10.3 M_{\text{Jupiter}}$, $R_P = 1.1 R_{\text{Jupiter}}$). Even though a rapid orbital decay was predicted theoretically (Hellier et al., 2009), it is not observed yet (Wilkins et al., 2017) and new theoretical models proposed a variation of less than 4 seconds in the transit time over a 20-yr baseline (Collier Cameron and Jardine, 2018).

The hot Jupiter WASP-19b was first reported by Hebb et al. (2010). It is known as one of the currently hot Jupiters with shortest orbital period ($P = 0.788$ days). With a mass of $1.15 M_{\text{Jupiter}}$ and a radius of $1.31 R_{\text{Jupiter}}$, the planet orbits an active G8 dwarf.

The third exoplanet we followed-up in this work, WASP-77Ab, was first presented by Maxted et al. (2013a). WASP-77Ab has a mass of $1.8 M_{\text{Jupiter}}$ and a radius of $1.2 R_{\text{Jupiter}}$, and orbital period of 1.36 days. It transits a G8 star in the visual binary system with a separation of 3.3 arcsec.

This paper is organized as follows. In Section 3.2 are summarized the photometric observations and their reduction process. In Section 3.3 we present the new light curves of the targets and the description of the technique used to obtain their orbital and physical parameters. The principal results and their consequences are presented in Section 3.4. Finally, a summary and conclusions are described in Section 3.5.

3.2 Observations and Data Reduction

We collected 8 light curves for WASP-18b between 2009 and 2017, 9 light curves for WASP-19b between 2011 and 2017, and 5 light curves for WASP-77Ab between 2015 and 2017. We included 4 transits of WASP-77Ab from the Exoplanet Transit Database (ETD) in order to cover a larger timespan.

All of the photometry are collected by using either the Danish 1.54 m telescope at ESO La Silla Observatory, or the SMARTS 1 m at Cerro Tololo Observatory (CTIO), except for one transit of WASP-77Ab that was observed with the Warsaw 1.3 m at Las Campanas Observatory (LCO). The log of our observations is shown in Table 3.1. All the new light

Table 3.1: Log of Observations

Target	Date (UTC)	Epoch ^a	Telescope	Filter	N	t_{exp}^b (seconds)	RMS ^c (mmag)
WASP-18	2009 Oct 28	-1904	SMARTS 1 m	<i>I</i>	1412	1.5	8.49
	2009 Oct 29	-1903	SMARTS 1 m	<i>I</i>	1435	2	5.67
	2009 Oct 30	-1902	SMARTS 1 m	<i>I</i>	1198	2	4.50
	2011 Sep 06	-1184	SMARTS 1 m	<i>I</i>	203	15	2.40
	2016 Sep 24 ^d	776	Danish 1.54 m	<i>I</i>	138	90	1.05
	2016 Sep 25 ^d	777	Danish 1.54 m	<i>I</i>	159	90	0.96
	2016 Sep 26 ^d	778	Danish 1.54 m	<i>I</i>	113	90	0.87
	2017 Sep 29 ^d	1169	Danish 1.54 m	<i>R</i>	330	30	2.53
WASP-19	2011 Apr 22	-923	SMARTS 1 m	<i>I</i>	626	12	4.31
	2011 Dec 24	-611	SMARTS 1 m	<i>I</i>	364	18	35.9
	2013 Mar 13	-47	Danish 1.54 m	<i>R</i>	336	35	2.15
	2013 Apr 20	1	Danish 1.54 m	<i>R</i>	153	100	0.80
	2015 Mar 04	867	Danish 1.54 m	<i>R</i>	235	60	0.84
	2016 Apr 14	1383	Danish 1.54 m	<i>I</i>	87	100	0.71
	2017 Feb 14	1771	Danish 1.54 m	<i>I</i>	137	90	0.79
	2017 Apr 08	1838	Danish 1.54 m	<i>R</i>	125	90	0.81
	2017 Oct 03	2064	Danish 1.54 m	<i>R</i>	43	110	1.70
WASP-77	2013 Aug 20	-659	ETD ^e	<i>clear</i>	103	120	3.87
	2013 Oct 30	-606	ETD ^e	<i>clear</i>	690	12	5.91
	2015 Sep 29	-92	Danish 1.54 m	<i>R</i>	244	30	0.84
	2015 Oct 03	-89	Danish 1.54 m	<i>R</i>	138	60	1.84
	2016 Sep 26	175	Danish 1.54 m	<i>I</i>	90	90	0.47
	2016 Sep 30	177	ETD ^e	<i>clear</i>	66	180	2.74
	2016 Oct 07	183	Warsaw 1.3 m	<i>I</i>	237	60	2.38
	2016 Dec 09	229	ETD ^e	<i>R</i>	57	180	2.11
	2017 Oct 01	447	Danish 1.54 m	<i>B</i>	224	30	3.48

^a The epoch 0 is T_0 in Tables 3.3,3.4 and 3.5, for WASP-18b, WASP-19b and WASP-77Ab, respectively.

^b For the variable exposure times, we consider the average during the night.

^c RMS values were computed from the best fitted model of each light curve.

^d Light curves obtained with only one reference star.

^e These light curves were obtained from the Exoplanet Transit Database (ETD) var2.astro.cz/ETD.

curves used for this work are presented in Figure 3.1.

For the photometric observations conducted on the Danish telescope, we used the Danish Faint Object Spectrograph and Camera (DFOSC) instrument, which has a $2\text{K} \times 2\text{K}$ CCD with a 13.7×13.7 arcmin 2 field of view (FoV) and a pixel scale of $0.39''$ per pixel. To reduce the readout time, some of the Danish 1.54 m images were windowed to only include the target star and its closest reference stars. The observations of the transits of WASP-18b during 2016 and 2017 were forced to be windowed due to a malfunction of the CCD. For those transits, only one reference star was used to perform the photometry.

The SMARTS 1 m has the Y4KCam instrument which is a $4\text{K} \times 4\text{K}$ CCD camera with a 20×20 arcmin 2 FoV and a pixel scale of $0.289''$ per pixel.

For the observation on the Warsaw 1.3 m telescope, we used a 2048×4096 CCD camera chip with a 1.4 square degrees of FoV and $0.26''$ per pixel scale. No windowing or binning was used during the observations on both SMARTS 1m and the Warsaw 1.3m telescope.

Most of our observation, especially those conducted after 2011, used the defocus technique as suggested by Southworth et al. (2009), which allows longer exposure times in bright targets and improves the photometric precision. We adjust the exposure time during the observations if the weather is not ideal. The recorded Julian Date in the Coordinated Universal Time (JD_{UTC}) were converted into Barycentric Julian Date in the Barycentric Dynamical Time standard (BJD_{TDB}) by following the procedure as in Eastman et al. (2010).

We reduced the data by using our custom pipeline. It follows the standard procedures of reduction, calibration, and aperture photometry, but customized for each used instrument. The pipeline semi-automatically finds the best aperture and ring size, for the sky that produces the light curve with less RMS. Then, we manually choose the reference stars to produce the differential light curves for each targets.

3.3 Light curve and RV analysis

To obtain the refined orbital and physical parameters of WASP-18b, WASP-19b, and WASP-77Ab, as well as their transit mid-time (T_c), we used EXOFASTv2 (Eastman et al., 2013; Eastman, 2017) to model the light curves together with archived RV data Hellier et al. (2009); Hebb et al. (2010); Maxted et al. (2013a).

EXOFASTv2 is an IDL code designed to simultaneously fit transits and radial velocity measurements obtained from different filters or different telescopes. It uses the Differential Evolution Markov chain Monte Carlo (DE-MCMC) method to derive the values and their uncertainties of the stellar, orbital and physical parameters of the system.

The stellar parameters of WASP-18, WASP-19, and WASP-77A were computed using the MESA Isochrones and Stellar Tracks (MIST) model (Dotter, 2016) included in EXOFASTv2. We applied Gaussian priors in surface gravity $\log g$, effective temperature T_{eff} , and metallicity [Fe/H] of the stars, from Hellier et al. (2009), Hebb et al. (2010) and Maxted et al. (2013a)

Table 3.2: Example photometry of WASP-18, WASP-19 and WASP-77A

Target	BJD _{TDB} ^a	Relative flux	Error
WASP-18b	2457658.658241	1.00168	0.00078
	2457658.660591	1.00138	0.00080
	2457658.661771	1.00195	0.00082
	2457658.662940	1.00261	0.00085
	2457658.664109	1.00137	0.00086

WASP-19b	2457086.543926	1.00099	0.00086
	2457086.544916	1.00173	0.00091
	2457086.545905	1.00139	0.00086
	2457086.546895	1.00045	0.00094
	2457086.547886	1.00064	0.00093

WASP-77Ab	2457299.78624	1.00229	0.00028
	2457299.78764	1.00116	0.00022
	2457299.78855	1.00201	0.00022
	2457299.78946	1.00216	0.00022
	2457299.79092	1.00133	0.00021

These tables are available in machine-readable form.

^a The column time was converted to (BJD_{TDB}), following the procedure of Eastman et al. (2010).

for WASP-18, WASP-19 and WASP-77A, respectively. We were not able to separate the contribution of the two companions of the binary system WASP-77, because the separation is 3.3 arcsec, but our photometry aperture is about 10 arcsec. Thus, we computed the dilution factor – fraction of the light that comes from the companion star – for each filter of our data set in order to get the real transit depth of WASP-77Ab. Because of the lack of good quality magnitude measurements for the fainter companion WASP-77B in the *B*, *I*, *R* and *clear* pass bands, we derived them from the *Gaia* magnitude ($G = 11.8356$) assuming Black Body radiation. The derived magnitudes for WASP-77B are $V = 11.97$, $B = 12.72$, $R = 11.57$, $I = 10.95$ and $clear = 11.78$.

We set previous published values as uniform priors for the DE-MCMC in all the transit, RV parameters, quadratic limb darkening coefficients and T_c . The priors were taken from the discovery papers of WASP-18b (Hellier et al., 2009), WASP-19b (Hebb et al., 2010) and WASP-77Ab (Maxted et al., 2013a).

In order to reduce significantly the convergence time of the chains during the EXOFASTv2 fitting, we started from shorter chains. Thus, the total time to complete that run is reduced. After it finished, we took the values from its best model and used them as priors for the next short run. This process was repeated until the chains converged and were well-mixed.

The best-fitted model is presented in Figure 3.1 for our transit data from the TraMoS

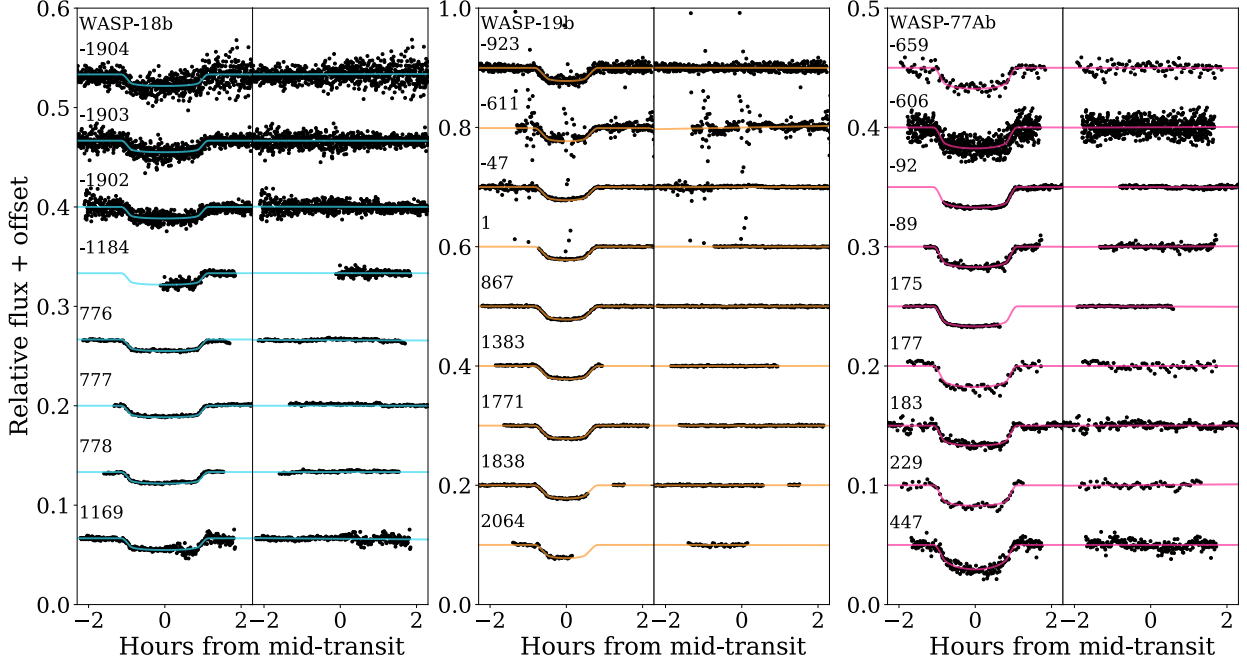


Figure 3.1: Light curves of WASP-18, WASP19 and WASP77 during 8, 9 and 9 different transits, respectively, from the TraMoS project. The fitted best model from EXOFASTv2 is shown as a light blue solid line for WASP-18b, orange for WASP-19b and pink for WASP-77Ab. To the right of each panel are the corresponding residuals of the model. For clarity, both light curves and their residual are offset artificially. The epoch number is indicated above each light curve. The technical information about each observation is listed in Table 3.1.

project, and in Figure 3.2 for the RV archival data.

3.4 Results and Discussion

3.4.1 Transit Parameters and Physical Properties

3.4.1.1 WASP-18b

The resulting parameters from the global fit of WASP-18 in comparison the with results of the discovery paper Hellier et al. (2009) and the most recent analysis with TESS data (Shporer et al., 2018), are listed in Table 3.3. While in Hellier et al. (2009) the analysis was performed combining photometry and RV data, in Shporer et al. (2018) only photometric data was used.

As the stellar spectroscopic priors were taken from the discovery paper Hellier et al. (2009), our results for the stellar mass M_* and radius R_* are in good agreement with theirs, as expected, as well as the rest of the stellar parameters. Shporer et al. (2018) do not present results of stellar parameters.

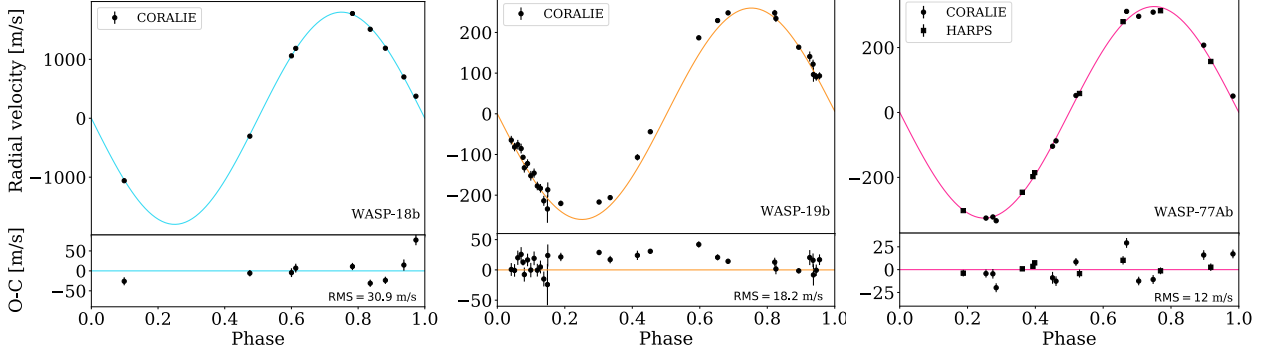


Figure 3.2: Radial velocity observations of WASP-18, WASP-19 and WASP-77A from Hellier et al. (2009), Hebb et al. (2010) and Maxted et al. (2013a), respectively. The best fitted model from the joint modeling of RV and light curves with EXOFASTv2 is in solid line color: light blue for WASP-18b, orange for WASP-19b and pink for WASP-77Ab. The residuals of the model are shown at the bottom panel of each figure.

In the case of the primary transit parameters, the greatest difference is found in the radius of the planet in stellar radii R_p/R_* . Our reported R_p/R_* is 7.8σ and 4.4σ larger than the reported by Hellier et al. (2009) on the discovery paper and the recent result from Shporer et al. (2018), respectively. Our transit duration T_{14} is also 3.4σ larger than the value from Hellier et al. (2009).

For the radial velocity parameters, the RV semi-amplitude derived from our analysis is consistent with the value of Hellier et al. (2009), as the same data was used.

Finally, the derived parameters of the system are, in general, in good agreement with the values from Hellier et al. (2009) and Shporer et al. (2018).

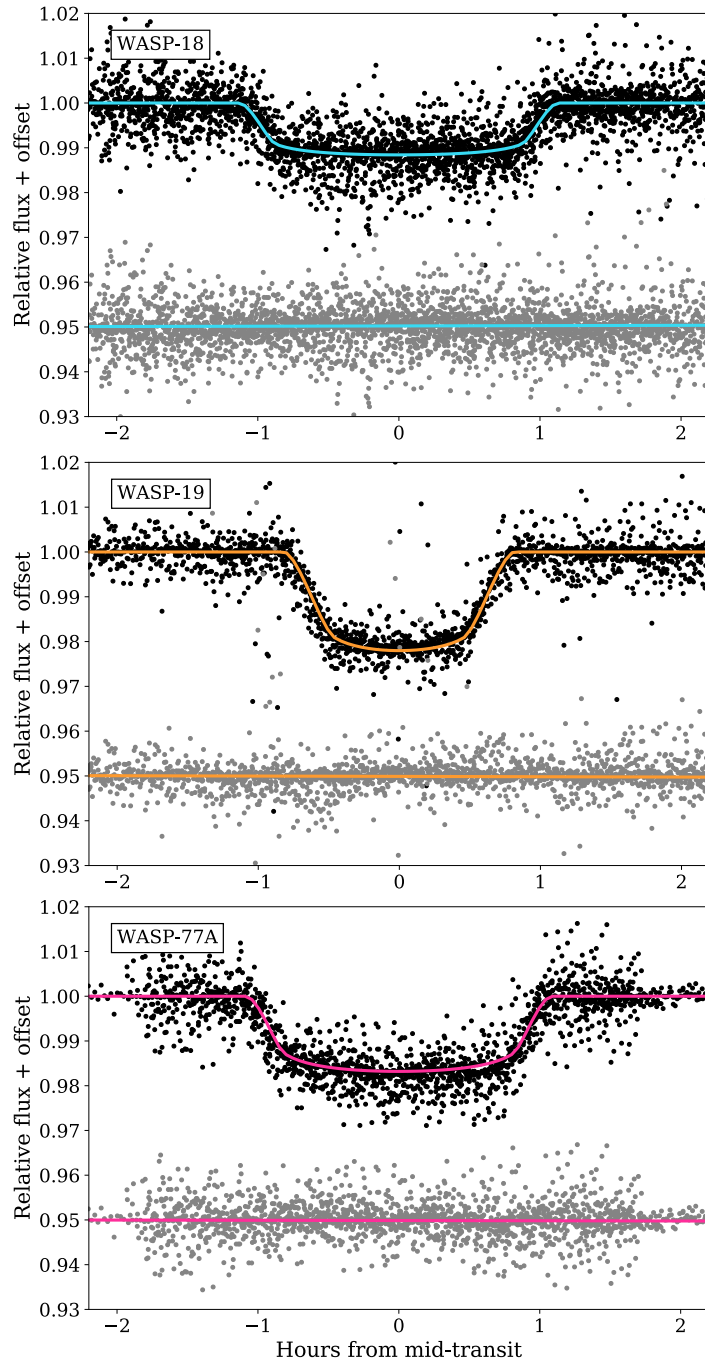


Figure 3.3: Phased light curve of WASP-18b, WASP-19b and WASP-77Ab transits, from the TraMoS project. The three data set of light curves are fitted simultaneously with RV archival data using EXOFASTv2, in order to estimate the orbital and physical parameters of the system. In the top panel, the light blue solid line is the best fitting model for WASP-18b, and bellow are the residuals in color grey. The same for WASP-19b in color orange at the center panel, and for WASP-77Ab in color pink at the bottom panel.

Table 3.3: System parameter of WASP-18

Parameter	Units	This work	Hellier et al. (2009)	Shporer et al. (2018)
Stellar Parameters:				
M_* ..	Mass (M_\odot)	$1.294^{+0.063}_{-0.061}$	1.25 ± 0.13	
R_* ..	Radius (R_\odot)	$1.319^{+0.061}_{-0.062}$	$1.26^{+0.067}_{-0.054}$	
L_* ..	Luminosity (L_\odot)	$2.68^{+0.28}_{-0.26}$		
ρ_* ..	Density (cgs)	$0.795^{+0.11}_{-0.089}$	$0.707^{+0.056}_{-0.096}$	
$\log g$..	Surface gravity (cgs)	$4.310^{+0.036}_{-0.033}$	$4.367^{+0.028}_{-0.042}$	
T_{eff} ..	Effective Temperature (K)	6432 ± 48	6400 ± 100	
[Fe/H]	Metallicity	0.107 ± 0.080	0.00 ± 0.09	
Age ..	Age (Gyr)	$1.57^{+1.4}_{-0.94}$	$0.5 - 1.5$	
Planetary Parameters:				
R_P ..	Radius (R_J)	1.310 ± 0.071	$1.106^{+0.072}_{-0.054}$	1.192 ± 0.038
M_P ..	Mass (M_J)	$10.48^{+0.42}_{-0.40}$	10.30 ± 0.69	
P ..	Period (days)	$0.94145236 \pm (49)$	$0.94145299 \pm (87)$	$0.9414576^{(+34)}_{(-35)}$
e ..	Eccentricity	$0.0061^{+0.0089}_{-0.0044}$		
a ..	Semi-major axis (AU)	$0.02054^{+0.00033}_{-0.00032}$	0.02045 ± 0.00067	
ω_* ..	Argument of Periastron (Degrees) .	-100^{+110}_{-120}		
ρ_P ..	Density (cgs)	$5.79^{+0.97}_{-0.78}$	$7.73^{+0.78a}_{-1.27}$	
$\log g_P$..	Surface gravity	$4.180^{+0.044}_{-0.041}$	$4.289^{+0.027}_{-0.050}$	
T_{eq} ..	Equilibrium temperature (K)	2485^{+53}_{-56}	2384^{+58}_{-30}	
Θ ..	Safronov Number	$0.254^{+0.015}_{-0.014}$		
$\langle F \rangle$..	Incident Flux (10^9 erg s $^{-1}$ cm $^{-2}$) ..	$8.66^{+0.77}_{-0.75}$		
Primary Transit Parameters:				
T_0 ..	Transit time (BJD _{TDB})	$2456740.80560 \pm (19)$	$2454221.48163 \pm (38)$	$2458361.048072^{(+34)}_{(-35)}$
i ..	Inclination (Degrees)	$83.5^{+2.0}_{-1.6}$	86.0 ± 2.5	$84.31^{+0.40}_{-0.37}$
R_P/R_*	Radius of planet in stellar radii ..	0.1021 ± 0.0011	0.0935 ± 0.0011	$0.09721^{+0.00016}_{-0.00017}$

Table 3.3 – *Continued from previous page*

Parameter	Units	This work	Hellier et al. (2009)	Shporer et al. (2018)
a/R_* ..	Semi-major axis in stellar radii ..	$3.35^{+0.15}_{-0.13}$		$3.523^{+0.028}_{-0.027}$
b ...	Impact parameter	$0.433^{+0.07}_{-0.10}$	0.25 ± 0.15	$0.349^{+0.020}_{-0.022}$
δ ...	Transit depth (fraction)	0.01041 ± 0.00022		$0.009449^{+0.000032}_{-0.000032}$
$u_{1,I}$..	linear LD coeff., I band	0.207 ± 0.019		
$u_{2,I}$..	quadratic LD coeff., I band	0.313 ± 0.019		
$u_{1,R}$..	linear LD coeff., R band	0.257 ± 0.045		
$u_{2,R}$..	quadratic LD coeff., R band	0.309 ± 0.048		
T_{14} ..	Total transit duration (days)	$0.0931^{+0.0011}_{-0.0010}$	0.08932 ± 0.00068	
P_T ..	A priori non-grazing transit prob .	$0.268^{+0.011}_{-0.012}$		
$P_{T,G}$..	A priori transit prob	$0.328^{+0.014}_{-0.015}$		
τ ...	Ingress/egress transit duration (days)	0.0107 ± 0.0010		
RV Parameters:				
$e \cos \omega_*$	$-0.0004^{+0.0038}_{-0.0045}$		
$e \sin \omega_*$	$-0.0008^{+0.0056}_{-0.0092}$		
K ..	RV semi-amplitude (m/s)	1807^{+34}_{-36}	1818.3 ± 8.0	
$M_P \sin i$	Minimum mass (M_J)	10.40 ± 0.40		
Secondary Eclipse Parameters:				
T_S ..	Time of eclipse (BJD _{TDB})	$2457657.3076^{+0.0023}_{-0.0027}$		
b_S ..	Eclipse impact parameter	$0.431^{+0.070}_{-0.100}$		
τ_S ..	Ingress/egress eclipse duration (days)	$0.0106^{+0.0011}_{-0.0010}$		
$T_{S,14}$..	Total eclipse duration (days)	0.0929 ± 0.0017		
P_S ..	A priori non-grazing eclipse prob .	$0.269^{+0.010}_{-0.011}$		
$P_{S,G}$..	A priori eclipse prob	$0.330^{+0.013}_{-0.014}$		

Values enclosed in parentheses correspond to the uncertainties of the last digits of the nominal value.

^a Value converted to cgs units multiplying by the Jupiter density $\rho_J = 1.33$ cgs.

3.4.1.2 WASP-19b

The results of the global fit of WASP-19 are listed in Table 3.4, in comparison with the previous values from the discovery paper (Hebb et al., 2010), and a more recent work (Lendl et al., 2013).

To estimate the stellar parameters of WASP-19, we used as priors the stellar spectroscopic parameters from Hebb et al. (2010). Thus, in general, our results are in agreement with those from the discovery paper. The most important discrepancies are the density of the star ρ_* and the surface gravity $\log g$, showing $+2.5\sigma$ and -3.2σ difference, respectively. Comparing with the results from Lendl et al. (2013), ours are all in good agreement.

For values of the primary transit parameters obtained from the light curves, the greatest differences are found in the orbital inclination i and the total transit duration T_{14} . We report an inclination value 5.1σ smaller than Hebb et al. (2010), but in agreement with the estimate of Lendl et al. (2013). In the other hand, our estimation of T_{14} is significantly larger than Hebb et al. (2010) by 9σ , but the difference is only 3.5σ when compared with Lendl et al. (2013). We also report a more precise impact parameter b and transit depth δ .

As the same RV data set from the discovery paper (Hebb et al., 2010) was used to perform our analysis, the almost identical values in the RV semi-amplitude K is not a surprise. Moreover, the values from Lendl et al. (2013) are also in agreement.

The planetary parameters derived from the light curve and radial velocity analysis are almost all in good agreement with the comparison works. The only parameter with a difference greater than 3σ is our estimation of the Equilibrium Temperature T_{eq} compared with the result of Hebb et al. (2010). However, our result is in better agreement with Lendl et al. (2013) by less than 2σ .

Table 3.4: System parameter of WASP-19

Parameter	Units	This work	Hebb et al. (2010) ^a	Lendl et al. (2013)
Stellar Parameters:				
M_* ..	Mass (M_\odot)	$0.965^{+0.091}_{-0.095}$	0.95 ± 0.10	$0.968^{+0.084}_{-0.079}$
R_* ..	Radius (R_\odot)	$1.006^{+0.031}_{-0.034}$	$0.93^{+0.05}_{-0.04}$	0.994 ± 0.031
L_* ..	Luminosity (L_\odot)	$0.905^{+0.071}_{-0.069}$		
ρ_* ..	Density (cgs)	$1.339^{+0.056}_{-0.058}$	$1.19^{+0.12b}_{-0.11}$	$1.384^{+0.055b}_{-0.051}$
$\log g$..	Surface gravity (cgs)	$4.417^{+0.020}_{-0.021}$	4.48 ± 0.03	
T_{eff} ..	Effective Temperature (K)	5616^{+66}_{-65}	5500 ± 100	
[Fe/H]	Metallicity	$0.04^{+0.25}_{-0.30}$	0.02 ± 0.09	
Age ..	Age (Gyr)	$6.4^{+4.1}_{-3.5}$	$5.5^{+9.0}_{-4.5}$	
Planetary Parameters:				
R_P ..	Radius (R_J)	$1.415^{+0.044}_{-0.048}$	1.28 ± 0.07	1.376 ± 0.046
M_P ..	Mass (M_J)	$1.154^{+0.078}_{-0.080}$	1.14 ± 0.07	1.165 ± 0.068
P ..	Period (days)	$0.78883852^{+(75)}_{-(82)}$	$0.7888399 \pm (8)$	$0.7888390 \pm (2)$
e ..	Eccentricity	$0.0126^{+0.014}_{-0.0089}$		$0.0077^{+0.0068}_{-0.0032}$
a ..	Semi-major axis (AU)	$0.01652^{+0.00050}_{-0.00056}$	$0.0164^{+0.0005}_{-0.0006}$	0.01653 ± 0.00046
ω_* ..	Argument of Periastron (Degrees) ..	51^{+89}_{-190}	-76^{+112}_{-23}	43^{+28}_{-67}
ρ_P ..	Density (cgs)	$0.506^{+0.031}_{-0.030}$	$0.54^{+0.07}_{-0.06}$	$0.595^{+0.036c}_{-0.033}$
$\log P$..	Surface gravity	$3.155^{+0.018}_{-0.019}$	3.20 ± 0.03	3.184 ± 0.015
T_{eq} ..	Equilibrium temperature (K)	2113 ± 29	1993^{+32}_{-33}	2058 ± 40
Θ ..	Safronov Number	$0.0279^{+0.0012}_{-0.0011}$		
$\langle F \rangle$..	Incident Flux (10^9 erg s $^{-1}$ cm $^{-2}$) ..	$4.52^{+0.26}_{-0.24}$		
Primary Transit Parameters:				
T_0 ..	Transit Time (BJD _{TDB})	$2456402.7128^{+(17)}_{-(14)}$	$2454775.3372 \pm (2)$	$2456029.59204 \pm (13)$
i ..	Inclination (Degrees)	$79.08^{+0.34}_{-0.37}$	80.8 ± 0.8	79.54 ± 0.33
R_P/R_*	Radius of planet in stellar radii ..	$0.14410^{+0.00049}_{-0.00050}$	0.1425 ± 0.0014	

Table 3.4 – *Continued from previous page*

Parameter	Units	This work	Hebb et al. (2010) ^a	Lendl et al. (2013)
a/R_* ..	Semi-major axis in stellar radii ..	$3.533_{-0.052}^{+0.048}$		3.573 ± 0.046
b ...	Impact parameter	$0.6671_{-0.0091}^{+0.0087}$	0.62 ± 0.03	0.645 ± 0.012
δ ...	Transit depth (fraction)	0.02077 ± 0.00014	0.0203 ± 0.0004	0.02018 ± 0.00021
$u_{1,I}$..	linear LD coeff., I band.....	$0.287_{-0.029}^{+0.027}$		
$u_{2,I}$..	quadratic LD coeff., I band.....	0.263 ± 0.024		
$u_{1,R}$..	linear LD coeff., R band	$0.383_{-0.032}^{+0.029}$		
$u_{2,R}$..	quadratic LD coeff., R band	$0.246_{-0.025}^{+0.027}$		
T_{14} ..	Total transit duration (days)....	$0.06697_{-0.00030}^{+0.00031}$	$0.0643_{-0.0007}^{+0.0006}$	$0.06586_{-0.00031}^{+0.00033}$
P_T ..	A priori non-grazing transit prob .	$0.2426_{-0.0051}^{+0.0066}$		
$P_{T,G}$..	A priori transit prob	$0.3246_{-0.0069}^{+0.0089}$		
τ ...	Ingress/egress transit duration (days)	0.01459 ± 0.00035		
RV Parameters:				
$e \cos \omega_*$	$-0.0027_{-0.013}^{+0.0077}$	0.004 ± 0.009	0.0024 ± 0.0020
$e \sin \omega_*$	$0.0016_{-0.0092}^{+0.014}$	-0.02 ± 0.02	0.000 ± 0.005
K ..	RV semi-amplitude (m/s)	$255.4_{-6.2}^{+6.1}$	256 ± 5	257.7 ± 2.9
$M_P \sin i$	Minimum mass (M_J).....	$1.133_{-0.079}^{+0.078}$		
Secondary Eclipse Parameters:				
T_S ..	Time of eclipse (BJD _{TDB})	$2455169.3621_{-(51)}^{+(41)}$	$2456030.77766 \pm (88)$	
b_S ..	Eclipse impact parameter	$0.670_{-0.017}^{+0.020}$	0.652 ± 0.015	
τ_S ..	Ingress/egress eclipse duration (days)	$0.01472_{-0.00066}^{+0.00085}$		
$T_{S,14}$..	Total eclipse duration (days)....	$0.06812_{-0.00074}^{+0.00087}$		
P_S ..	A priori non-grazing eclipse prob .	0.2415 ± 0.0021		
$P_{S,G}$..	A priori eclipse prob	0.3232 ± 0.0030		

Values enclosed in parentheses correspond to the uncertainties of the last digits of the nominal value.

^a For comparison, the results from Hellier et al. (2009) that considered free eccentricity were used.

^b Values converted to cgs units multiplying by the Sun density $\rho_\odot = 1.408$ cgs.

^c Value converted to cgs units multiplying by the Jupiter density $\rho_J = 1.33$ cgs.

3.4.1.3 WASP-77Ab

Table 3.5 lists the results of the global fit of WASP-77Ab, in comparison with the values from its discovery paper (Maxted et al., 2013a) on which photometry and RV data were used. No other previous work has reported bulk measurements for this system.

Almost all the stellar parameters are in agreement with (Maxted et al., 2013a), except for a -9.7σ difference in the stellar surface gravity $\log g$, where our reported value is more precise.

The primary transit parameters, as well as the RV parameters and the derived planetary parameters, are consistent with the results from Maxted et al. (2013a).

Table 3.5: System parameter of WASP-77A

Parameter	Units	This work	Maxted et al. (2013a)
Stellar Parameters:			
M_* ..	Mass (M_\odot)	$0.903^{+0.066}_{-0.059}$	1.002 ± 0.045
R_* ..	Radius (R_\odot)	$0.910^{+0.025}_{-0.023}$	0.955 ± 0.015
L_* ..	Luminosity (L_\odot)	$0.743^{+0.065}_{-0.058}$	
ρ_* ..	Density (cgs)	$1.692^{+0.056a}_{-0.069}$	$1.629^{+0.023a}_{-0.028}$
$\log g$.	Surface gravity (cgs)	$4.476^{+0.014}_{-0.015}$	4.33 ± 0.08
T_{eff} ..	Effective Temperature (K)	5617 ± 72	5500 ± 80
[Fe/H]	Metallicity	$-0.10^{+0.10}_{-0.11}$	0.00 ± 0.11
Age .	Age (Gyr)	$6.2^{+4.0}_{-3.5}$	$0.5 - 1.0$
Planetary Parameters:			
R_P ..	Radius (R_J)	$1.183^{+0.034}_{-0.031}$	1.21 ± 0.02
M_P ..	Mass (M_J)	$1.650^{+0.082}_{-0.075}$	1.76 ± 0.06
P ...	Period (days)	$1.3600290^{+(18)}_{-(20)}$	$1.3600309 \pm (20)$
e ...	Eccentricity	$0.0074^{+0.0075}_{-0.0051}$	
a ...	Semi-major axis (AU)	$0.02323^{+0.00056}_{-0.00052}$	0.0240 ± 0.00036
ω_* ..	Argument of Periastron (Degrees) .	-30^{+170}_{-120}	
ρ_P ..	Density (cgs)	$1.240^{+0.060}_{-0.067}$	1.33 ± 0.04^b
$\log g_P$.	Surface gravity	$3.467^{+0.012}_{-0.015}$	3.441 ± 0.008
T_{eq} ..	Equilibrium temperature (K)	1695^{+25}_{-24}	
Θ ...	Safronov Number	0.0717 ± 0.0021	
$\langle F \rangle$..	Incident Flux (10^9 erg s $^{-1}$ cm $^{-2}$) ..	$1.87^{+0.11}_{-0.10}$	
Primary Transit Parameters:			
T_0 ..	Transit Time (BJD _{TDB})	$2457420.88439^{(+80)}_{(-85)}$	$2455870.44977 \pm (20)$
i ...	Inclination (Degrees)	$88.91^{+0.74}_{-0.95}$	$89.4^{+0.4}_{-0.7}$
R_P/R_*	Radius of planet in stellar radii ..	$0.13352^{+0.00074}_{-0.00070}$	

Table 3.5 – *Continued from previous page*

Parameter	Units	This work	Maxted et al. (2013a)
a/R_* .	Semi-major axis in stellar radii ..	$5.493^{+0.060}_{-0.075}$	
b . . .	Impact parameter	$0.105^{+0.089}_{-0.071}$	$0.06^{+0.07}_{-0.05}$
δ . . .	Transit depth (fraction)	$0.01783^{+0.00020}_{-0.00019}$	
$u_{1,B}$. . .	linear LD coeff., B band	0.680 ± 0.054	
$u_{2,B}$. . .	quadratic LD coeff., B band	$0.140^{+0.052}_{-0.053}$	
$u_{1,clear}$	linear LD coeff., <i>clear</i> band	0.386 ± 0.029	
$u_{2,clear}$	quadratic LD coeff., <i>clear</i> band ..	0.227 ± 0.029	
$u_{1,I}$. . .	linear LD coeff., I band	0.311 ± 0.025	
$u_{2,I}$. . .	quadratic LD coeff., I band	0.294 ± 0.033	
$u_{1,R}$. . .	linear LD coeff., R band	0.312 ± 0.023	
$u_{2,R}$. . .	quadratic LD coeff., R band	$0.237^{+0.029}_{-0.028}$	
T_{14} ..	Total transit duration (days)	$0.08952^{+0.00053}_{-0.00051}$	
P_T ..	A priori non-grazing transit prob .	$0.1578^{+0.0029}_{-0.0025}$	
$P_{T,G}$.	A priori transit prob	$0.2064^{+0.0039}_{-0.0033}$	
τ . . .	Ingress/egress transit duration (days)	$0.01075^{+0.00032}_{-0.00015}$	

RV Parameters:

$e \cos \omega_*$	$-0.0033^{+0.0041}_{-0.0065}$
$e \sin \omega_*$	$-0.0002^{+0.0061}_{-0.0073}$
K ..	RV semi-amplitude (m/s)	$323.4^{+3.7}_{-3.3}$
$M_P \sin i$	Minimum mass (M_J)	$1.649^{+0.082}_{-0.075}$

Secondary Eclipse Parameters:

T_S ..	Time of eclipse (BJD _{TDB})	$2457659.5665^{+0.0038}_{-0.0056}$
b_S ..	Eclipse impact parameter	$0.104^{+0.089}_{-0.071}$
τ_S ..	Ingress/egress eclipse duration (days)	$0.01076^{+0.00035}_{-0.00023}$
$T_{S,14}$..	Total eclipse duration (days)	$0.0895^{+0.0013}_{-0.0014}$
P_S ..	A priori non-grazing eclipse prob .	$0.1578^{+0.0018}_{-0.0012}$
$P_{S,G}$.	A priori eclipse prob	$0.2063^{+0.0025}_{-0.0016}$

Table 3.5 – *Continued from previous page*

Parameter	Units	This work	Maxted et al. (2013a)
-----------	-------	-----------	-----------------------

Values enclosed in parentheses correspond to the uncertainties of the last digits of the nominal value.

^a Values converted to cgs units multiplying by the Sun density $\rho_{\odot} = 1.408$ cgs.

^b Value converted to cgs units multiplying by the Jupiter density $\rho_J = 1.33$ cgs.

3.4.2 Transit Timing Variations

A transit timing variation is represented through a difference in time from the transit mid-time T_c , for a planet in Keplerian motion following a linear ephemeris of the orbital period. The TTVs were computed considering our transit times from the TraMoS project, as well as including previous published ones. A refined orbital period was linearly fitted, considering 19, 59 and 11 transit times of WASP-18b, WASP-19b, and WASP-77Ab, respectively. Along the linear fit, we also tested a second degree polynomial fit to analyze a possible orbital decay. Both fits considered the errors of the data. In Figure 3.4 are presented all the TTV values for the transit times of WASP-18b, WASP-19b and WASP-77Ab, respectively.

If the planet stays in a Keplerian orbit, its transit time T_c of each epoch E should follow a linear function of the orbital period P .

$$T_C(E) = T_C(0) + E \cdot P \quad (3.1)$$

Where $T_C(0)$ is the optimal transit time in an arbitrary zero epoch. The best-fitted values of $T_C(0)$ for WASP-18b, WASP-19b and WASP-77Ab, are listed in Tables 3.3, 3.4 and 3.5, respectively.

3.4.2.1 WASP-18b

For this system, the proposed linear ephemeris equation is:

$$T_C(E) = 2456926.27460 \pm (94) + E \cdot 0.941452232 \pm (89) \quad (3.2)$$

The orbital period P in Eq. 3.2 is in complete agreement with the value computed only with the TraMoS light curves in Table 3.3.

Table 3.6 lists the TTV of our transit times and also, of data from previous works (Triaud et al., 2010; Hellier et al., 2009; Maxted et al., 2013b) of WASP-18b.

The top panel of Figure 3.4 is the linear plot of TTV versus epoch for this planet. The deviations of the transit times from the linear ephemeris has an RMS of 83 seconds. The greater deviations come from the transit time of the epochs -1904 and -1184 , which are over the linear ephemeris by 2.5σ and 1.9σ , respectively. If those values are removed, the RMS decreases to 61 seconds. Considering all the transit times in Table 3.6 without the epochs -1904 and -1184 , all the TTVs lie within 1.6σ in the linear fit. The epoch -1184 has the greatest error in our sample because it is not a complete transit.

When testing the goodness of the linear fit, $\chi^2_{red} = 0.56$, while for a second degree polynomial is $\chi^2_{red} = 0.48$, therefore an orbital decay can be discarded in agreement with theoretical estimations (Collier Cameron and Jardine, 2018).

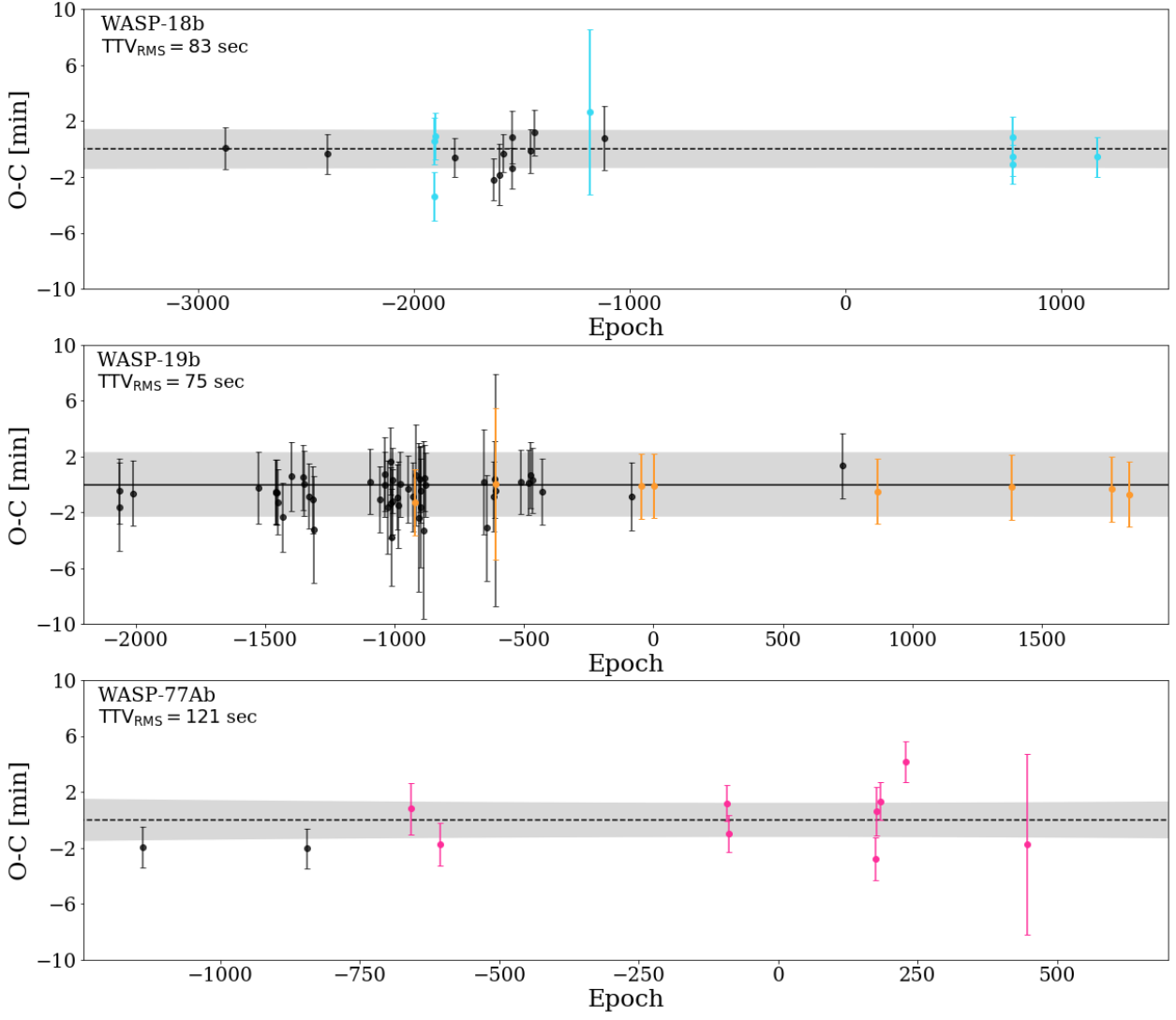


Figure 3.4: Observed minus calculated mid-transit times (TTV) for WASP-18b (top), WASP-19b (center) and WASP-77Ab (bottom). The dashed black line corresponds to the proposed linear ephemeris, i.e. zero deviation from the predicted transit time (See Section 3.4.2) computed from our refined orbital period. For that, we considered 19, 59 and 11 transit times of WASP-18b, WASP-19b, and WASP-77Ab, respectively. The grey area corresponds to the error propagation at 1σ , where the quadratic trend looks almost horizontal. The points in color are the TTV from the newly light curves of the TraMoS project (WASP-18b: light blue, WASP-19b: orange, WASP-77Ab: pink) and the black points in the three panels are TTVs measured from previous published transit times. The RMS scatter from the linear ephemeris are 83 seconds for WASP-18b; 75 seconds for WASP-19b, and 121 seconds for WASP-77Ab.

Table 3.6: Transit mid-times for WASP-18b

Epoch	Transit mid-time (BJD _{TDB})	TTV (min)	References
-2873	2454221.48238	0.1 ± 1.5	1
-2402	2454664.9061	-0.4 ± 1.4	2
-1904	2455133.7472	-3.4 ± 1.7	This work
-1903	2455134.6914	0.6 ± 1.7	This work
-1902	2455135.6331	0.9 ± 1.7	This work
-1811	2455221.3042	-0.6 ± 1.4	3
-1629	2455392.6474	-2.2 ± 1.5	3
-1601	2455419.0083	-1.8 ± 2.2	3
-1587	2455432.1897	-0.3 ± 1.4	3
-1546	2455470.7885	-1.4 ± 1.4	3
-1543	2455473.6144	0.9 ± 1.9	3
-1457	2455554.5786	-0.2 ± 1.5	3
-1440	2455570.5842	1.2 ± 1.6	3
-1184	2455811.5970	2.7 ± 5.9	This work
-1115	2455876.5559	0.8 ± 2.3	3
776	2457656.84078	-1.1 ± 1.4	This work
777	2457657.78359	0.9 ± 1.4	This work
778	2457658.72404	-0.6 ± 1.4	This work
1169	2458026.83186	-0.6 ± 1.5	This work

References: (1) Hellier et al. (2009); (2) Triaud et al. (2010); (3) Maxted et al. (2013a)

3.4.2.2 WASP-19b

The proposed equation for linear ephemeris, considering 59 transit times of WASP-19b is:

$$T_C(E) = 2456402.7128 \pm (16) + E \cdot 0.788838858 \pm (47) \quad (3.3)$$

The TTV values from the proposed linear ephemeris are listed in Table 3.7, including transit times from the previous works (Hebb et al., 2010; Anderson et al., 2010; Lendl et al., 2013; Tregloan-Reed et al., 2013; Bean et al., 2013; Mancini et al., 2013).

At the middle panel of Figure 3.4 are the TTV values versus epoch, for all the transit time considered in this work.

The RMS from the linear ephemeris is about 75 seconds. The epoch of -1011 is the only one with a transit time deviation above 1.5σ from the linear ephemeris. If it is removed, then the RMS decreases to 69 seconds. Moreover, in our data the epoch -611 has one of the greatest errors due to bad weather conditions.

Considering all the transit times from Table 3.7, the linear fit has $\chi^2_{red} = 0.16$. This is an indication of an overestimation of the errors. A second degree polynomial was also tested in order to reject or not a possible orbital decay. The goodness of that fit is $\chi^2_{red} = 0.12$.

Table 3.7: Transit mid-times for WASP-19b

Epoch	Transit mid-time (BJD _{TDB})	TTV (min)	References
-2063	2454775.3372	-1.6 ± 3.2	1
-2061	2454776.91566	-0.5 ± 2.3	2
-2010	2454817.14633	-0.6 ± 2.3	3
-1525	2455199.73343	-0.2 ± 2.6	4
-1459	2455251.79657	-0.6 ± 2.3	5
-1458	2455252.58544	-0.5 ± 2.3	5
-1454	2455255.74077	-0.6 ± 2.3	5
-1449	2455259.68448	-1.3 ± 2.4	4
-1431	2455273.88282	-2.4 ± 2.5	4
-1399	2455299.12768	0.6 ± 2.4	4
-1354	2455334.6254	0.5 ± 2.3	6
-1349	2455338.56927	0.1 ± 2.3	3
-1330	2455353.55659	-0.8 ± 2.3	6
-1317	2455363.81131	-1.1 ± 2.4	4
-1311	2455368.54285	-3.3 ± 3.8	6
-1094	2455539.72327	0.2 ± 2.4	3
-1056	2455569.69826	-1.1 ± 2.4	3
-1039	2455583.10979	0.8 ± 2.6	4
-1037	2455584.68693	0.0 ± 2.3	3
-1025	2455594.15188	-1.6 ± 3.3	6
-1016	2455601.25164	-1.3 ± 2.5	6
-1014	2455602.83138	1.7 ± 2.4	3
-1011	2455605.19414	-3.8 ± 3.5	6
-1009	2455606.77464	0.3 ± 2.3	3
-1008	2455607.56241	-1.2 ± 2.4	3
-989	2455622.55057	-0.9 ± 2.3	3
-987	2455624.12787	-1.5 ± 3.1	6
-976	2455632.80612	0.0 ± 2.3	3
-947	2455655.68222	-0.3 ± 2.4	3
-928	2455670.66976	-0.9 ± 2.5	3
-923	2455674.61367	-1.3 ± 2.4	This work
-919	2455677.77038	0.7 ± 3.6	6
-905	2455688.81201	-2.4 ± 5.3	6
-904	2455689.60276	0.4 ± 2.4	6
-900	2455692.75674	-1.6 ± 4.3	6
-899	2455693.54639	-0.5 ± 2.3	6
-886	2455703.79933	-3.3 ± 6.4	6
-885	2455704.59078	0.5 ± 2.4	6
-880	2455708.534626	0.0 ± 2.3	6
-654	2455886.81234	0.2 ± 3.8	6
-642	2455896.27611	-3.1 ± 3.8	6
-618	2455915.20980	-0.9 ± 2.5	6
-613	2455919.15485	0.4 ± 2.7	6

Table 3.7 – *Continued from previous page*

Epoch	Transit mid-time (BJD _{TDB})	TTV (min)	References
-611	2455920.7353	0.0 ± 5.4	This work
-609	2455922.30966	-0.4 ± 8.3	6
-511	2455999.6163	0.2 ± 2.3	7
-483	2456021.70374	0.1 ± 2.3	7
-473	2456029.5925	0.7 ± 2.4	3
-468	2456033.53643	0.3 ± 2.3	6
-430	2456063.51174	-0.5 ± 2.3	3
-86	2456334.87208	-0.8 ± 2.4	4
-47	2456365.6373	-0.1 ± 2.3	This work
1	2456403.50158	-0.1 ± 2.3	This work
729	2456977.77722	1.3 ± 2.3	8
867	2457086.63571	-0.5 ± 2.3	This work
1383	2457493.67676	-0.2 ± 2.3	This work
1771	2457799.74612	-0.3 ± 2.3	This work
1838	2457852.597807	-0.7 ± 2.3	This work
2064	2458030.8751	-1.5 ± 3.2	This work

References: (1) Hebb et al. (2010); (2) Anderson et al. (2010); (3) Lendl et al. (2013); (4) Exoplanet Transit Database (ETD) `var2.astro.cz/ETD`; (5) Tregloan-Reed et al. (2013); (6) Mancini et al. (2013); (7) Bean et al. (2013); (8) Sedaghati et al. (2015).

3.4.2.3 WASP-77Ab

As in the previous targets, we computed a refined linear ephemeris equation for WASP-77A considering 11 transit times:

$$T_C(E) = 2457420.88439 \pm (85) + E \cdot 1.36002854 \pm (52) \quad (3.4)$$

In Table 3.5 are listed the TTV values of our transit times and from previous works (Turner et al., 2016; Maxted et al., 2013a) of WASP-77Ab and, at the bottom of Figure 3.4 are plotted versus epoch. The scatter of all the transit times is about $RMS = 121$ seconds.

The epochs 175 and 229 are above 2σ from the expected transit time following the linear ephemeris, while all the others epochs lie within 1.5σ from it. When removing the epochs 175 and 229, the RMS decreases to 88 seconds.

Considering all the transit times, the linear fit has $\chi^2_{red} = 1.4$, and the second degree polynomial has $\chi^2_{red} = 1.39$. However, we chose the linear fit as it suppose a simpler model.

Table 3.8: Transit mid-times for WASP-77Ab

Epoch	Transit mid-time (BJD _{TDB})	TTV (min)	References
-1140	2455870.45054	-2.0 ± 1.5	1
-845	2456271.65888	-2.0 ± 1.4	2
-659	2456524.62617	0.8 ± 1.8	This work ^a
-606	2456596.70591	-1.7 ± 1.5	This work ^a
-92	2457295.7626	1.2 ± 1.3	This work
-89	2457299.84119	-1.0 ± 1.3	This work
175	2457658.88744	-2.8 ± 1.5	This work
177	2457661.60987	0.6 ± 1.7	This work ^a
183	2457669.77054	1.4 ± 1.4	This work
229	2457732.33382	4.2 ± 1.4	This work ^a
447	2458028.8159	-1.8 ± 6.5	This work

References: (1) Maxted et al. (2013a); (2) Turner et al. (2016).

^a From the Exoplanet Transit Database (ETD) `var2.astro.cz/ETD`

3.4.3 Limits on an Additional Perturber

The results from our mid-transit time study in Section 3.4.2, allow us to infer an upper mass limit for an additional planet in each system. A perturbing planet will introduce a change in the mid-transit times of a known planet, which can be quantified by the RMS scatter around the nominal (unperturbed) linear ephemeris. The TTV effect is amplified for orbital configurations involving mean-motion resonances (Agol et al., 2005; Holman and Murray, 2005; Nesvorný and Morbidelli, 2008b). In principle, this amplification would allow the detection of a low-mass planetary perturbing body. A larger perturbation implies a larger RMS scatter around the nominal ephemeris.

The applied method follows the technique described in Wang et al. (2018b, 2017b, 2018c). The calculation of an upper mass limit is performed numerically via direct orbit integrations. For this task, we have modified the FORTRAN-based **MICROFARM**³ package (Goździewski, 2003; Goździewski et al., 2008) which utilizes OpenMPI⁴ to spawn hundreds of single-task parallel jobs on a suitable super-computing facility. The package’s main purpose is the numerical computation of the Mean Exponential Growth factor of Nearby Orbits (Cincotta and Simó, 2000; Goździewski et al., 2001; Cincotta et al., 2003, MEGNO) over a grid of initial values of orbital parameters for an n -body problem. The calculation of the RMS scatter of TTVs in the present work follows a direct brute-force method, which proved to be robust given the availability of computing power.

Within the framework of the three-body problem, we integrated the orbits of one of our three hot Jupiters and an additional perturbing planet around their host stars. The mid-

³<https://bitbucket.org/chdianthus/microfarm/src>

⁴<https://www.open-mpi.org>

transit time was calculated iteratively to a high precision from a series of back-and-forth integrations once a transit of the transiting planet was detected. The best-fit radii of both the planet and the host star were accounted for. We then calculated an analytic least-squares regression to the time-series of transit numbers and mid-transit times to determine a best-fitting linear ephemeris with an associated RMS statistic for the TTVs. The RMS statistic was based on a 20-year integration corresponding to 7763 transits for WASP-18b, 9270 transits for WASP-19b, and 5371 transit events for WASP-77Ab. This procedure was then applied to a grid of masses and semi-major axes of the perturbing planet while fixing all the other orbital parameters. In this study, we have chosen to start the perturbing planet on a circular orbit that is co-planar with the transiting planet; this implies that $\Omega_2 = 0^\circ$ and $\omega_2 = 0^\circ$ for the perturbing and $\Omega_1 = 0^\circ$ for the transiting planet. This setting provides a most conservative estimate of the upper mass limit of a possible perturber (Bean, 2009; Fukui et al., 2011; Hoyer et al., 2011, 2012). For the interested readers, we refer to Wang et al. (2018c), which has studied the effects of TTVs on varying initial orbital parameters.

Table 3.9: Approximate upper mass limits of a putative perturber in various orbital resonances for each system

MMR (P_2/P_1)	WASP-18 [M_\oplus]	WASP-19 [M_\oplus]	WASP-77A [M_\oplus]
1:3	1.9	500 ^b	1.0
2:5	4.0	-	-
1:2	5.0 ^a	2.0	3.5
3:5	-	-	2.0
2:3	-	-	7.0 ^a
5:3	-	6.0	6.0
7:4	-	-	10.0
2:1	25 ^a	0.9	3.5
7:3	80.0 ^c	-	-
5:2	10.0	3.0	-
3:1	7.0	2.0	4.5
17:5	500.0 ^d	-	-
4:1	50.0	100.0 ^e	60.0 ^f

^a Very close to the general instability area.

^b Constraint by RV limit of 17.8 [M_\oplus]

^c Constraint by RV limit of 74.6 [M_\oplus]

^d Constraint by RV limit of 82.8 [M_\oplus]

^e Constraint by RV limit of 40.8 [M_\oplus]

^f Constraint by RV limit of 30.8 [M_\oplus]

In order to calculate the location of mean-motion resonances, we have used the same code to calculate MEGNO on the same parameter grid. However, this time we integrated each initial grid point for 1000 years, allowing this study to highlight the location of weak chaotic high-order mean-motion resonances. In short, MEGNO quantitatively measures the degree of stochastic behaviour of a non-linear dynamical system and has been proven useful in the detection of chaotic resonances (Goździewski et al., 2001; Hinse et al., 2010). In addition

to the Newtonian equations of motion, the associated variational equations of motion are solved simultaneously allowing the calculation of MEGNO at each integration time step. The MICROFARM package implements the ODEX⁵ extrapolation algorithm to numerically solve the system of first-order differential equations.

Following the definition of MEGNO (Cincotta and Simó, 2000) (denoted as $\langle Y \rangle$ in Figures 3.5-3.7), in a dynamical system that evolves quasi-periodically, the quantity $\langle Y \rangle$ will asymptotically approach 2.0 for $t \rightarrow \infty$. In that case, often the orbital elements associated with that orbit are bounded. In case of a chaotic time evolution, the $\langle Y \rangle$ diverges away from 2.0 with orbital parameters exhibiting erratic temporal excursions. For quasi-periodic orbits, we typically have $|\langle Y \rangle - 2.0| < 0.001$ at the end of each integration.

Importantly, MEGNO is unable to prove that a dynamical system is evolving quasi-periodically, meaning that a given system cannot be proven to be stable or bounded for all times. The integration of the equations of motion only considers a limited time period. However, once a given initial condition has found to be chaotic, there is no doubt about its erratic nature in the future.

In the following, we will present the results of each system for which we have calculated the RMS scatter of TTVs on a grid of the masses and semi-major axes of a perturbing planet in a circular, co-planar orbit. Results are shown in Figures 3.5 - 3.7 and Table 3.9. In each of the three cases, we find the usual instability region located in the proximity of the transiting planet with MEGNO color-coded as yellow (corresponding to $\langle Y \rangle > 5$). The extent of these regions coincides with the results presented in Barnes and Greenberg (2006). The locations of mean-motion resonances are indicated by arrows in each map.

3.4.3.1 WASP-18b

For the WASP-18b system we find a large region of instability when compared to the other two systems with the boundaries at the 1:2 interior and 2:1 exterior mean-motion resonance. By over-plotting the RMS scatter of mid-transit times (TTV_{RMS}) for a certain value, we find that the TTVs are relatively more sensitive at orbital architectures involving mean-motion resonances confirming the results by Agol et al. (2005) and Holman and Murray (2005). This also applies to WASP-19 and WASP-77A.

As shown in Figure 3.5, we find that a perturbing body of mass (upper limit) around $7 - 500 M_\oplus$ will produce an RMS of 83 s when located in the $P_2/P_1 = 7:3, 5:2, 3:1, 17:5$ and 4:1 exterior resonance. For the 1:3 interior resonance, a perturber mass (upper limit) as small as $1.9 M_\oplus$ could also cause a RMS mid-transit time scatter of 83 s.

⁵<https://www.unige.ch/~hairer/prog/nonstiff/odex.f>

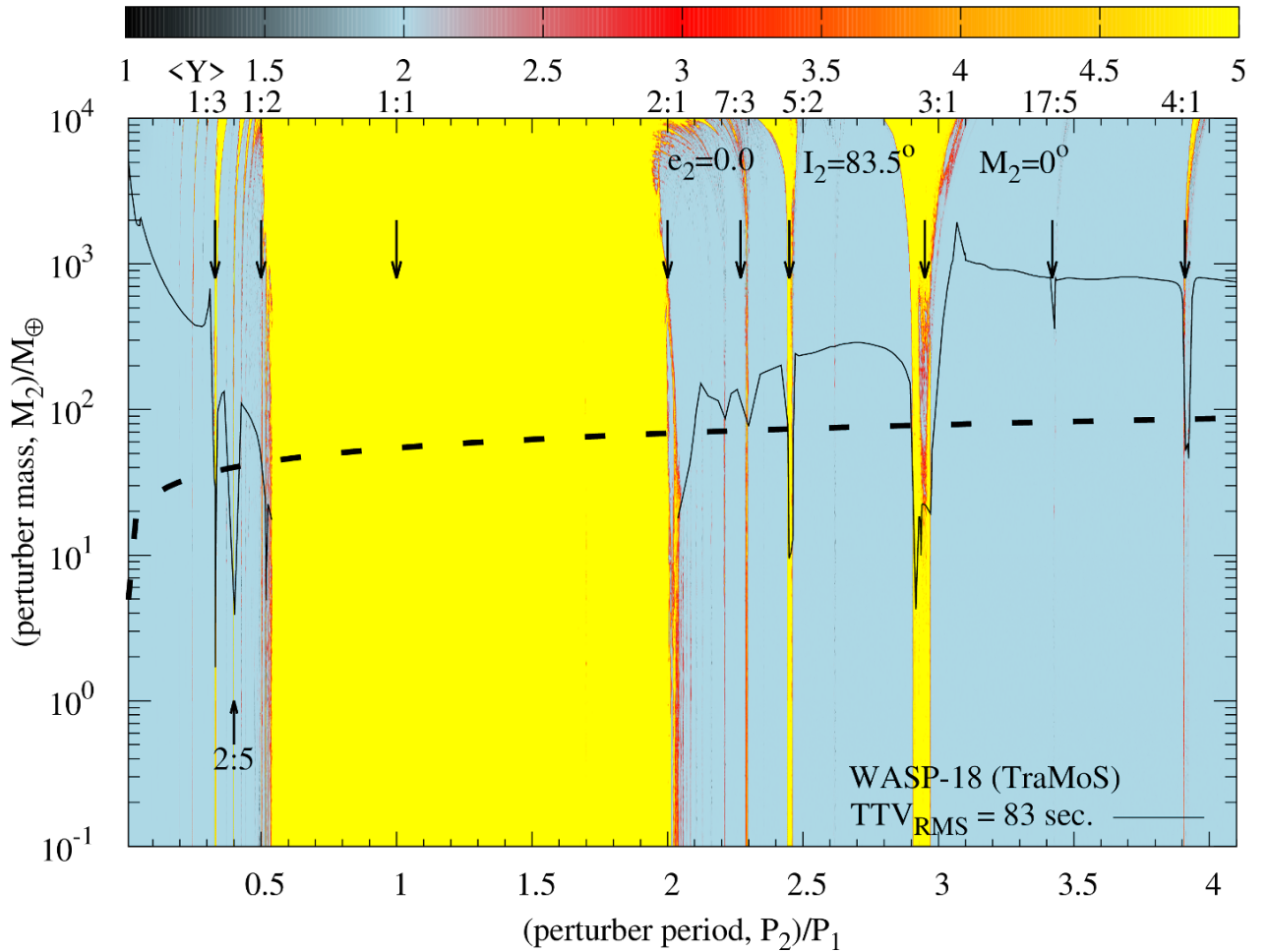


Figure 3.5: MEGNO ($\langle Y \rangle$) stability map for the WASP-18 system. We over-plot the map with an upper mass of a hypothetical perturbing planet introducing a mid-transit time TTV_{RMS} scatter of 83 s (solid line) as obtained in this study. The stipulated line is the upper mass limit as obtained from the RMS scatter (30.9 m/s) of the radial-velocity curve. For initial conditions resulting in a quasi-periodic (i.e bounded) motion of the system, the $\langle Y \rangle$ value is close to 2.0 (color coded blue). For chaotic (i.e unstable) motion, the $\langle Y \rangle$ is diverging away from 2.0 (color coded red to yellow). Vertical arrows indicate (P_2/P_1) orbital resonances between the perturbing body and the transiting planet. The two planets were assumed to be co-planar, and the perturbing planet's eccentricity was initially set to zero. *See electronic version for colors.*

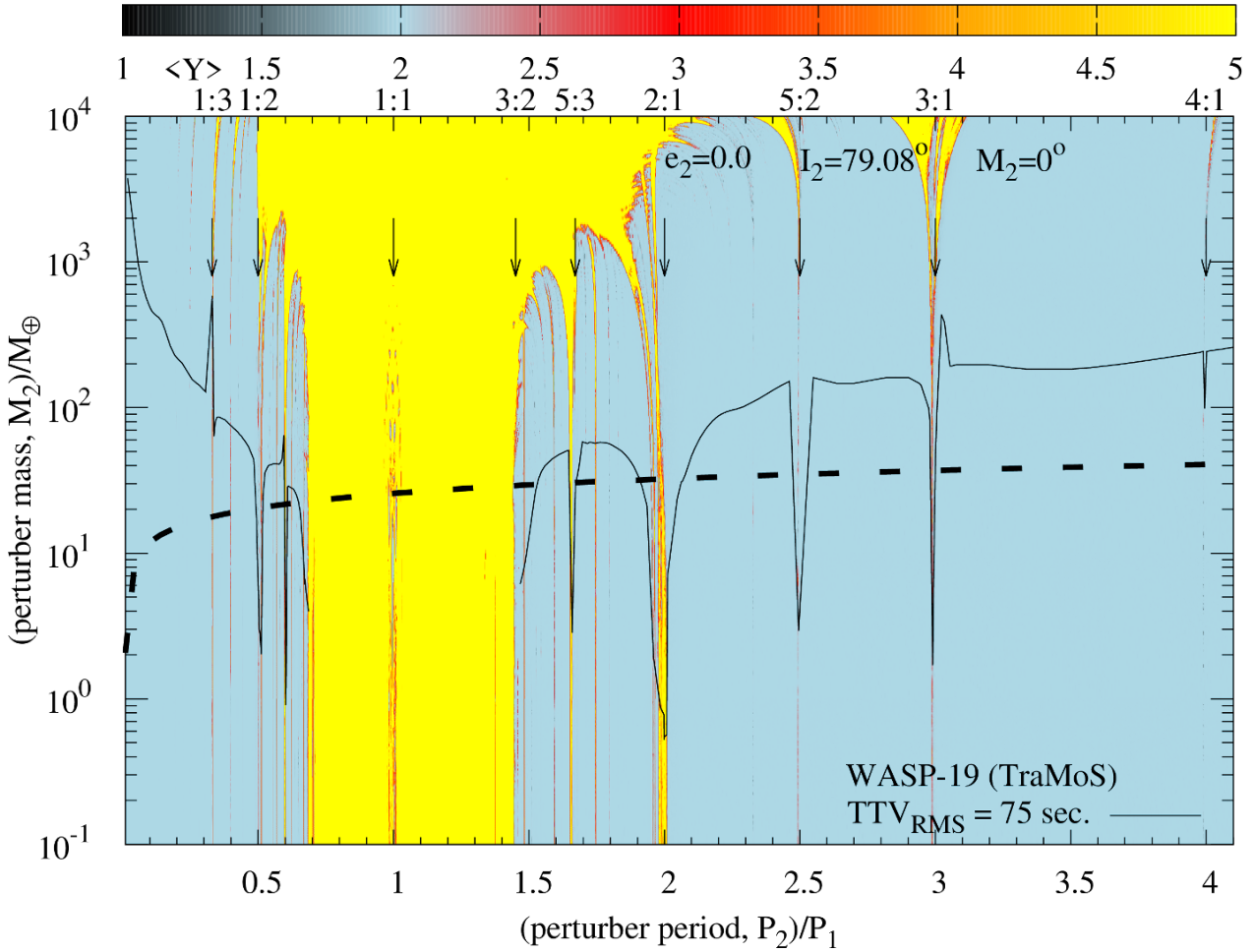


Figure 3.6: Same as Fig. 3.5, but this time for WASP-19 with an TTV_{RMS} of 75 s. The RMS for the radial-velocity measurements was (18.2 m/s). *See electronic version for colors.*

3.4.3.2 WASP-19b

For the WASP-19b system the measured transit-timing RMS scatter was $\text{TTV}_{\text{RMS}} = 75$, s. Additional bodies with a mass of $500 M_{\oplus}$ and as low as $2.0 M_{\oplus}$ and $0.9 M_{\oplus}$ at the 1:3, 1:2 (interior) and 2:1 (exterior) mean-motion resonances could cause the observed RMS scatter. Hypothetical planets of $6 M_{\oplus}$, $3 M_{\oplus}$ and $2 M_{\oplus}$ could cause the observed RMS scatter at the 5:3, 5:2 and 3:1 exterior mean-motion resonances, respectively. We refer to Fig. 3.6.

3.4.3.3 WASP-77Ab

For the WASP-77Ab system the results are somewhat similar to WASP-19b. We refer to Fig. 3.7. The measured RMS of mid-transit timing variations around the linear ephemeris was $\text{TTV}_{\text{RMS}} = 121$ s. For interior mean-motion resonances the 1:2 and 2:3 commensurabilities could cause the observed TTV_{RMS} by an additional planet of mass around $3.5 M_{\oplus}$ and $7 M_{\oplus}$. However, the 2:3 resonance is very close to the general instability area rendering the orbit likely to be unstable. Further a $1 M_{\oplus}$ mass planet at the 1:3 interior resonance could also cause

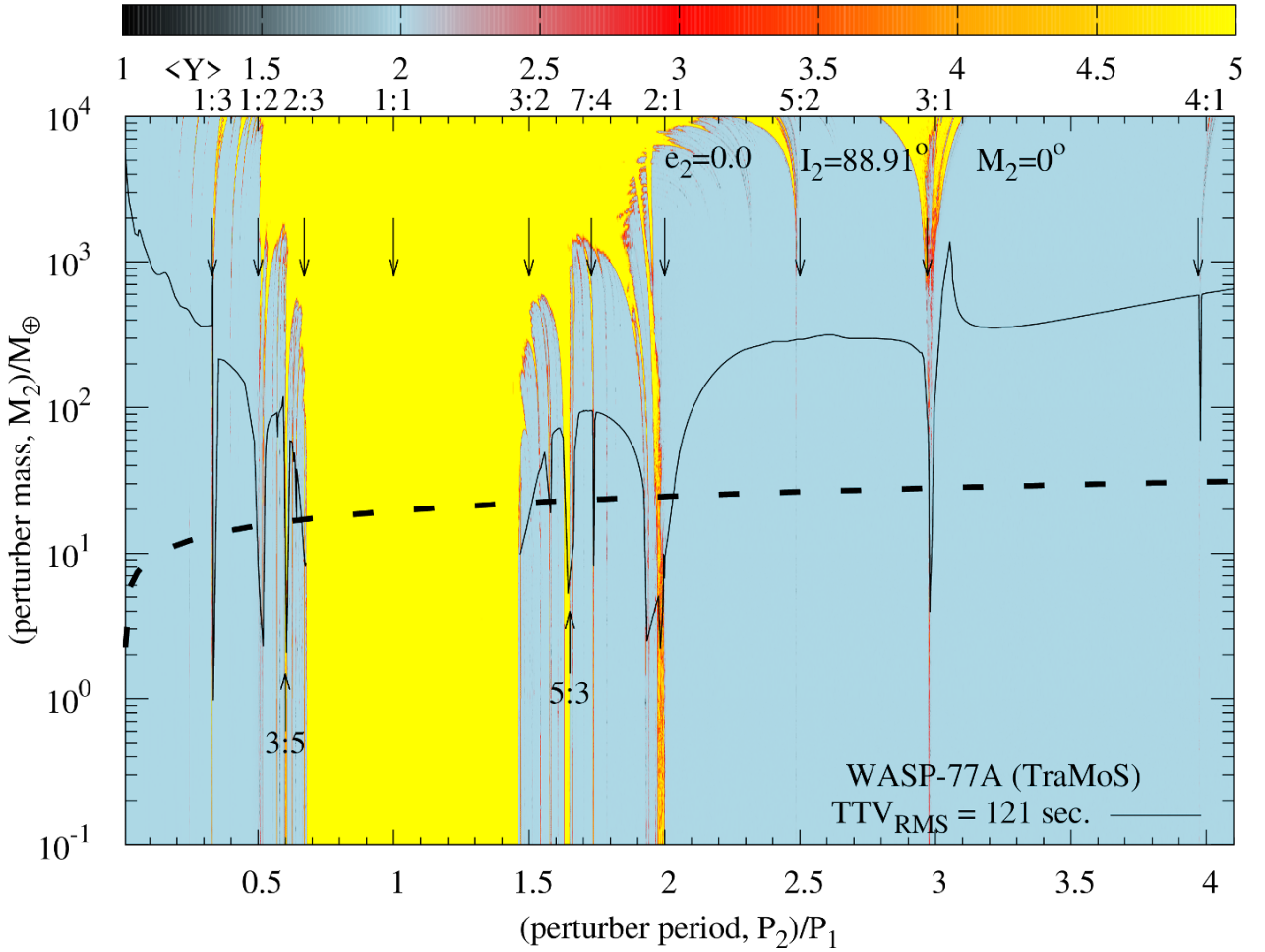


Figure 3.7: Same as Fig. 3.5, but this time for WASP-77 with an TTV_{RMS} of 121 s. The RMS for the radial-velocity measurements was (12.0 m/s). *See electronic version for colors.*

a TTV_{RMS} of 121 s. A $2 M_{\oplus}$ mass planet located at the 3:5 resonance, although relatively close to the inner edge of the general instability region, could also explain the observed timing variation. For exterior mean-motion resonances of 2:1, 3:1 and 4:1 an additional planet of mass $3.5 M_{\oplus}$, $4.5 M_{\oplus}$ and $60 M_{\oplus}$, could cause a $\text{TTV}_{\text{RMS}} = 121$ s, respectively. A subtle difference from the WASP-19b system is found at the 5:2 resonance, which does not exhibit any significant decrease in upper mass planet detection sensitivity.

3.4.4 TTV period search

We have carried out a Lomb-Scargle period analysis (Lomb, 1976; Scargle, 1982) for each system's TTVs residuals to search for a significant periodic trend. For this we applied the `LombScargle`⁶ (LS) algorithm available within the `Astropy` (v3.1.1) Python package (VanderPlas et al., 2012; VanderPlas and Ivezić, 2015).

The algorithm is suitable for unevenly-sampled data. We chose to carry out computations

⁶<http://docs.astropy.org/en/stable/stats/lombscargle.html>

using the observed transit epochs for each system as the independent variable. Each epoch is determined with a high degree of confidence. TTV measurement uncertainties were not accounted for since no convincing periodic trend were detected. Default settings were avoided in order to safeguard the analysis from an inappropriate frequency grid choice. We made use of the minimum and maximum frequency heuristic. Periods between 1 and 5000 epochs were searched for. Furthermore, we sampled each peak twelve times. Noteworthy to mention, and often overlooked, is the possible detection of frequencies much larger than the Nyquist sampling frequency (VanderPlas, 2018).

The result for each system is shown in Figs. 3.8 to 3.10, where we show the Lomb-Scargle power P from the standard normalization method with $0 \leq P < 1$. The final period is found by multiplying with the final best-fit period for each system. To quantify the significance of period-peaks we calculated the false-alarm probability (FAP) for three different p -values. The FAP encodes the probability of detecting a peak of a given height (or higher) and is conditioned on the null-hypothesis that the data is characterized by normal random noise.

To avoid misinterpretation of the FAP we have calculated synthetic random TTVs for each system in a single realization. For each known epoch, we drew a normal random point with mean zero and standard deviation in accordance with the measured RMS for each timing data set (83 s for WASP-18, 75 s for WASP-19 and 121 s for WASP-77A).

We then recomputed the LS periodogram for each synthetic data set. This method enables a meaningful quantitative assessment of a minimum requirement of the FAP to detect a true periodic signal which clearly stands out from Gaussian noise. We plot the LS periodograms for the synthetic TTVs in the bottom panels of Figs. 3.8 to 3.10. For the case of WASP-19 and WASP-77, we found that a reasonable minimum FAP of 0.01% is required in order to distinguish any signal from white noise. For the case of WASP-18 the threshold is just above 0.01%. In generally, we found no significant (99.99% level) periodicity peaks for all three cases.

3.5 Summary and Conclusions

We performed photometric follow-ups of the transiting exoplanets WASP-18b, WASP-19b and WASP-77Ab with one meter-class telescopes within the TraMoS project. Our 22 new high-precision light curves and archive data were combined together to refine physical and orbital parameters of the systems.

For WASP-18b we find a larger value for the fraction of the radius R_p/R_* than the most recent work with TESS data Shporer et al. (2018), and a larger total transit duration T_{14} comparing with Hellier et al. (2009). The rest of stellar and planetary parameters are all in good agreement with previous results.

In the analysis of WASP-19b, our results are in general, in good agreement with previous works (Hebb et al., 2010; Lendl et al., 2013). Only the inclination i and the total duration of the transit T_{14} show important differences.

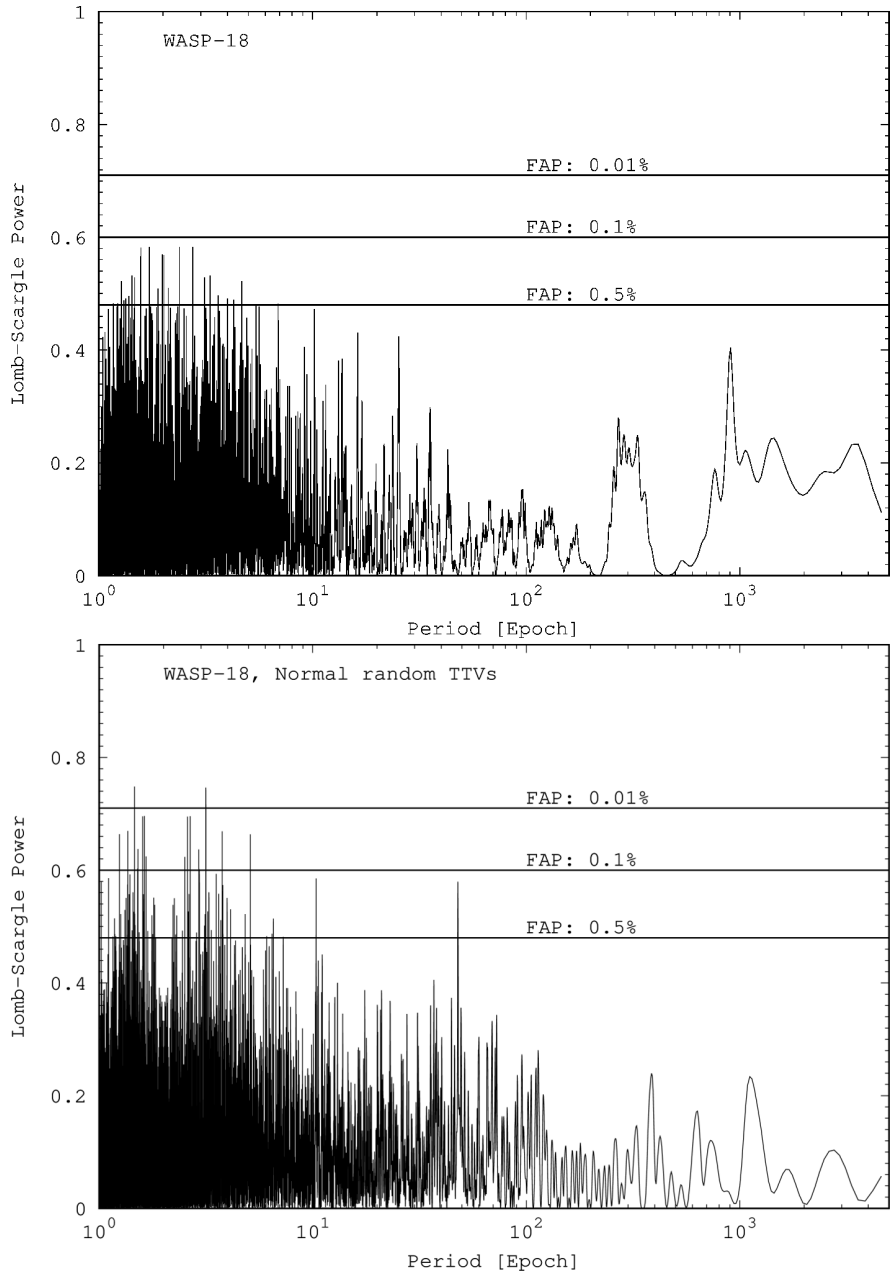


Figure 3.8: Lomb-Scargle (standard normalized) power vs period for observed TTV residuals of WASP-18 (*top panel*) and for a simulated set of TTVs randomly drawn from a normal distribution with mean zero and standard deviation of 1.38 minutes (*lower panel*). See text for more details.

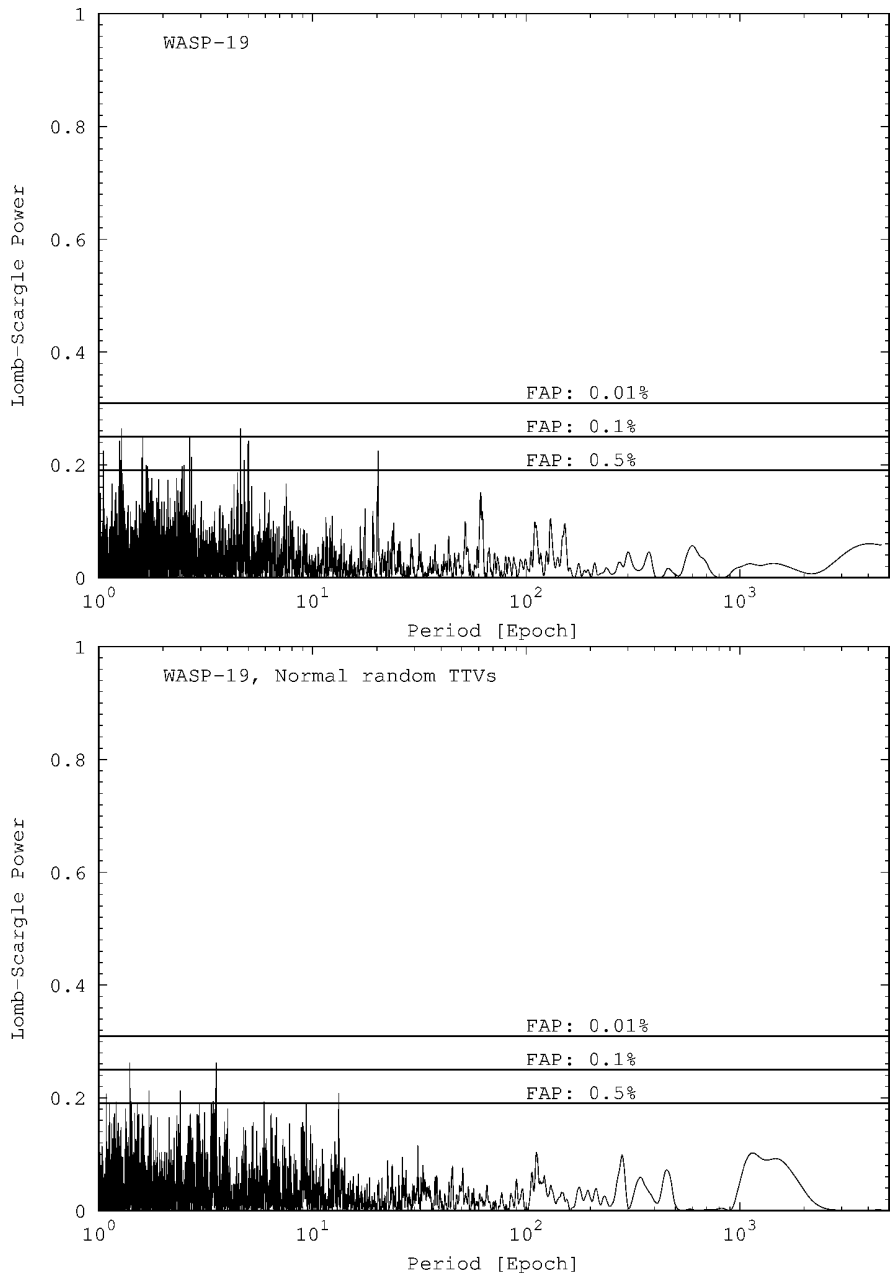


Figure 3.9: Lomb-Scargle (standard normalized) power vs period for observed TTV residuals of WASP-19 (*top panel*) and for a simulated set of TTVs randomly drawn from a normal distribution with mean zero and standard deviation of 1.33 minutes (*lower panel*). See text for more details.

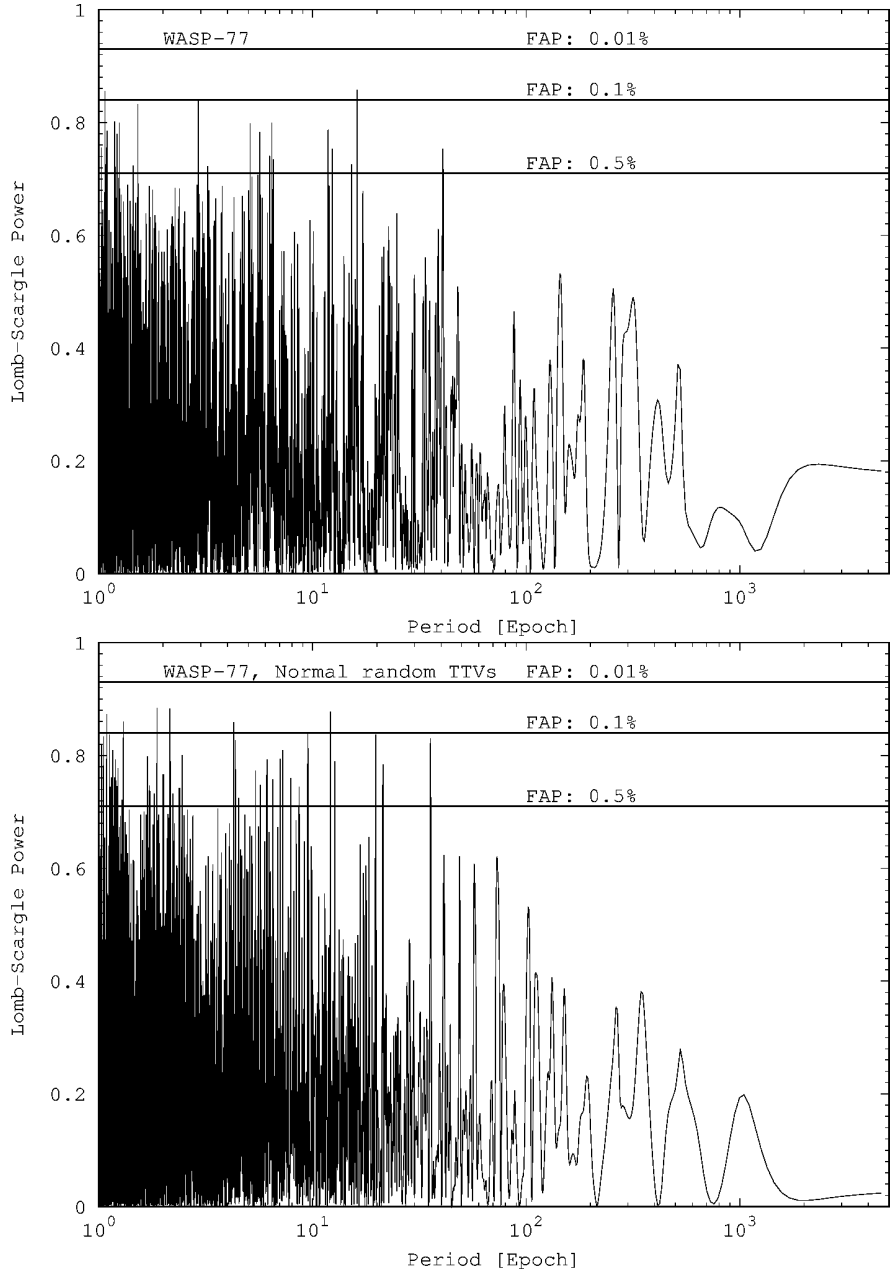


Figure 3.10: Lomb-Scargle (standard normalized) power vs period for observed TTV residuals of WASP-77 (*top panel*) and for a simulated set of TTVs randomly drawn from a normal distribution with mean zero and standard deviation of 2.02 minutes (*lower panel*). See text for more details.

In this work we reported the first bulk measurements of the WASP-77Ab system. We find almost no disagreement in the orbital and physical parameters with the discovery paper Maxted et al. (2013a).

We included archival transit times along with the transits from the TraMoS project to obtain refined values for the period P of the three exoplanets, as well as updated linear ephemeris. We report a period of $P = 0.94145223 \pm 9 \times 10^{-8}$ days for WASP-18b, $P = 0.788838852 \pm 5 \times 10^{-9}$ days for WASP-19b, and $P = 1.3600285 \pm 5 \times 10^{-7}$ days for WASP-77Ab. With the proposed linear ephemeris we found TTV_{RMS} of 83 seconds, 75 seconds, and 121 seconds, for WASP-18b, WASP-19b, and WASP-77Ab, respectively. Also, we find a lack of significant TTV periodic signals.

The TTV_{RMS} could be produced by a perturber body bounded gravitationally with our targets. Thus, we performed orbit integrations in order to find upper mass limits for possible companions. We find that, for WASP-18b, the observed RMS could be produced by a perturber with an upper limit mass of $7 - 80 M_{\oplus}$ in 3:1, 4:1, 5:2, and 7:3 exterior resonances. For the interior resonances 1:3 and 2:5, a body with a limit mass of $1.9 M_{\oplus}$ and $4 M_{\oplus}$, respectively, could produce the observed TTV_{RMS}.

In the case WASP-19b, companions with masses of 0.9, 3, 6 and $2 M_{\oplus}$, in 2:1, 5:2, 5:3 and 3:1 exterior resonances, could reproduce the 75 seconds of scatter. For WASP-77Ab a planet with masses 3.5, 1, 3.5, 4.5, 2, and $10 M_{\oplus}$ in resonances 1:2, 1:3, 2:1, 3:1, 3:5, and 7:4 could produce the observed RMS in the TTVs.

The hypothetical perturbers with the greatest masses for the three targets are discarded, as they are constrained by RV variations. These cases are: a body up to $500 M_{\oplus}$ in 17:5 resonance for WASP-18b, $500 M_{\oplus}$ and $100 M_{\oplus}$ in 1:3 and 3:1 resonances for WASP-19b, and $60 M_{\oplus}$ in 4:1 resonances for WASP-77Ab.

We found no significant periodicity in any of the systems by performing a Lomb-Scargle period analysis.

The absence of a significant TTV signal in WASP-18b and the poor quality of a second order fit, support the conclusion that there is no evidence for a rapid orbital decay, as proposed by Wilkins et al. (2017). As the TTV technique is sensitive to detect tidal decays on the exoplanets orbits, we could detect any trending in the TTV data, which is not the case. Moreover, theoretical studies (Collier Cameron and Jardine, 2018) suggest a time span of around 20 years to observe a variation of 4 seconds in this system. Our result supports that prediction.

Previous photometric studies of WASP-19b (Lendl et al., 2013; Wong et al., 2016) also suggest the lack of TTV on this system. Our results include more transit times, 59 versus 56 in Wong et al. (2016) and 14 in Lendl et al. (2013), and also more recent transits being the last one from the end of 2017. Finding a no periodic TTV signal is consistent with their results.

This is the first detailed study of WASP-77Ab. Our results will serve as base for future photometric and dynamic studies where an extensive follow-up should be performed. WASP-

77Ab shows the larger deviation for the linear ephemeris of our targets, with more than 2 minutes. Furthermore, the linear fit on the TTV is not fully representing the data as $\chi^2_{red} = 1.4$, and a second degree fit shows almost the same value of χ^2_{red} . More consecutive transit times are needed in order to understand the truly nature of this planet and its possible companions.

Chapter 4

TraMoS in the TESS era

With the end of the Kepler mission, thousands of possible exoplanets remain as candidates known as Kepler Objects of Interest (KOI). The Kepler Object of Interest Network (KOINet: (von Essen et al., 2018; Freudenthal et al., 2018)) in the Northern hemisphere, is a network of ground-based telescopes performing a photometric follow-up of KOIs to continue what Kepler left undone. The main goal of KOINet is to combine Kepler data with ground-based observations to confirm and characterize the masses of exoplanet candidates using TTVs.

TTV studies must continue the work of space missions from the ground. Ground-based photometric follow-up observations are important and contribute with significant scientific measurements and complement space-based observations to detect astrophysical interesting signals like TTVs. In Figure 4.1, new data from ground-based telescopes were fundamental to confirm the TTV signal, and therefore to perform a proper characterization of the system.

The new space telescope Transiting Exoplanet Survey Satellite (TESS: Ricker (2014)) is delivering its first discoveries. The TESS observation plan divided into 13 sectors will challenge the confirmation process and characterization of possible exoplanets. During the ~ 27 days of each sector, many candidates will not be observed for a long enough time to confirm and characterize them. However, this special feature will provide a huge amount of new transit events of already known transiting exoplanets, especially for those with short-period. Combining the new TESS data with ground-based follow- up observations, many possible TTVs could be confirmed or ruled out. Moreover, Ballard (2018) predicted that around 5% of the planets discovered by TESS will exhibit measurable TTV signals, similar to Kepler's results.

Between Sector 1 and Sector 13 – sectors dedicated to the southern hemisphere – TESS observed around 15% (see Figure 4.2) of the stars with confirmed exoplanets but not all of them will produce a transit event within the 27 days sector's duration (see Figure 4). Anyway, several complete light curves could be obtained and analyzed. TESS data are reduced by the Science Processing Operations Center (SPOC: Jenkins et al. (2016)) and after being processed, they are archived in the Mikulski Archive for Space Telescopes (MAST¹) catalog, where can be downloaded directly by anyone.

¹<http://archive.stsci.edu/>

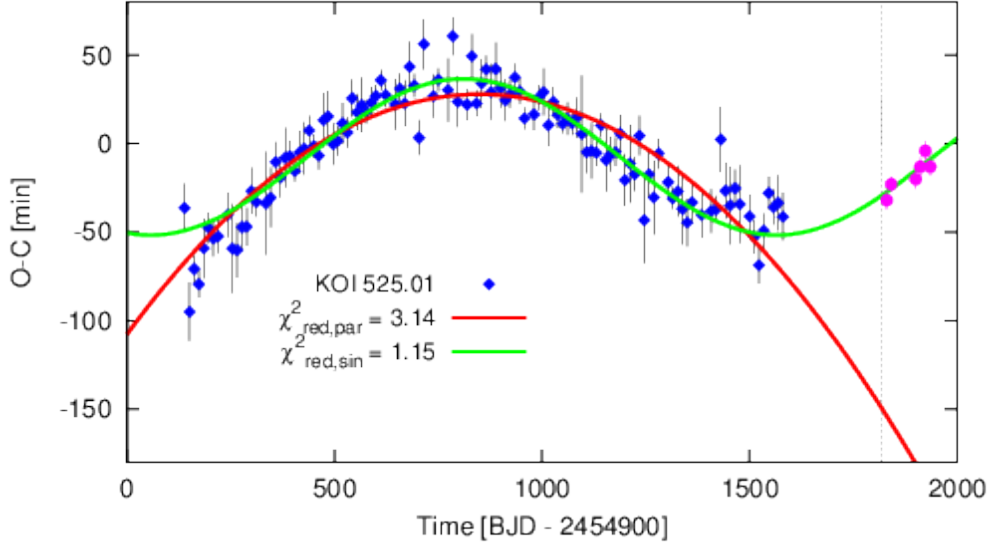


Figure 4.1: Observed minus calculated (O-C) diagram of the KOI-525b transit times, from the KOINet project. The observations from Kepler are in blue, and two different models were fitted on those data: an orbital decay model is in red, and a periodical TTV model is in green. If only Kepler data is considered, the two models could be plausible. The new ground-based observations (in pink) were essential to confirm the TTV nature of the system, discarding an orbital decay

Thus, for the current and future stage of the TraMoS project, archival data – collected since 2008 – will be combined with the upcoming TESS data and new ground-based observations using one-meter class telescopes. The main goal of the project remains the same: refine orbital and physical parameters of the exoplanetary system and search for variations in those parameters, that could suggest the presence of additional small bodies in the system. The KOINet project proved that ground-based follow-up is, in some cases, essential to complete a possible TTV signal, and therefore, to confirm or rule out variations in the transit time. During its first year of the mission, TESS will supply with consecutive transit light curves from southern targets, especially from short-period planets, such as hot Jupiters. This special feature is fundamental to construct TTV curves and then, complete them from ground-based follow-up.

In the following subsections, I present a re-analysis of the TTV curves of the hot Jupiters: WASP-18b, WASP-19b, and WASP-77Ab including new transit times from TESS: 45, 28, and 15 for WASP-18b, WASP-19b and WASP-77Ab respectively. To compute the transit time of each light curve, I used EXOFASTv2² (Eastman et al., 2013) to only fit the transit time and the flux’s baseline. The remaining planetary parameters were fixed with the values from Tables 3.3, 3.4, 3.5.

²<https://github.com/jdeast/EXOFASTv2>

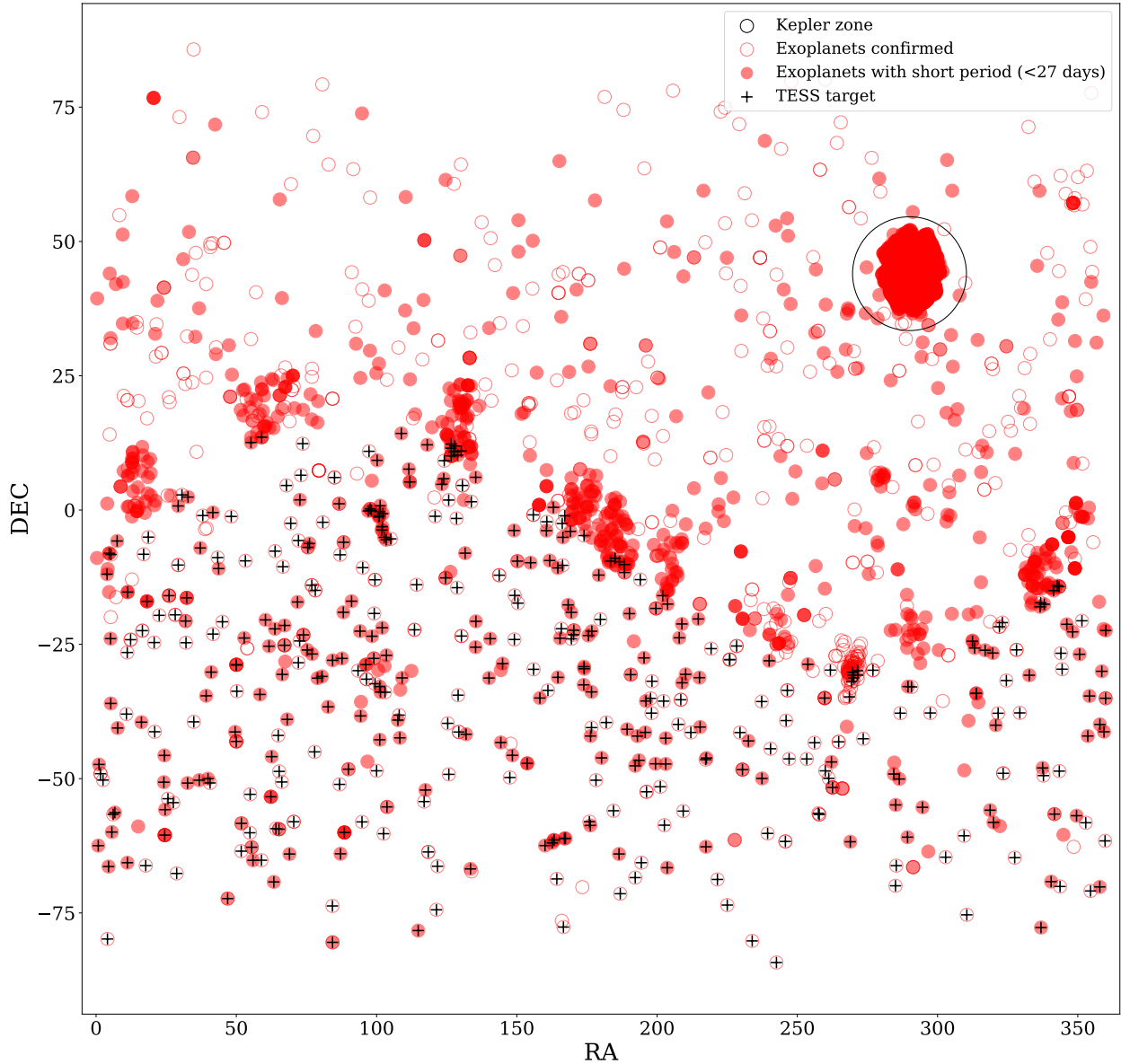


Figure 4.2: Match between all the stars with confirmed exoplanets and the TESS targets from Sector 1 to Sector 13. The empty red circles correspond to the star with confirmed exoplanets distributed by its position in the sky, while the filled red circles indicate if the exoplanet has an orbital period of fewer than 27 days, which is the duration of one TESS sector. The black cross indicates which star was already observed by TESS. However, this does not indicate that transit light curves will be provided for sure since the orbital period of the exoplanet needs to be considered. Thus, the first-year mission of TESS will provide for sure transit data of the exoplanets with a filled red circle and a black cross. The zone in the sky within the big black circle corresponds to the Kepler field of view, where the bulk of discovered exoplanets are located.

4.1 WASP-18b

The star WASP-18 was observed continuously during Sector 2 and 3 of the TESS mission, between August 22nd and October 18th, 2018. These observations provided 47 transits events of WASP-18b, but only 45 of them were complete transits, and therefore included in the TTV analysis.

The new linear ephemeris equation considering a total of 63 transit mid-times is:

$$T_C(E) = 2456926.27460 \pm (94) + E \cdot 0.941452232 \pm (27) \quad (4.1)$$

The best fit for the period $P = 0.941452232 \pm 2.7 \times 10^{-8}$ days differs from the previously reported in Eq. 3.2 by 0.016 seconds, and the error was reduced to a third.

Figure 4.3 shows the extension of the TTV curve of WASP-18b considering the new data from TESS. Including these new transit times, the scatter from the linear ephemeris was reduced to 47 seconds. A possible second-order fit of a hypothetical orbital decay has a reduced chi-squared of $\chi^2_{red,quad} = 0.35$, while the linear fit - which corresponds to the linear ephemeris - has $\chi^2_{red,lin} = 0.36$. Furthermore, as there is no strong evidence for orbital decay in this system as proposed by Wilkins et al. (2017), the simpler model should be chosen: the linear model.

Considering the lack of a clear sinusoidal TTV signal with even more transit time data, suggest that this exoplanet does not have a close-in companion in MMR. Moreover, the existence of a possible far-out companion is rejected by the lack of an additional signal in RV data. With this study, I can not discard the presence of any kind of companion of WASP-18b but if there is one, it should be small.

4.2 WASP-19b

WASP-19 was observed during Sector 9 between February 28th and March 26th, 2019. During this time, 29 complete transit event was provided and then considered to compute the new TTVs of WASP-19b shown in Figure 4.4. The new proposed linear ephemeris equation considering a total of 88 transit times is:

$$T_C(E) = 2456402.7128 \pm (16) + E \cdot 0.788838940 \pm (30) \quad (4.2)$$

The new best fit value for the period $P = 0.788838940 \pm 3.0 \times 10^{-8}$ days is 0.007 seconds larger than the previously reported value in Eq. 3.1.

As in the case of WASP-18b, the TTV scatter of WASP-19b was reduced when including new transit times data from TESS to: $TTV_{RMS} = 65$ seconds. Again, a second order fit is not better than the linear one: $\chi^2_{red,lin} = 0.65$ and $\chi^2_{red,quad} = 0.64$.

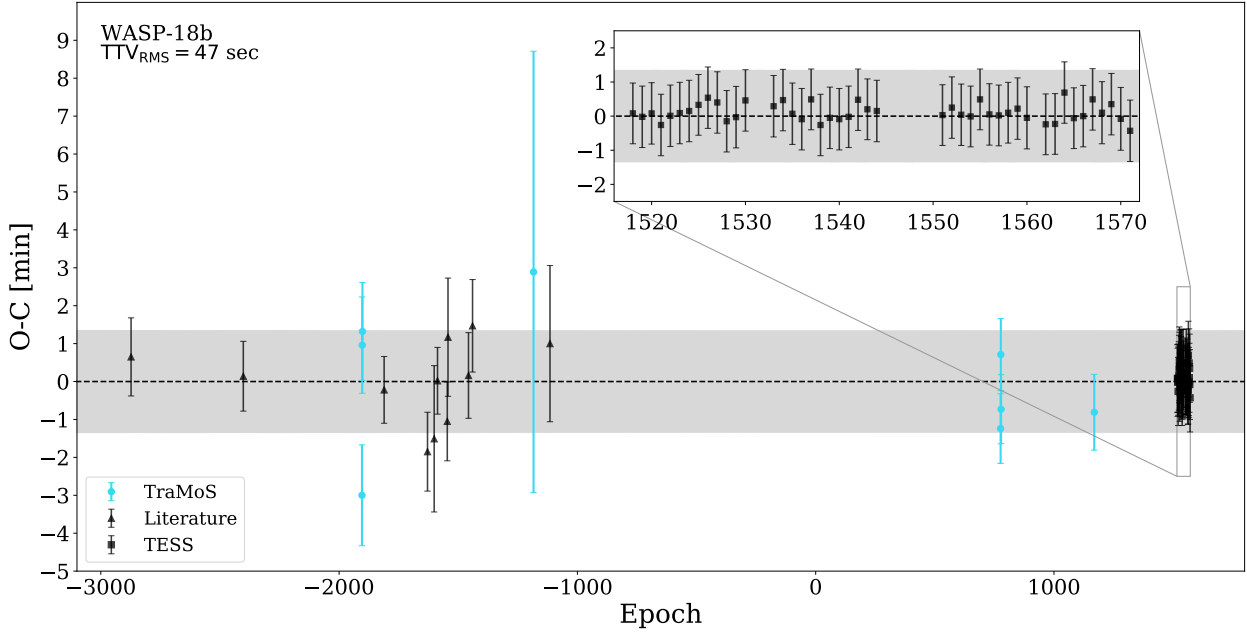


Figure 4.3: Observed minus calculated mid-transit times (TTV) for WASP-18b. The dashed black line corresponds to the proposed linear ephemeris, i.e. zero deviation from the predicted transit time computed from our refined orbital period. For that, we considered 63 transit times from the TraMoS project (in light blue), published works and TESS (both in black). The grey area corresponds to the error propagation at 1σ , which follows an imperceptible quadratic trend. The RMS scatter from the linear ephemeris is 47 seconds.

4.3 WASP-77Ab

The third target presented in Cortés-Zuleta et al. 2019 (submitted), was observed in Sector 4 between October 18th and November 15th, 2018. During this time, the planet transited its host star 17 times, but only 15 were complete light curves. From the previous study presented in this thesis, WASP-77Ab was the most interesting target, since its variation from the linear ephemeris was around 121 seconds. After including the new transit times, the new proposed linear ephemeris equation is:

$$T_C(E) = 2457420.88439 \pm (85) + E \cdot 1.36002866 \pm (17) \quad (4.3)$$

With a best fit period of $P = 1.36002866 \pm 1.7 \times 10^{-7}$ days. In Eq. 3.4, the value for the orbital period P is 0.01 seconds lower, and the scatter from the linear ephemeris was reduced to 86 seconds. The linear fit has a reduced chi-squared of $\chi^2_{red,lin} = 1.03$, while a second-degree polynomial has $\chi^2_{red,quad} = 0.72$. Anyway, the second-order fit is highly dominated by the outlier transit time of epoch 229 (see Figure 4.5). After removing it, the reduced chi-squared is $\chi^2_{red,quad} = 0.37$. In all cases, the best fit corresponds to the linear ephemeris.

Like the previous two targets, extending the TTV curve of WASP-77Ab with transit times from TESS light curve supported the conclusion from the previous study: there is not a clear sinusoidal signal in the variations of the transit times, that could suggest a periodic TTV in

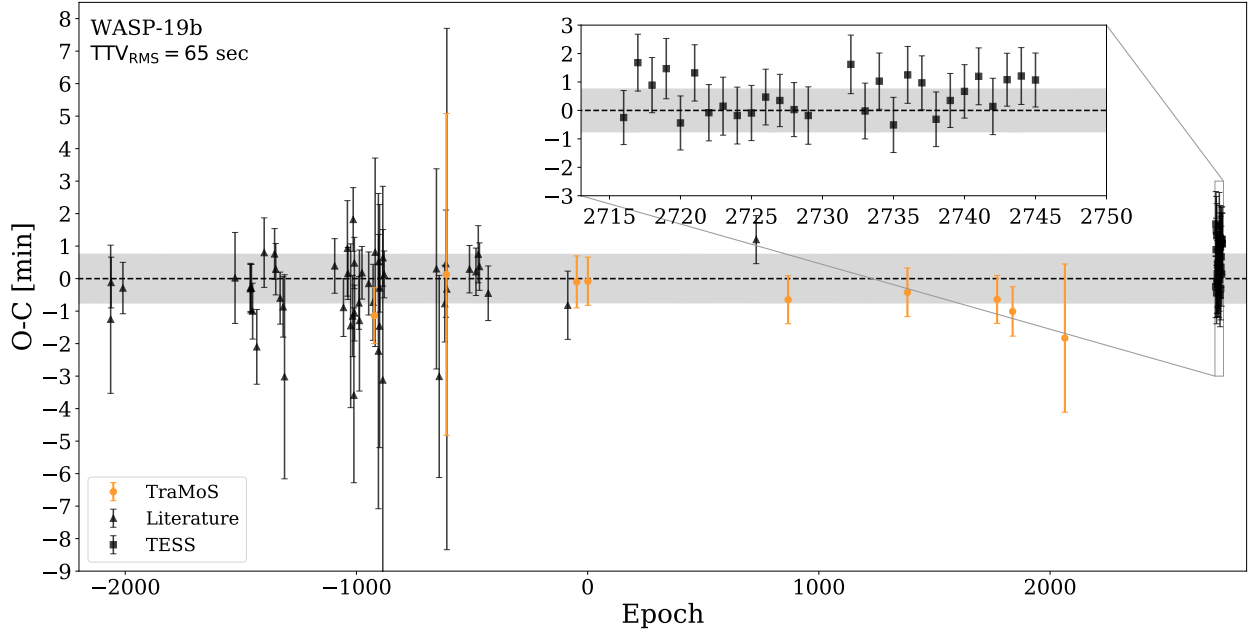


Figure 4.4: Observed minus calculated mid-transit times (TTV) for WASP-19b. The dashed black line corresponds to the proposed linear ephemeris, i.e. zero deviation from the predicted transit time computed from our refined orbital period. For that, we considered 87 transit times from the TraMoS project (in light blue), published works and TESS (both in black). The grey area corresponds to the error propagation at 1σ , which follows an imperceptible quadratic trend.. The RMS scatter from the linear ephemeris is 65 seconds.

WASP-77Ab. However, from the current work, this target is the one with less transit time data, thus, follow-up observations would be required to confirm the no existence of close-in companions in MMR.

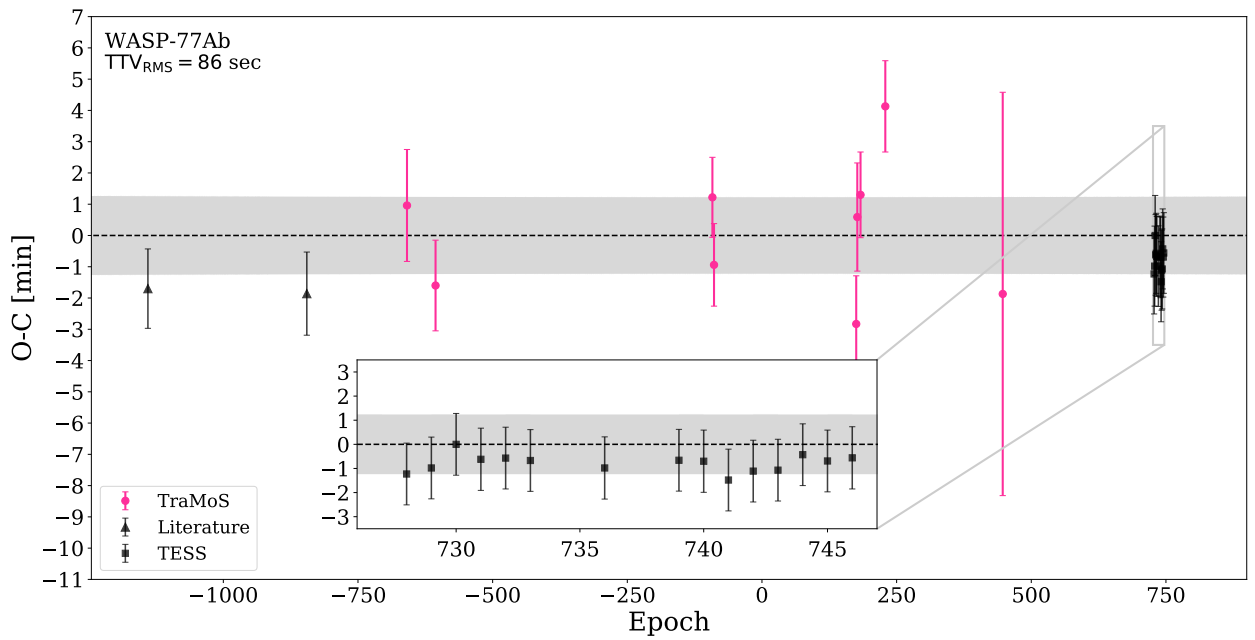


Figure 4.5: Observed minus calculated mid-transit times (TTV) for WASP-77Ab. The dashed black line corresponds to the proposed linear ephemeris, i.e. zero deviation from the predicted transit time computed from our refined orbital period. For that, we considered 26 transit times from the TraMoS project (in light blue), published works and TESS (both in black). The grey area corresponds to the error propagation at 1σ , which follows an imperceptible quadratic trend. The RMS scatter from the linear ephemeris is 86 seconds.

Chapter 5

Summary and future work

The TraMos project started more than 10 years ago aiming to refine orbital and physical parameters of already known exoplanets, and to search for variation in the transit time – or other planet parameters – that could suggest the existence of additional massive bodies on their systems. Our search focused on hot Jupiter planetary systems on short orbital periods, allowing to obtain additional photometric data from ground as well as space-based telescopes.

The Transit Timing Variation (TTV) technique was proposed as a technique to detect Earth-mass planet in gas giant systems, due to their mutual dynamical interaction. The variation in the transit time is enhanced when the two bodies are near to Mean Motion Resonances (MMR), therefore, this kind of interaction is easier to detect from ground-based follow-up. Through the years, the TTV technique has demonstrated to be an efficient and powerful tool not only to detect small exoplanets in the Earth-mass regime but to obtain essential information of multi-exoplanetary systems. By analyzing and modeling TTV curves of planetary systems in near MMR, the bodies' masses can be estimated, whence RV could be no longer a requirement for masses estimation.

During this Master project, I studied three exoplanets: WASP-18b, WASP-19b, and WASP-77Ab. For these targets, I analyzed a total of twenty-six new light curves: eight of WASP-18b, nine of WASP-19b and nine of WASP-77Ab. In the case of WASP-77Ab, four light curves were taken from the Exoplanet Transit Database (ETD)¹ to obtain a wider time coverage. For the light curves coming from the TraMoS project, I started from performing aperture photometry of the targets using our data reduction pipeline (for further details see Appendix A), to obtain high-precision light curves. Then, I used EXOFASTv2 Eastman et al. (2013); Eastman (2017) to get the best fit for the light curve's data and hence, to refine their orbital and physical parameters and obtain their transit times.

The TTV curves were constructed from the residuals between the observed transit time and the expected from the linear ephemeris. None of the targets studied in this thesis shows a clear, periodic sinusoidal signal in the variation of their transit mid-times and moreover, the structure of the transit times are comparable with a random distribution after a Lomb-Scargle analysis. This suggests the lack of close-in companions in MMR in their systems.

¹<https://var2.astro.cz/ETD>

However, upper mass limits of hypothetical perturbers – placed not only in near MMR – could be computed with the time-scatter from the linear ephemeris. The hot Jupiter WASP-18b shows 83 seconds of scatter, WASP-19b shows 75 seconds and WASP-77ab shows 121 seconds. The latter being the target with a larger deviation from the linear ephemeris, but at the same time, the target with fewer transit times.

In summary, the upper mass limit for possible perturbers that could produced the observed scatter in the transit time are:

- WASP-18b: $1.9 M_{\oplus}$, $4.0 M_{\oplus}$, $5.0 M_{\oplus}$, $25 M_{\oplus}$, $10 M_{\oplus}$, $7.0 M_{\oplus}$, $50 M_{\oplus}$ in 1:3, 2:5, 1:2, 2:1, 5:2, 3:1 and 4:1 resonances, respectively.
- WASP-19b: $2.0 M_{\oplus}$, $6.0 M_{\oplus}$, $0.9 M_{\oplus}$, $3.0 M_{\oplus}$, $2.0 M_{\oplus}$ in 1:2, 5:3, 2:1, 5:2 and 3:1 resonances, respectively.
- WASP-77Ab: $1.0 M_{\oplus}$, $3.5 M_{\oplus}$, $2.0 M_{\oplus}$, $7.0 M_{\oplus}$, $6.0 M_{\oplus}$, $10 M_{\oplus}$, $3.5 M_{\oplus}$, $4.5 M_{\oplus}$ in 1:3, 1:2, 3:5, 2:3, 5:3, 7:4, 2:1 and 3:1 resonances, respectively.

After the release of TESS data, I included transit times of the targets studied in this thesis, to extend their TTV curves and confirm the lack of periodic variations in the transit time. The results came out as expected and the scatter in the transit time were reduced for the three targets: 47 seconds for WASP-18b, 65 seconds for WASP-19b and 86 seconds for WASP-77Ab. Moreover, I refined each orbital period obtaining a precision of the order of milliseconds.

To date, none of the previous and current targets of the TraMoS project have shown TTVs. As they are all hot Jupiters, these studies support the theory of "isolated hot Jupiters", on which this kind of exoplanets are probably alone in their systems or accompanied of small bodies, not in MMR. How WASP-47b and Kepler-730b, the only two hot Jupiters showing TTVs, have close-in companions is still unknown. The migration theory of hot Jupiters could give us a possible explanation of how these gas giant ended-up with companions in MMR, as they are supposed to start their migration process in far-away orbits. While migrating, they could catch other bodies to then settling down in close orbits. But the lack of more hot Jupiters with TTVs suggest that probably during migration they cleaned-up their orbits of small bodies.

The TraMoS catalog stores more than 400 transits events of near 140 exoplanets. As future work, I propose to continue performing a ground-based photometric follow-up of the targets in this catalog, as well as new targets. Combining the efforts of TESS and TraMoS the amount of mid-transit times will cover a wider time-span and hence detect possible long-periodic TTV trends. TESS can provide hints of possible short and long-term TTVs – or TPVs in general – with an important amount of consecutive transit light curves. Then, performing ground-based follow-up is the most efficient way to prove or discard this variations, as the number of possible transit data from TESS is constrain by the duration of the sectors – for most of the targets –. We proved that our current used telescopes provides high-precision light curves, comparable with TESS.

In the near future, given the new scatter of the transit time in the three targets analyzed in this thesis, more accurate upper mass limits for hypothetical perturbers could be computed. Also, the next step is to analyze the exoplanets WASP-36b and HATS-34b, which each one

has five transit times from TraMoS and twelve and twenty-six from TESS, respectively. For WASP-22, WASP-46, WASP-45, WASP-23, and WASP-123, TESS provided five, seventeen, eight, seven and thirteen light curves, respectively. These targets are within the 30 targets with most light curves from TraMoS, therefore, they should be the next in line.

The reduction pipeline is fully functional and provides high-precision photometry. During this thesis project, I included dictionaries that allows the reduction photometry of new telescopes. Currently, the pipelines works for data coming from: Danish 1.54 m, Warsaw, Swope, Du Pont, REM, SMARTS 0.9 m and 1 m and SOAR. Nevertheless, several improvements were left behind because of the lack of time to implement them. For example, the coordinates selection could be done inside the program, to avoid mistakes when typing them by hand before calling the pipeline. Any new idea to improve the reduction pipeline could be done within an undergrad project or graduate semester-workshop.

Bibliography

- Adams, F. C. and Laughlin, G. (2006). Long-Term Evolution of Close Planets Including the Effects of Secular Interactions. *The Astrophysical Journal*, 649(2):1004–1009.
- Agol, E., Steffen, J., Sari, R., and Clarkson, W. (2005). On detecting terrestrial planets with timing of giant planet transits. *MNRAS*, 359:567–579.
- Agol, E. and Steffen, J. H. (2007). A limit on the presence of Earth-mass planets around a Sun-like star. *MNRAS*, 374(3):941–948.
- Alonso, R., Brown, T. M., Charbonneau, D., Dunham, E. W., Belmonte, J. A., Deeg, H. J., Fernández, J. M., Latham, D. W., Mandushev, G., O’Donovan, F. T., Rabus, M., and Torres, G. (2007). The Transatlantic Exoplanet Survey (TrES): A Review. In Afonso, C., Weldrake, D., and Henning, T., editors, *Transiting Extrapolar Planets Workshop*, volume 366 of *Astronomical Society of the Pacific Conference Series*, page 13.
- Anderson, D. R., Gillon, M., Maxted, P. F. L., Barman, T. S., Collier Cameron, A., Hellier, C., Queloz, D., Smalley, B., and Triaud, A. H. M. J. (2010). H-band thermal emission from the 19-h period planet WASP-19b. *A&A*, 513:L3.
- Bakos, G. (2012). Planet Hunting With HATNet and HATSouth. *Journal of the American Association of Variable Star Observers (JAAVSO)*, 40:241.
- Ballard, S. (2018). Predicted number, multiplicity, and orbital dynamics of TESS M dwarf exoplanets. *ArXiv e-prints*, arXiv:1801.04949.
- Ballard, S., Fabrycky, D., Fressin, F., Charbonneau, D., Desert, J.-M., Torres, G., Marcy, G., Burke, C. J., Isaacson, H., Henze, C., Steffen, J. H., Ciardi, D. R., Howell, S. B., Cochran, W. D., Endl, M., Bryson, S. T., Rowe, J. F., Holman, M. J., Lissauer, J. J., Jenkins, J. M., Still, M., Ford, E. B., Christiansen, J. L., Middour, C. K., Haas, M. R., Li, J., Hall, J. R., McCauliff, S., Batalha, N. M., Koch, D. G., and Borucki, W. J. (2011). The Kepler-19 System: A Transiting 2.2 R \oplus Planet and a Second Planet Detected via Transit Timing Variations. *ApJ*, 743:200.
- Barnes, R. and Greenberg, R. (2006). Stability Limits in Extrasolar Planetary Systems. *ApJ*, 647:L163–L166.
- Bean, J. L. (2009). An analysis of the transit times of CoRoT-1b. *A&A*, 506:369–375.
- Bean, J. L., Désert, J.-M., Seifahrt, A., Madhusudhan, N., Chilingarian, I., Homeier, D., and Szentgyorgyi, A. (2013). Ground-based Transit Spectroscopy of the Hot-Jupiter WASP-19b in the Near-infrared. *ApJ*, 771:108.

- Becker, J. C., Vanderburg, A., Adams, F. C., Rappaport, S. A., and Schwengeler, H. M. (2015). WASP-47: A Hot Jupiter System with Two Additional Planets Discovered by K2. *ApJ*, 812:L18.
- Cañas, C. I., Wang, S., Mahadevan, S., Bender, C. F., De Lee, N., Fleming, S. W., García-Hernández, D. A., Hearty, F. R., Majewski, S. R., Roman-Lopes, A., Schneider, D. P., and Stassun, K. G. (2019). Kepler-730: A Hot Jupiter System with a Close-in, Transiting, Earth-sized Planet. *ApJ*, 870:L17.
- Cincotta, P. M., Giordano, C. M., and Simó, C. (2003). Phase space structure of multi-dimensional systems by means of the mean exponential growth factor of nearby orbits. *Physica D Nonlinear Phenomena*, 182:151–178.
- Cincotta, P. M. and Simó, C. (2000). Simple tools to study global dynamics in non-axisymmetric galactic potentials - I. *A&AS*, 147:205–228.
- Collier Cameron, A. and Jardine, M. (2018). Hierarchical Bayesian calibration of tidal orbit decay rates among hot Jupiters. *MNRAS*, 476(2):2542–2555.
- Dawson, R. I., Huang, C. X., Lissauer, J. J., Collins, K. A., Sha, L., Armstrong, J., Conti, D. M., Collins, K. I., Evans, P., Gan, T., Horne, K., Ireland, M., Murgas, F., Myers, G., Relles, H. M., Sefako, R., Shporer, A., Stockdale, C., Žerjal, M., Zhou, G., Ricker, G., Vand erspek, R., Latham, D. W., Seager, S., Winn, J., Jenkins, J. M., Bouma, L. G., Caldwell, D. A., Daylan, T., Doty, J. P., Dynes, S., Esquerdo, G. A., Rose, M., Smith, J. C., and Yu, L. (2019). TOI-216b and TOI-216 c: Two Warm, Large Exoplanets in or Slightly Wide of the 2:1 Orbital Resonance. *AJ*, 158(2):65.
- Dotter, A. (2016). MESA Isochrones and Stellar Tracks (MIST) 0: Methods for the Construction of Stellar Isochrones. *ApJS*, 222:8.
- Eastman, J. (2017). EXOFASTv2: Generalized publication-quality exoplanet modeling code.
- Eastman, J., Gaudi, B. S., and Agol, E. (2013). EXOFAST: A Fast Exoplanetary Fitting Suite in IDL. *PASP*, 125:83.
- Eastman, J., Siverd, R., and Gaudi, B. S. (2010). Achieving Better Than 1 Minute Accuracy in the Heliocentric and Barycentric Julian Dates. *PASP*, 122:935.
- Fabrycky, D. C., Ford, E. B., Steffen, J. H., Rowe, J. F., Carter, J. A., Moorhead, A. V., Batalha, N. M., Borucki, W. J., Bryson, S., Buchhave, L. A., Christiansen, J. L., Ciardi, D. R., Cochran, W. D., Endl, M., Fanelli, M. N., Fischer, D., Fressin, F., Geary, J., Haas, M. R., Hall, J. R., Holman, M. J., Jenkins, J. M., Koch, D. G., Latham, D. W., Li, J., Lissauer, J. J., Lucas, P., Marcy, G. W., Mazeh, T., McCauliff, S., Quinn, S., Ragozzine, D., Sasselov, D., and Shporer, A. (2012). Transit Timing Observations from Kepler. IV. Confirmation of Four Multiple-planet Systems by Simple Physical Models. *ApJ*, 750:114.
- Ford, E. B., Fabrycky, D. C., Steffen, J. H., Carter, J. A., Fressin, F., Holman, M. J., Lissauer, J. J., Moorhead, A. V., Morehead, R. C., Ragozzine, D., Rowe, J. F., Welsh, W. F., Allen, C., Batalha, N. M., Borucki, W. J., Bryson, S. T., Buchhave, L. A., Burke, C. J., Caldwell, D. A., Charbonneau, D., Clarke, B. D., Cochran, W. D., Désert, J.-M., Endl, M., Everett, M. E., Fischer, D. A., Gautier, Thomas N., I., Gilliland, R. L., Jenkins, J. M., Haas, M. R., Horch, E., Howell, S. B., Ibrahim, K. A., Isaacson, H., Koch, D. G., Latham, D. W., Li, J., Lucas, P., MacQueen,

P. J., Marcy, G. W., McCauliff, S., Mullally, F. R., Quinn, S. N., Quintana, E., Shporer, A., Still, M., Tenenbaum, P., Thompson, S. E., Torres, G., Twicken, J. D., Wohler, B., and Kepler Science Team (2012). Transit Timing Observations from Kepler. II. Confirmation of Two Multiplanet Systems via a Non-parametric Correlation Analysis. *ApJ*, 750:113.

Fressin, F., Torres, G., Charbonneau, D., Bryson, S. T., Christiansen, J., Dressing, C. D., Jenkins, J. M., Walkowicz, L. M., and Batalha, N. M. (2013). The False Positive Rate of Kepler and the Occurrence of Planets. *ApJ*, 766(2):81.

Freudenthal, J., von Essen, C., Dreizler, S., Wedemeyer, S., Agol, E., Morris, B. M., Becker, A. C., Mallonn, M., Hoyer, S., Ofir, A., Tal-Or, L., Deeg, H. J., Herrero, E., Ribas, I., Khalafinejad, S., Hernández, J., and Rodríguez S., M. M. (2018). Kepler Object of Interest Network. II. Photodynamical modelling of Kepler-9 over 8 years of transit observations. *A&A*, 618:A41.

Fukui, A., Narita, N., Tristram, P. J., Sumi, T., Abe, F., Itow, Y., Sullivan, D. J., Bond, I. A., Hirano, T., Tamura, M., Bennett, D. P., Furusawa, K., Hayashi, F., Hearnshaw, J. B., Hosaka, S., Kamiya, K., Kobara, S., Korpela, A., Kilmartin, P. M., Lin, W., Ling, C. H., Makita, S., Masuda, K., Matsubara, Y., Miyake, N., Muraki, Y., Nagaya, M., Nishimoto, K., Ohnishi, K., Omori, K., Perrott, Y., Rattenbury, N., Saito, T., Skuljan, L., Suzuki, D., Sweatman, W. L., and Wada, K. (2011). Measurements of Transit Timing Variations for WASP-5b. *PASJ*, 63:287–300.

Goździewski, K. (2003). A dynamical analysis of the HD 37124 planetary system. *A&A*, 398:315–325.

Goździewski, K., Bois, E., Maciejewski, A. J., and Kiseleva-Eggleton, L. (2001). Global dynamics of planetary systems with the MEGNO criterion. *A&A*, 378:569–586.

Goździewski, K., Breiter, S., and Borczyk, W. (2008). The long-term stability of extrasolar system HD37124. Numerical study of resonance effects. *MNRAS*, 383:989–999.

Hebb, L., Collier-Cameron, A., Triaud, A. H. M. J., Lister, T. A., Smalley, B., Maxted, P. F. L., Hellier, C., Anderson, D. R., Pollacco, D., Gillon, M., Queloz, D., West, R. G., Bentley, S., Enoch, B., Haswell, C. A., Horne, K., Mayor, M., Pepe, F., Segransan, D., Skillen, I., Udry, S., and Wheatley, P. J. (2010). WASP-19b: The Shortest Period Transiting Exoplanet Yet Discovered. *ApJ*, 708:224–231.

Hellier, C., Anderson, D. R., Collier Cameron, A., Gillon, M., Hebb, L., Maxted, P. F. L., Queloz, D., Smalley, B., Triaud, A. H. M. J., West, R. G., Wilson, D. M., Bentley, S. J., Enoch, B., Horne, K., Irwin, J., Lister, T. A., Mayor, M., Parley, N., Pepe, F., Pollacco, D. L., Segransan, D., Udry, S., and Wheatley, P. J. (2009). An orbital period of 0.94days for the hot-Jupiter planet WASP-18b. *Nature*, 460:1098–1100.

Heyl, J. S. and Gladman, B. J. (2007). Using long-term transit timing to detect terrestrial planets. *Monthly Notices of the Royal Astronomical Society*, 377(4):1511–1519.

Hinse, T. C., Christou, A. A., Alvarellos, J. L. A., and Goździewski, K. (2010). Application of the MEGNO technique to the dynamics of Jovian irregular satellites. *MNRAS*, 404:837–857.

Holman, M. J., Fabrycky, D. C., Ragozzine, D., Ford, E. B., Steffen, J. H., Welsh, W. F., Lissauer, J. J., Latham, D. W., Marcy, G. W., Walkowicz, L. M., Batalha, N. M., Jenkins, J. M., Rowe, J. F., Cochran, W. D., Fressin, F., Torres, G., Buchhave, L. A., Sasselov, D. D., Borucki, W. J.,

- Koch, D. G., Basri, G., Brown, T. M., Caldwell, D. A., Charbonneau, D., Dunham, E. W., Gautier, T. N., Geary, J. C., Gilliland, R. L., Haas, M. R., Howell, S. B., Ciardi, D. R., Endl, M., Fischer, D., Fürész, G., Hartman, J. D., Isaacson, H., Johnson, J. A., MacQueen, P. J., Moorhead, A. V., Morehead, R. C., and Orosz, J. A. (2010). Kepler-9: A System of Multiple Planets Transiting a Sun-Like Star, Confirmed by Timing Variations. *Science*, 330:51.
- Holman, M. J. and Murray, N. W. (2005). The Use of Transit Timing to Detect Terrestrial-Mass Extrasolar Planets. *Science*, 307:1288–1291.
- Hoyer, S., López-Morales, M., Rojo, P., Minniti, D., and Adams, E. R. (2016a). TraMoS - IV. Discarding the Quick Orbital Decay Hypothesis for OGLE-TR- 113b. *MNRAS*, 455:1334–1340.
- Hoyer, S., López-Morales, M., Rojo, P., Nascimbeni, V., Hidalgo, S., Astudillo-Defru, N., Concha, F., Contreras, Y., Servajean, E., and Hinse, T. C. (2013). TraMoS project - III. Improved physical parameters, timing analysis and starspot modelling of the WASP-4b exoplanet system from 38 transit observations. *MNRAS*, 434:46–58.
- Hoyer, S., Pallé, E., Dragomir, D., and Murgas, F. (2016b). Ruling out the Orbital Decay of the WASP-43b Exoplanet. *AJ*, 151(6):137.
- Hoyer, S., Rojo, P., and López-Morales, M. (2012). Transit Monitoring in the South (TraMoS) Project: Discarding Transit Timing Variations in WASP-5b. *ApJ*, 748:22.
- Hoyer, S., Rojo, P., López-Morales, M., Díaz, R. F., Chambers, J., and Minniti, D. (2011). Five New Transit Epochs of the Exoplanet OGLE-TR-111b. *ApJ*, 733:53.
- Jenkins, J. M., Twicken, J. D., McCauliff, S., Campbell, J., Sanderfer, D., Lung, D., Mansouri-Samani, M., Girouard, F., Tenenbaum, P., Klaus, T., Smith, J. C., Caldwell, D. A., Chacon, A. D., Henze, C., Heiges, C., Latham, D. W., Morgan, E., Swade, D., Rinehart, S., and Vanderspek, R. (2016). The TESS science processing operations center. In *Software and Cyberinfrastructure for Astronomy IV*, volume 9913 of *Proc. SPIE*, page 99133E.
- Kipping, D. M. (2009a). Transit timing effects due to an exomoon. *MNRAS*, 392(1):181–189.
- Kipping, D. M. (2009b). Transit timing effects due to an exomoon - II. *MNRAS*, 396(3):1797–1804.
- Lendl, M., Gillon, M., Queloz, D., Alonso, R., Fumel, A., Jehin, E., and Naef, D. (2013). A photometric study of the hot exoplanet WASP-19b. *A&A*, 552:A2.
- Lomb, N. R. (1976). Least-squares frequency analysis of unequally spaced data. *Ap&SS*, 39:447–462.
- Mackebrandt, F., Mallonn, M., Ohlert, J. M., Granzer, T., Lalitha, S., García Muñoz, A., Gibson, N. P., Lee, J. W., Sozzetti, A., Turner, J. D., Vaňko, M., and Strassmeier, K. G. (2017). Transmission spectroscopy of the hot Jupiter TrES-3 b: Disproof of an overly large Rayleigh-like feature. *A&A*, 608:A26.
- Mancini, L., Ciceri, S., Chen, G., Tregloan-Reed, J., Fortney, J. J., Southworth, J., Tan, T. G., Burgdorf, M., Calchi Novati, S., Dominik, M., Fang, X. S., Finet, F., Gerner, T., Hardis, S., Hinse, T. C., Jørgensen, U. G., Liebig, C., Nikolov, N., Ricci, D., Schäfer, S., Schönebeck, F., Skottfelt, J., Wertz, O., Alsubai, K. A., Bozza, V., Browne, P., Dodds, P., Gu, S. H., Harpsøe, K., Henning, T., Hundertmark, M., Jessen-Hansen, J., Kains, N., Kerins, E., Kjeldsen, H., Lund,

M. N., Lundkvist, M., Madhusudhan, N., Mathiasen, M., Penny, M. T., Prof, S., Rahvar, S., Sahu, K., Scarpetta, G., Snodgrass, C., and Surdej, J. (2013). Physical properties, transmission and emission spectra of the WASP-19 planetary system from multi-colour photometry. *MNRAS*, 436:2–18.

Mancini, L., Giordano, M., Mollière, P., Southworth, J., Brahm, R., Ciceri, S., and Henning, T. (2016a). An optical transmission spectrum of the transiting hot Jupiter in the metal-poor WASP-98 planetary system. *MNRAS*, 461:1053–1061.

Mancini, L., Lillo-Box, J., Southworth, J., Borsato, L., Gandolfi, D., Ciceri, S., Barrado, D., Brahm, R., and Henning, T. (2016b). Kepler-539: A young extrasolar system with two giant planets on wide orbits and in gravitational interaction. *A&A*, 590:A112.

Mandel, K. and Agol, E. (2002). Analytic Light Curves for Planetary Transit Searches. *The Astrophysical Journal*, 580(2):L171–L175.

Maxted, P. F. L., Anderson, D. R., Collier Cameron, A., Doyle, A. P., Fumel, A., Gillon, M., Hellier, C., Jehin, E., Lendl, M., Pepe, F., Pollacco, D. L., Queloz, D., Ségransan, D., Smalley, B., Southworth, K., Smith, A. M. S., Triaud, A. H. M. J., Udry, S., and West, R. G. (2013a). WASP-77 Ab: A Transiting Hot Jupiter Planet in a Wide Binary System. *PASP*, 125:48.

Maxted, P. F. L., Anderson, D. R., Doyle, A. P., Gillon, M., Harrington, J., Iro, N., Jehin, E., Lafrenière, D., Smalley, B., and Southworth, J. (2013b). Spitzer 3.6 and 4.5 μm full-orbit light curves of WASP-18. *MNRAS*, 428:2645–2660.

Millholland, S. and Laughlin, G. (2018). Obliquity Tides May Drive WASP-12b Rapid Orbital Decay. *ApJ*, 869:L15.

Miralda-Escudé, J. (2002). Orbital Perturbations of Transiting Planets: A Possible Method to Measure Stellar Quadrupoles and to Detect Earth-Mass Planets. *ApJ*, 564:1019–1023.

Nesvorný, D. (2009). Transit Timing Variations for Eccentric and Inclined Exoplanets. *ApJ*, 701(2):1116–1122.

Nesvorný, D. and Morbidelli, A. (2008a). Mass and Orbit Determination from Transit Timing Variations of Exoplanets. *ApJ*, 688(1):636–646.

Nesvorný, D. and Morbidelli, A. (2008b). Mass and Orbit Determination from Transit Timing Variations of Exoplanets. *ApJ*, 688:636–646.

Nutzman, P. A., Fabrycky, D. C., and Fortney, J. J. (2011). Using Star Spots to Measure the Spin-orbit Alignment of Transiting Planets. *ApJ*, 740:L10.

Pál, A., Sárneczky, K., Szabó, G. M., Szing, A., Kiss, L. L., Mező, G., and Regály, Z. (2011). Transit timing variations in the HAT-P-13 planetary system. *MNRAS*, 413:L43–L46.

Patra, K. C., Winn, J. N., Holman, M. J., Yu, L., Deming, D., and Dai, F. (2017). The Apparently Decaying Orbit of WASP-12b. *AJ*, 154:4.

Pepper, J., Pogge, R. W., DePoy, D. L., Marshall, J. L., Stanek, K. Z., Stutz, A. M., Poindexter, S., Siverd, R., O'Brien, T. P., Trueblood, M., and Trueblood, P. (2007). The Kilodegree Extremely Little Telescope (KELT): A Small Robotic Telescope for Large-Area Synoptic Surveys.

Publications of the Astronomical Society of the Pacific, 119:923–935.

- Pollacco, D. L., Skillen, I., Collier Cameron, A., Christian, D. J., Hellier, C., Irwin, J., Lister, T. A., Street, R. A., West, R. G., Anderson, D. R., Clarkson, W. I., Deeg, H., Enoch, B., Evans, A., Fitzsimmons, A., Haswell, C. A., Hodgkin, S., Horne, K., Kane, S. R., Keenan, F. P., Maxted, P. F. L., Norton, A. J., Osborne, J., Parley, N. R., Ryans, R. S. I., Smalley, B., Wheatley, P. J., and Wilson, D. M. (2006). The WASP Project and the SuperWASP Cameras. *Publications of the Astronomical Society of the Pacific*, 118:1407–1418.
- Ricker, G. R. (2014). The Transiting Exoplanet Survey Satellite Mission. *Journal of the American Association of Variable Star Observers (AAVSO)*, 42:234.
- Sanchis-Ojeda, R. and Winn, J. N. (2011). Starspots, Spin-Orbit Misalignment, and Active Latitudes in the HAT-P-11 Exoplanetary System. *ApJ*, 743:61.
- Sanchis-Ojeda, R., Winn, J. N., and Fabrycky, D. C. (2013). Starspots and spin-orbit alignment for Kepler cool host stars. *Astronomische Nachrichten*, 334:180–183.
- Scargle, J. D. (1982). Studies in astronomical time series analysis. II - Statistical aspects of spectral analysis of unevenly spaced data. *ApJ*, 263:835–853.
- Seager, S. and Mallén-Ornelas, G. (2003). A Unique Solution of Planet and Star Parameters from an Extrasolar Planet Transit Light Curve. *ApJ*, 585(2):1038–1055.
- Sedaghati, E., Boffin, H. M. J., Csizmadia, S., Gibson, N., Kabath, P., Mallonn, M., and Van den Ancker, M. E. (2015). Regaining the FORS: optical ground-based transmission spectroscopy of the exoplanet WASP-19b with VLT+FOURS2. *A&A*, 576:L11.
- Shporer, A., Wong, I., Huang, C. X., Line, M. R., Stassun, K. G., Fetherolf, T., Kane, S., Ricker, G. R., Latham, D. W., Seager, S., Winn, J. N., Jenkins, J. M., Glidden, A., Berta-Thompson, Z., Ting, E. B., Li, J., and Haworth, K. (2018). TESS full orbital phase curve of the WASP-18b system. *arXiv e-prints*, page arXiv:1811.06020.
- Southworth, J., Hinse, T. C., Jørgensen, U. G., Dominik, M., Ricci, D., Burgdorf, M. J., Hornstrup, A., Wheatley, P. J., Anguita, T., Bozza, V., Novati, S. C., Harpsøe, K., Kjærgaard, P., Liebig, C., Mancini, L., Masi, G., Mathiasen, M., Rahvar, S., Scarpetta, G., Snodgrass, C., Surdej, J., Thöne, C. C., and Zub, M. (2009). High-precision photometry by telescope defocusing - I. The transiting planetary system WASP-5. *MNRAS*, 396:1023–1031.
- Steffen, J. H. and Agol, E. (2005). An analysis of the transit times of TrES-1b. *MNRAS*, 364(1):L96–L100.
- Steffen, J. H., Ford, E. B., Rowe, J. F., Fabrycky, D. C., Holman, M. J., Welsh, W. F., Batalha, N. M., Borucki, W. J., Bryson, S., Caldwell, D. A., Ciardi, D. R., Jenkins, J. M., Kjeldsen, H., Koch, D. G., Prša, A., Sanderfer, D. T., Seader, S., and Twicken, J. D. (2012a). Transit Timing Observations from Kepler. VI. Potentially Interesting Candidate Systems from Fourier-based Statistical Tests. *ApJ*, 756:186.
- Steffen, J. H., Ragozzine, D., Fabrycky, D. C., Carter, J. A., Ford, E. B., Holman, M. J., Rowe, J. F., Welsh, W. F., Borucki, W. J., Boss, A. P., Ciardi, D. R., and Quinn, S. N. (2012b). Kepler constraints on planets near hot Jupiters. *Proceedings of the National Academy of Science*,

109:7982–7987.

- Szabó, R., Szabó, G. M., Dálya, G., Simon, A. E., Hodosán, G., and Kiss, L. L. (2013). Multiple planets or exomoons in Kepler hot Jupiter systems with transit timing variations? *A&A*, 553:A17.
- Tregloan-Reed, J., Southworth, J., and Tappert, C. (2013). Transits and starspots in the WASP-19 planetary system. *MNRAS*, 428:3671–3679.
- Triaud, A. H. M. J., Collier Cameron, A., Queloz, D., Anderson, D. R., Gillon, M., Hebb, L., Hellier, C., Loeillet, B., Maxted, P. F. L., Mayor, M., Pepe, F., Pollacco, D., Ségransan, D., Smalley, B., Udry, S., West, R. G., and Wheatley, P. J. (2010). Spin-orbit angle measurements for six southern transiting planets. New insights into the dynamical origins of hot Jupiters. *A&A*, 524:A25.
- Turner, J. D., Pearson, K. A., Biddle, L. I., Smart, B. M., Zellem, R. T., Teske, J. K., Hardegree-Ullman, K. K., Griffith, C. C., Leiter, R. M., Cates, I. T., Nieberding, M. N., Smith, C.-T. W., Thompson, R. M., Hofmann, R., Berube, M. P., Nguyen, C. H., Small, L. C., Guvenen, B. C., Richardson, L., McGraw, A., Raphael, B., Crawford, B. E., Robertson, A. N., Tombleson, R., Carleton, T. M., Towner, A. P. M., Walker-LaFollette, A. M., Hume, J. R., Watson, Z. T., Jones, C. K., Lichtenberger, M. J., Hoglund, S. R., Cook, K. L., Crossen, C. A., Jorgensen, C. R., Romine, J. M., Thompson, A. R., Villegas, C. F., Wilson, A. A., Sanford, B., Taylor, J. M., and Henz, T. N. (2016). Ground-based near-UV observations of 15 transiting exoplanets: constraints on their atmospheres and no evidence for asymmetrical transits. *MNRAS*, 459:789–819.
- VanderPlas, J., Connolly, A. J., Ivezić, Z., and Gray, A. (2012). Introduction to astroML: Machine learning for astrophysics. In *Proceedings of Conference on Intelligent Data Understanding (CIDU)*, pp. 47–54, 2012., pages 47–54.
- VanderPlas, J. T. (2018). Understanding the Lomb-Scargle Periodogram. *ApJS*, 236:16.
- VanderPlas, J. T. and Ivezić, Ž. (2015). Periodograms for Multiband Astronomical Time Series. *ApJ*, 812:18.
- von Essen, C., Ofir, A., Dreizler, S., Agol, E., Freudenthal, J., Hernández, J., Wedemeyer, S., Parkash, V., Deeg, H. J., Hoyer, S., Morris, B. M., Becker, A. C., Sun, L., Gu, S. H., Herrero, E., Tal-Or, L., Poppenhaeger, K., Mallonn, M., Albrecht, S., Khalafinejad, S., Boumis, P., Delgado-Correal, C., Fabrycky, D. C., Janulis, R., Lalitha, S., Liakos, A., Mikolaitis, Š., Moyano D’Angelo, M. L., Sokov, E., Pakštienė, E., Popov, A., Krushinsky, V., Ribas, I., Rodríguez S., M. M., Rusov, S., Sokova, I., Tautvaišienė, G., and Wang, X. (2018). Kepler Object of Interest Network. I. First results combining ground- and space-based observations of Kepler systems with transit timing variations. *A&A*, 615:A79.
- Wang, S., Addison, B., Fischer, D. A., Brewer, J. M., Isaacson, H., Howard, A. W., and Laughlin, G. (2018a). Stellar Spin-Orbit Alignment for Kepler-9, a Multi-transiting Planetary System with Two Outer Planets Near 2:1 Resonance. *AJ*, 155:70.
- Wang, S., Wang, X.-Y., Wang, Y.-H., Liu, H.-G., Hinse, T. C., Eastman, J., Bayliss, D., Hori, Y., Hu, S.-M., Li, K., Liu, J., Narita, N., Peng, X., Wittenmyer, R. A., Wu, Z.-Y., Zhang, H., Zhang, X., Zhao, H., Zhou, J.-L., Zhou, G., Zhou, X., and Laughlin, G. (2018b). Transiting Exoplanet Monitoring Project (TEMP). I. Refined System Parameters and Transit Timing Variations of HAT-P-29b. *AJ*, 156:181.

- Wang, S., Wu, D.-H., Barclay, T., and Laughlin, G. P. (2017a). Updated Masses for the TRAPPIST-1 Planets. *arXiv e-prints*.
- Wang, S., Zhang, H., Zhou, J.-L., Zhou, X., Yang, M., Wang, L., Bayliss, D., Zhou, G., Ashley, M. C. B., Fan, Z., Feng, L.-L., Gong, X., Lawrence, J. S., Liu, H., Liu, Q., Luong-Van, D. M., Ma, J., Meng, Z., Storey, J. W. V., Wittenmyer, R. A., Wu, Z., Yan, J., Yang, H., Yang, J., Yang, J., Yuan, X., Zhang, T., Zhu, Z., and Zou, H. (2014). Planetary Transit Candidates in the CSTAR Field: Analysis of the 2008 Data. *The Astrophysical Journal Supplement Series*, 211:26.
- Wang, X.-Y., Wang, S., Hinse, T. C., Li, K., Wang, Y.-H., Laughlin, G., Liu, H.-G., Zhang, H., Wu, Z.-Y., Zhou, X., Zhou, J.-L., Hu, S.-M., Wu, D.-H., Peng, X.-Y., and Chen, Y.-Y. (2018c). Transiting Exoplanet Monitoring Project (TEMP). IV. Refined System Parameters, Transit Timing Variations, and Orbital Stability of the Transiting Planetary System HAT-P-25. *PASP*, 130(6):064401.
- Wang, Y.-H., Wang, S., Liu, H.-G., Hinse, T. C., Laughlin, G., Wu, D.-H., Zhang, X., Zhou, X., Wu, Z., Zhou, J.-L., Wittenmyer, R. A., Eastman, J., Zhang, H., Hori, Y., Narita, N., Chen, Y., Ma, J., Peng, X., Zhang, T.-M., Zou, H., Nie, J.-D., and Zhou, Z.-M. (2017b). Transiting Exoplanet Monitoring Project (TEMP). II. Refined System Parameters and Transit Timing Analysis of HAT-P-33b. *AJ*, 154:49.
- Weinberg, N. N., Sun, M., Arras, P., and Essick, R. (2017). Tidal Dissipation in WASP-12. *ApJ*, 849:L11.
- Wilkins, A. N., Delrez, L., Barker, A. J., Deming, D., Hamilton, D., Gillon, M., and Jehin, E. (2017). Searching for Rapid Orbital Decay of WASP-18b. *ApJ*, 836:L24.
- Winn, J. N. (2010). Transits and Occultations. *arXiv e-prints*, page arXiv:1001.2010.
- Wong, I., Knutson, H. A., Kataria, T., Lewis, N. K., Burrows, A., Fortney, J. J., Schwartz, J., Shporer, A., Agol, E., Cowan, N. B., Deming, D., Désert, J.-M., Fulton, B. J., Howard, A. W., Langton, J., Laughlin, G., Showman, A. P., and Todorov, K. (2016). 3.6 and 4.5 μm Spitzer Phase Curves of the Highly Irradiated Hot Jupiters WASP-19b and HAT-P-7b. *ApJ*, 823:122.
- Wu, D.-H., Wang, S., Zhou, J.-L., Steffen, J. H., and Laughlin, G. (2018). TTV-determined Masses for Warm Jupiters and Their Close Planetary Companions. *AJ*, 156:96.

Appendix A

Aperture photometry pipeline

Since the beginning of the TraMoS project, an aperture photometry pipeline has been in development, on which several graduates and undergraduates students worked and are currently working on it. This pipeline is Python-based and includes standard procedures of reduction, calibrations, and aperture photometry, including bias and flat-field corrections. The user needs to give the coordinates of the target and reference stars and a range of pixels for a possible aperture. Then, to produce high-precision light curves of the target and reference stars, the pipeline semi-automatically finds the best aperture and ring size, for the sky that produces the less RMS in the light curves.

The pipeline works with a specific directories' structure where all the needed information should be:

- raw: Folder containing the raw data of the observations. It could be FITS files or compressed FITS (e.g *fit.ZIP*).
- calib: This folder should include the flats – sky or dome – and bias files.
- data: Empty folder which will contain the output data after the aperture photometry procedure.
- figures: Empty folder on which all the figures generated in the reduction process will be stored.
- log: Folder containing the Python script to run the pipeline for the specific data set.
- extraction.tex: Latex file which generates the PDF file with all the important information related to the aperture photometry procedure process, such as images of the stamps, the radial profile of the target star, FWHM plots, preview of the light curve, etc.
- tramos_custom.sty: A customizable file containing the information related to the telescope, target's name, filter, date of the observation, RA, DEC and target's magnitude. When the pipeline finishes, it fills this file with the best aperture size obtained.

I have implemented dictionaries to ease the use of the pipeline with different telescopes. One of the biggest problems that I faced when I started reducing data, was the distinctness between the FITS headers produced from different telescopes. For example, while some of

them recorded the type of filter as *FILTER*, others use *FILTERB*. Also, as the TraMoS project has been collecting data for more than 10 years ago, some of our used telescopes were updated with new CCDs, producing that the pipeline was no longer functional. Currently, the pipeline works with data from the following telescopes:

- La Silla Observatory: Danish 1.54 m (previous and after 2017) and REM.
- Cerro Tololo Inter-American Observatory: SMARTS 0.9 m and 1 m.
- Las Campanas Observatory: Warsaw, Swope, Du Pont.
- Cerro Pachón: SOAR

In the sections ahead, I present the scripts for performing aperture photometry with the TraMoS pipeline of the targets studied in this thesis, following with an example of the PDF file generated by the pipeline, containing all the relevant information of the procedure.

A.1 Reduction script of WASP-18, WASP-19 and WASP-77A

WASP-18

2009 Oct 28:

```
coords_xy = [[691,1625],[1911,1349],[1644,925]]
ts, phot = pl.pipeline(files_path="raw/*.fits", calib_path="calib/*.fits",
                       coords_xy=coords_xy, target="WASP-18",
                       object_in_hdr = "WASP-18",
                       stamp_rad=20, recenter=True, brightest=1,
                       sector=[500,650], sky_test=[13,20],
                       aps=[5,12], filter_band = "I bessell Soar",
                       labelsize=16, ccd_lims_xy=[1,2072,1,2072],
                       max_counts = 60000, **pl.ctio_1m)
```

2009 Oct 29:

```
coords_xy = [[645,1625],[1865,1344],[1598,921]]
ts, phot = pl.pipeline(files_path="raw/*.fits", calib_path="calib/*.fits",
                       coords_xy=coords_xy, target="WASP-18",
                       object_in_hdr = "WASP-18",
                       stamp_rad=24, recenter=True, brightest=1,
                       sector=[1200,1350], sky_test=[15,23],
                       aps=[5,14], filter_band = "I bessell Soar",
                       labelsize=16, ccd_lims_xy=[1,2072,1,2072],
                       max_counts = 60000, **pl.ctio_1m)
```

2009 Oct 30:

```
coords_xy = [[640,1624],[1865,1344],[1598,920]]
ts, phot = pl.pipeline(files_path="raw/*.fits", calib_path="calib/*.fits",
                       coords_xy=coords_xy, target="WASP-18",
                       object_in_hdr = "WASP-18",
                       stamp_rad=28, recenter=True, brightest=1,
                       sector=[570,700], sky_test=[13,25],
                       aps=[5,12], filter_band = "I bessell Soar",
                       labelsize=16, ccd_lims_xy=[1,2072,1,2072],
                       max_counts = 60000, **pl.ctio_1m)
```

2011 Sep 06:

```
coords_xy = [[516,1496],[1731,1193],[1460,774]]
ts, phot = pl.pipeline(files_path="raw/*.fits", calib_path="calib/*.fits",
                       coords_xy=coords_xy, target="WASP-18",
                       object_in_hdr = "wasp18",
                       stamp_rad=24, recenter=True, brightest=1,
                       sector=[160,200], sky_test=[15,23],
                       aps=[5,14], filter_band = "I",
                       labelsize=16, ccd_lims_xy=[1,2072,1,2072],
                       max_counts = 60000, **pl.ctio_1m)
```

2016 Sep 24:

```
coords_xy = [[856,427],[455,710]]
ts, phot = pl.pipeline(files_path="raw/wasp18I*.fits", calib_path="calib/*.fits",
                       coords_xy=coords_xy, target="WASP-18",
                       object_in_hdr = "wasp18I",
                       stamp_rad=37, recenter=True, brightest=1,
                       sector=[1,20], sky_test=[30,35],
                       aps=[18,30], filter_band = "I",
                       labelsize=16, ccd_lims_xy=[1,1020,1,1052],
                       max_counts = 600000, **pl.dk154_old)
```

2016 Sep 25:

```
coords_xy = [[848,415],[445,699]]
ts, phot = pl.pipeline(files_path="raw/wasp*.fits", calib_path="calib/*.fits",
                       coords_xy=coords_xy,
                       target="WASP-18",
                       object_in_hdr = "wasp18I",
                       stamp_rad=48, recenter=True, brightest=1,
                       sector=[110,142], sky_test=[30,48],
```

```
    aps=[25,35], filter_band = "I",
    labelsize=16, ccd_lims_xy=[1,1020,1,1051],
    max_counts = 600000, **pl.dk154_2017)
```

2016 Sep 26:

```
coords_xy = [[469,873],[871,589]]
ts, phot = pl.pipeline(files_path="raw/wasp*.fits", calib_path="calib/*.fits",
                       coords_xy=coords_xy, target="WASP-18",
                       object_in_hdr = "wasp18",
                       stamp_rad=50, recenter=True, brightest=1,
                       sector=[100,110], sky_test=[40,50],
                       aps=[30,40], filter_band = "I",
                       labelsize=16, ccd_lims_xy=[1,1018,1,1293],
                       max_counts = 600000, **pl.dk154_2017)
```

2017 Sep 29:

```
coords_xy = [[1752,417],[1347,700]]
ts, phot = pl.pipeline(files_path="raw/Wasp-18*.fits", calib_path="calib/*.fits",
                       coords_xy=coords_xy, target="WASP-18",
                       object_in_hdr = "Wasp-18_R",
                       stamp_rad=37, recenter=True, brightest=1,
                       sector=[1,50], sky_test=[25,35],
                       aps=[16,25], filter_band = "R",
                       labelsize=16, ccd_lims_xy=[52,2099,1,1024],
                       max_counts = 600000, **pl.dk154_2017)
```

WASP-19

2011 Apr 22:

```
coords_xy = [[1198,459],[841,621],[937,737],[877,450]]
ts, phot = pl.pipeline(files_path="raw/*.fits", calib_path="calib/*.fits",
                       coords_xy=coords_xy, target="WASP-19",
                       object_in_hdr = "test",
                       stamp_rad=20, recenter=True, brightest=1,
                       sector=[30,90], sky_test=[10,20],
                       aps=[3,10], filter_band = "I",
                       labelsize=16, max_counts = 60000,
                       ccd_lims_xy=[0,2072,0,2072], **pl.ctio_1m)
```

2011 Dec 24:

```

coords_xy = [[1204,428],[1840,204],[1702,928],[1222,646]]
ts, phot = pl.pipeline(files_path="raw/*.fits", calib_path="calib/*.fits",
                       coords_xy=coords_xy, target="WASP-19",
                       object_in_hdr = "WASP19",
                       stamp_rad=20, recenter=True, brightest=3,
                       sector=[270,320], sky_test=[10,20],
                       aps=[3,10], filter_band = "I",
                       labelsize=16, ccd_lims_xy=[0,2072,0,2072],
                       max_counts = 60000, **pl.ctio_1m)

```

2013 Mar 13:

```

coords_xy = [[1202,1182],[1179,860]]
ts, phot = pl.pipeline(files_path="raw/WASP-19*.fits", calib_path="calib/*.fits",
                       coords_xy=coords_xy, target="WASP-19",
                       object_in_hdr=None,
                       stamp_rad=25, recenter=True, brightest=1,
                       sector=None, sky_test=[16,24],
                       aps=[8,20], filter_band="R",
                       labelsize=16, max_counts = 600000,
                       ccd_lims_xy=[52, 2048, 1, 2048], **pl.dk154_old)

```

2013 Apr 20:

```

coords_xy = [[109,515],[87,195],[445,201],[577,273],[601,369]]
ts, phot = pl.pipeline(files_path="raw/w19*.fits", calib_path="calib/*.fits",
                       coords_xy=coords_xy, target="WASP-19",
                       object_in_hdr="w19-20130420",
                       stamp_rad=25, recenter=True, brightest=1,
                       sky_test=[16,24], sector=[55,80],
                       filter_band="R", labelsize=16,
                       ccd_lims_xy=[0,700,0,650],
                       max_counts = 600000, **pl.dk154_old)

```

2015 Mar 04:

```

coords_xy = [[1074,967],[586,954],[1397,557],[1565,821],[1489,975],[1480,1201]]
ts, phot = pl.pipeline(files_path="raw/WASP19_*.fits", calib_path="calib/*.fits",
                       coords_xy=coords_xy, object_in_hdr="WASP19",
                       target="WASP-19",
                       stamp_rad=30, recenter=True, brightest=4,
                       sector=[1,30], labelsize=16,
                       filter_band="R", ccd_lims_xy=[0,2148,0,2048],
                       max_counts = 600000, **pl.dk154_old)

```

2016 Apr 14:

```
coords_xy = [[1125,1064], [708,1054], [718,828], [1318,151], [1031,524]]  
ts, phot = pl.pipeline(files_path="raw/wasp19_*.fits", calib_path="calib/*.fits",  
                      object_in_hdr="wasp19", target="WASP-19",  
                      coords_xy=coords_xy,  
                      stamp_rad=35, recenter=True, brightest=2,  
                      sector=[1,30], filter_band="I",  
                      labelsize=16, ccd_lims_xy=[0,2128,0,1376],  
                      max_counts = 600000, **pl.dk154_old)
```

2017 Feb 14:

```
coords_xy = [[525,686], [119,452], [432,149], [111,678],[192,1002]]  
ts, phot = pl.pipeline(files_path="raw/WASP_19_*.fits", calib_path="calib/*.fits",  
                      target="WASP-19",  
                      object_in_hdr= "WASP_19", coords_xy=coords_xy,  
                      stamp_rad=35, recenter=True, brightest=4,  
                      sector=[1,30], sky_test=[10,24],  
                      aps=[10,20], labelsize=16,  
                      ccd_lims_xy=[0,1019,0,1165], max_counts = 600000,  
                      filter_band="I", **pl.dk154_2017)
```

2017 Apr 08:

```
coords_xy = [[374,361], [866,215], [790, 369], [782, 595],[468,899]]  
ts, phot = pl.pipeline(files_path="raw/WASP19R*.fits", calib_path="calib/*.fits",  
                      target="WASP-19", object_in_hdr="WASP19R",  
                      coords_xy=coords_xy,  
                      stamp_rad=35, recenter=True, brightest=2,  
                      sector=[1,30], sky_test=[10,24],  
                      aps=[10,20], labelsize=16,  
                      filter_band="R", ccd_lims_xy=[0,1019,0,925],  
                      max_counts = 600000,  
                      filter_band="I", **pl.dk154_2017)
```

2017 Oct 03:

```
coords_xy = [[1087,1001],[892,1912],[1408,590],[1575,853],[1501,1009],[1491,1235]]  
ts, phot = pl.pipeline(files_path="raw/Wasp19_*.fits", calib_path="calib/*.fits",  
                      object_in_hdr="Wasp19", target="WASP-19",  
                      coords_xy=coords_xy,  
                      stamp_rad=25, recenter=True, brightest=1,  
                      aps=[10,20], sector=[1,15],  
                      sky_test=[10,24], labelsize=16,
```

```
filter_band="R", ccd_lims_xy=[0,2148,0,2048],  
max_counts = 600000, **pl.dk154_2017)
```

WASP-77A

2015 Sep 29:

```
coords_xy = [[1801,1558],[1558,681]]  
ts, phot = pl.pipeline(files_path="raw/*.fits", calib_path="calib/*.fits",  
                      coords_xy=coords_xy, target="WASP-77",  
                      object_in_hdr = "wasp77_",  
                      stamp_rad=40, recenter=True, brightest=1,  
                      sector=[55,90], sky_test=[30,35],  
                      aps=[20,28], filter_band = "R",  
                      labelsize=16, ccd_lims_xy=[1,1995,1,1655],  
                      max_counts = 600000, **pl.dk154_2017)
```

2015 Oct 03:

```
coords_xy = [[1572,118],[1819,996],[121,1433]]  
ts, phot = pl.pipeline(files_path="raw/wasp*.fits", calib_path="calib/*.fits",  
                      coords_xy=coords_xy, target="WASP-77",  
                      object_in_hdr = "wasp77",  
                      stamp_rad=40, recenter=True, brightest=2,  
                      sector=[50,75], sky_test=[31,35],  
                      aps=[20,30], filter_band = "R",  
                      labelsize=16, ccd_lims_xy=[1,1961,1,1546],  
                      max_counts = 600000, **pl.dk154_2017)
```

2016 Sep 26:

```
coords_xy = [[134,254],[378,1126],[518,1427]]  
ts, phot = pl.pipeline(files_path="raw/wasp*.fits", calib_path="calib/*.fits",  
                      coords_xy=coords_xy, target="WASP-77",  
                      object_in_hdr = "wasp77",  
                      stamp_rad=45, recenter=True, brightest=1,  
                      sector=[44,53], sky_test=[37,42],  
                      aps=[25,35], filter_band = "I",  
                      labelsize=16, ccd_lims_xy=[1,1010,1,1540],  
                      max_counts = 600000, **pl.dk154_2017)
```

2016 Oct 07:

```

coords_xy = [[1035,2120],[694,783],[1711,2094],[1820,2816]]
ts, phot = pl.pipeline(files_path="raw/*.ftsc", calib_path="calib/*.fts",
                       coords_xy=coords_xy, target="WASP-77",
                       object_in_hdr = "WASP-77",
                       stamp_rad=90, recenter=True, brightest=1,
                       sector=[145,160], sky_test=[50,70],
                       aps=[21,31], filter_band = "I",
                       labelsize=16, ccd_lims_xy=[1,2048,1,4102],
                       max_counts = 600000, **pl.warsaw_2016)

```

2017 Oct 01:

```

coords_xy = [[1054,1490],[1501,1471],[1520,372]]
ts, phot = pl.pipeline(files_path="raw/*.fits", calib_path="calib/*.fits",
                       coords_xy=coords_xy, target="WASP-77",
                       object_in_hdr = "Wasp-11",
                       stamp_rad=35, recenter=True, brightest=1,
                       sector=[10,30], sky_test=[21,34],
                       aps=[10,20], filter_band = "B",
                       labelsize=16, ccd_lims_xy=[1,2148,1,2048],
                       max_counts = 600000, **pl.dk154_2017)

```

A.2 Example of output file

The following joined document is an example of the PDF file generated by the data reduction pipeline. This corresponds to the reduction of the light curve of WASP-19 during March 4th, 2015.

TRAMOS Reduction Pipeline: WASP-19

	epoch	20150304
telescope/instrument	Danish	
period	0.78884 days	
semi-major axis	0.01616 AU	
RA	09:53:40.007	
Dec	-45:39:33.06	
V	11.35	
Chosen Apperture	14 pixels	

Reduction notes: The first data of the time series presents a big variation in comparison to the rest of the data that could be produced by atmospheric variations(cirrus clouds, turbulence, etc), this variations it's produced on the zone out of transit.

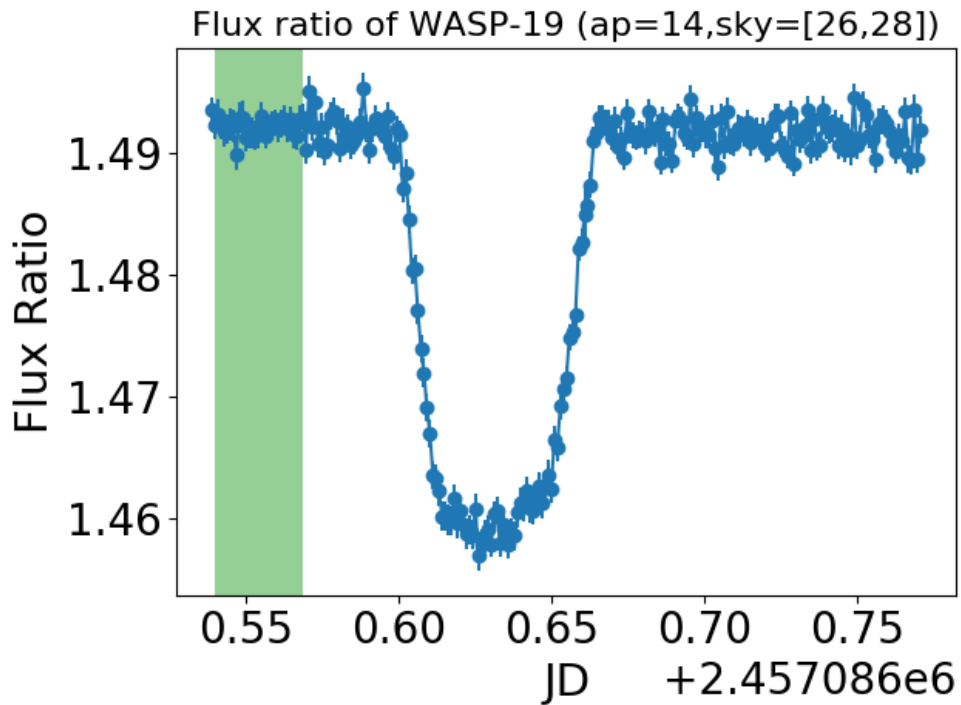


Figure 1: Flux ratio of the target. the x-axis is in units of Julian Date.

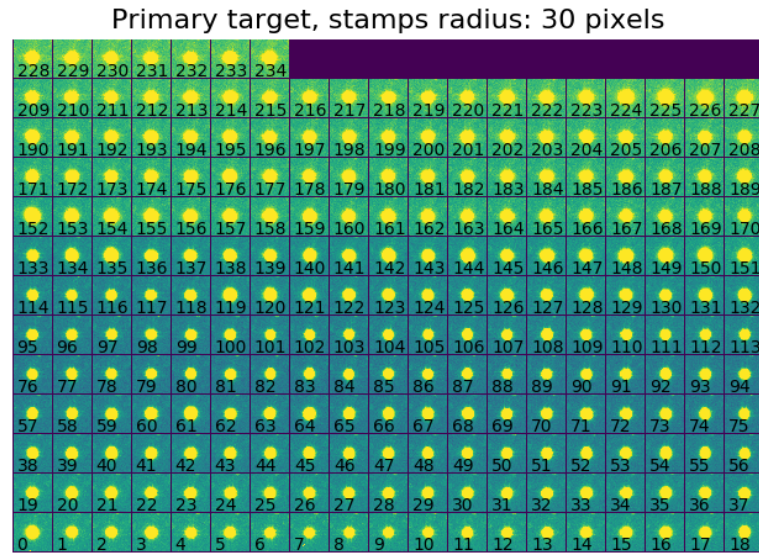
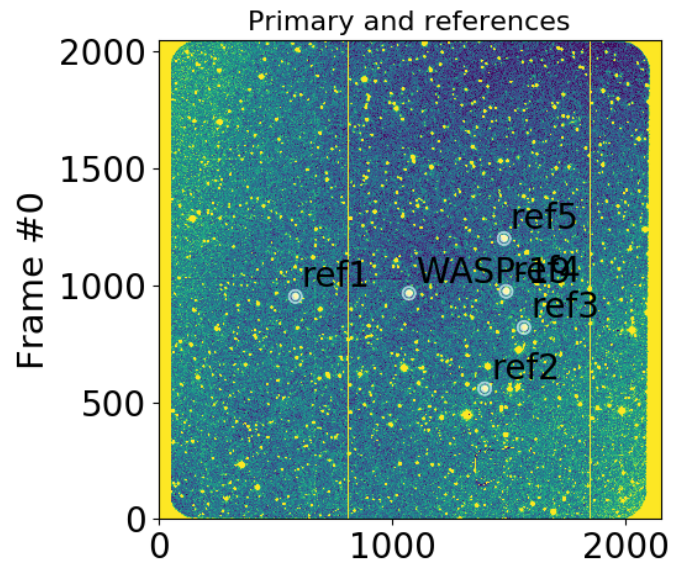


Figure 2: Timeseries stamps for target planet



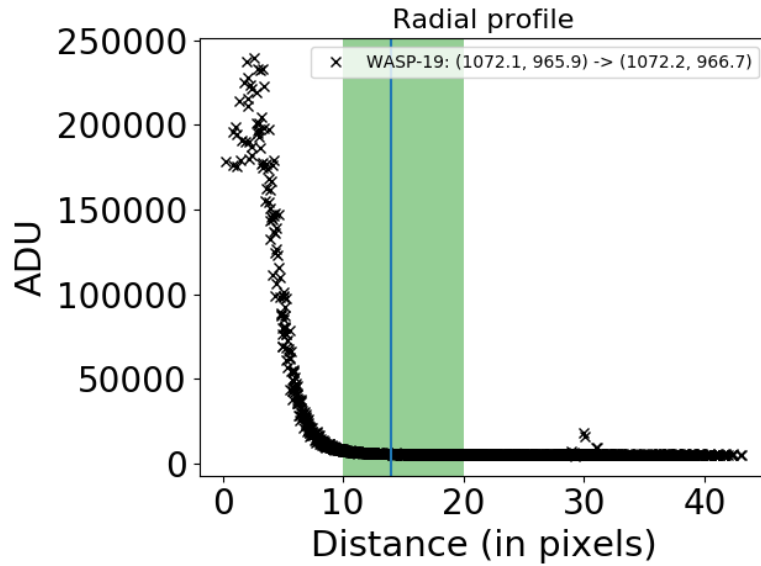


Figure 3: Radial profile with the range of apertures and the final aperture (optimal) indicated.

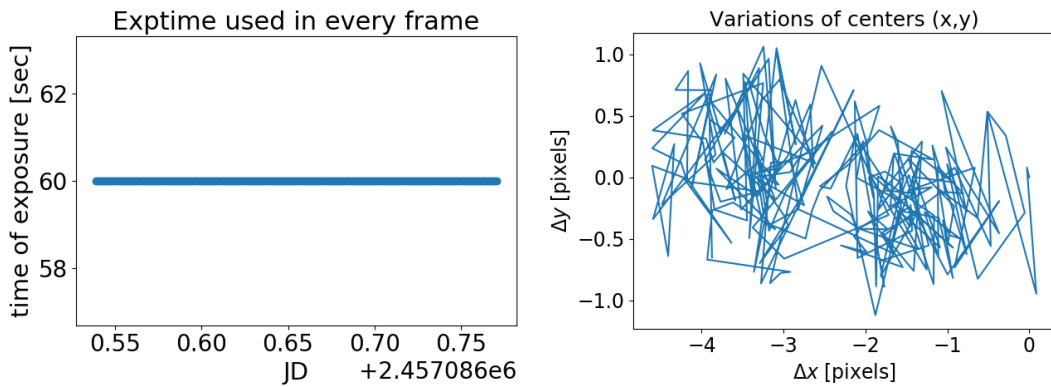


Figure 4: plot of variations of exposure time (left) and variations of positions for centers (right) for target and references, the variation is shown in $\Delta x = x_i - x_0$ and $\Delta y = y_i - y_0$ using position (x,y) of first frame as reference (x_0, y_0) .

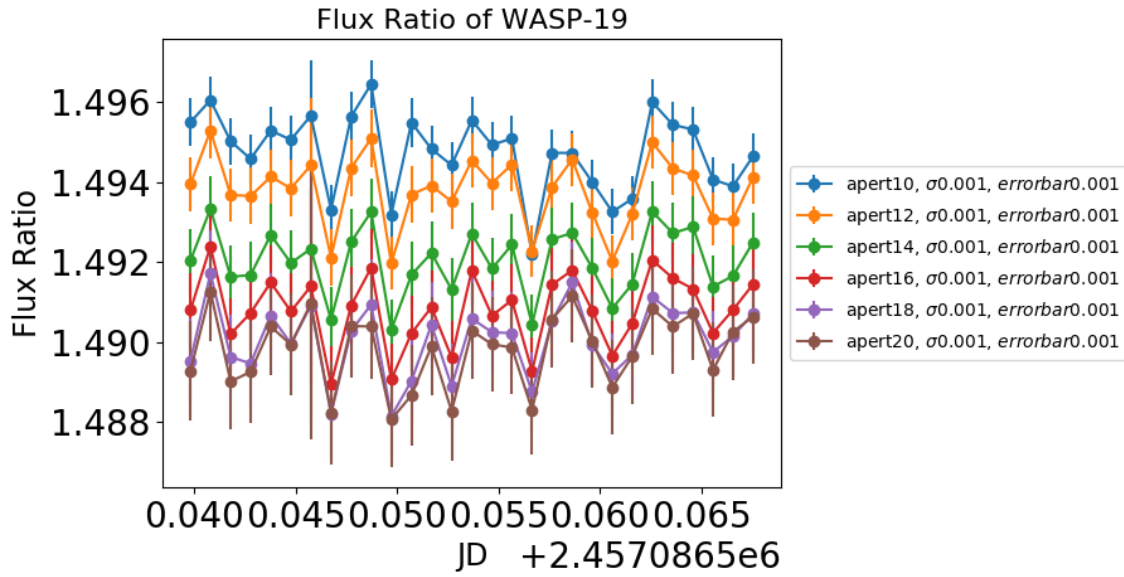


Figure 5: Flux out of transit for different apertures in a large range.

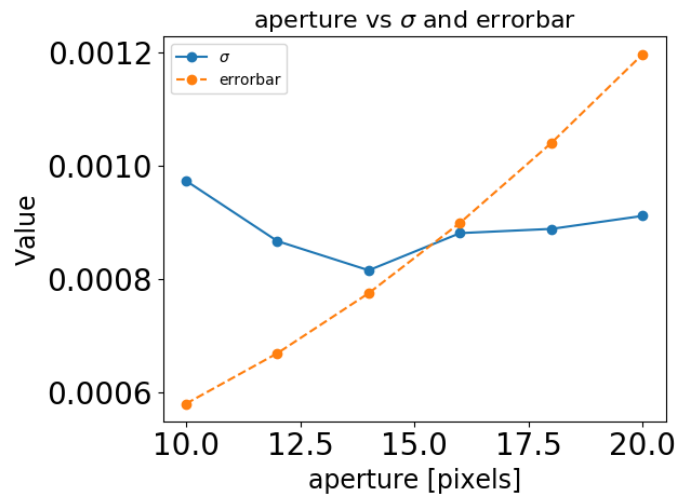


Figure 6: Plot of aperture vs standard deviation and mean errorbar for the different apertures used in Fig. 5

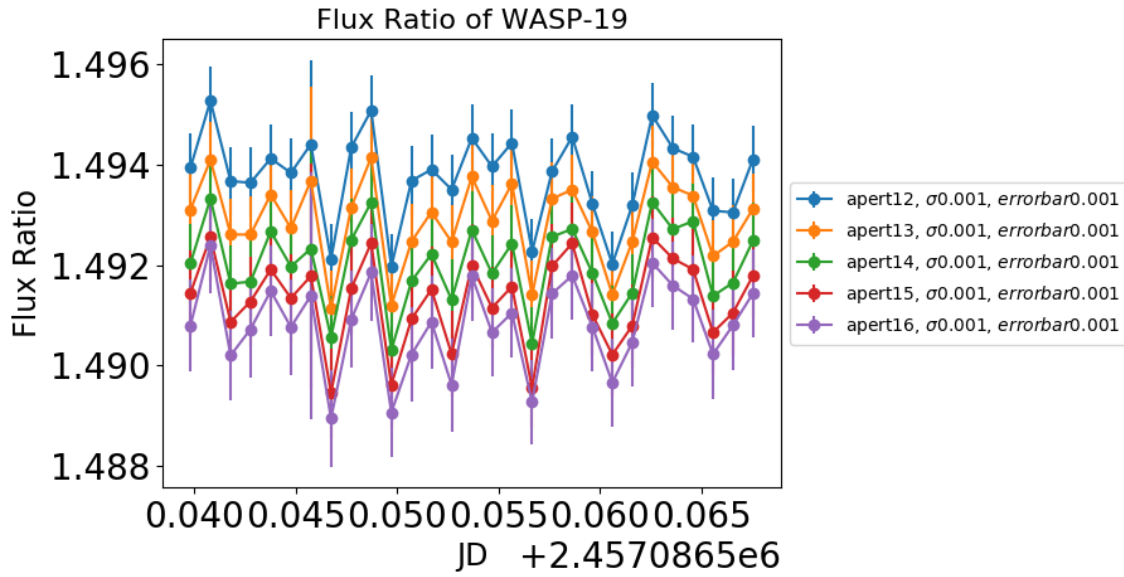


Figure 7: Flux out of transit for different apertures in a small range.

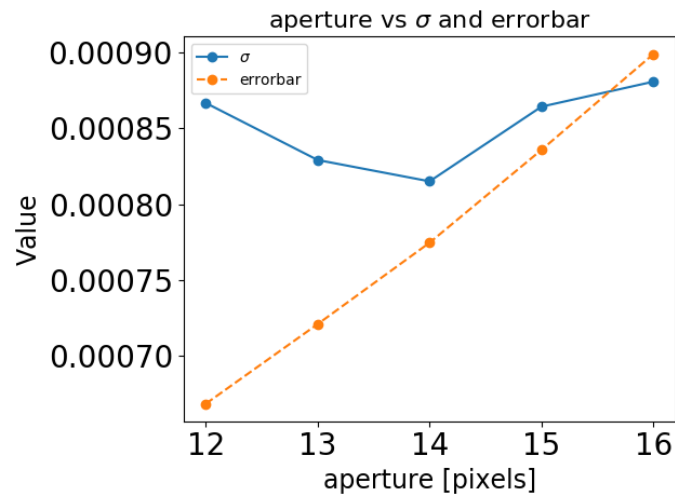


Figure 8: Plot of aperture vs standard deviation and mean errorbar for the different apertures used in Fig. 7.

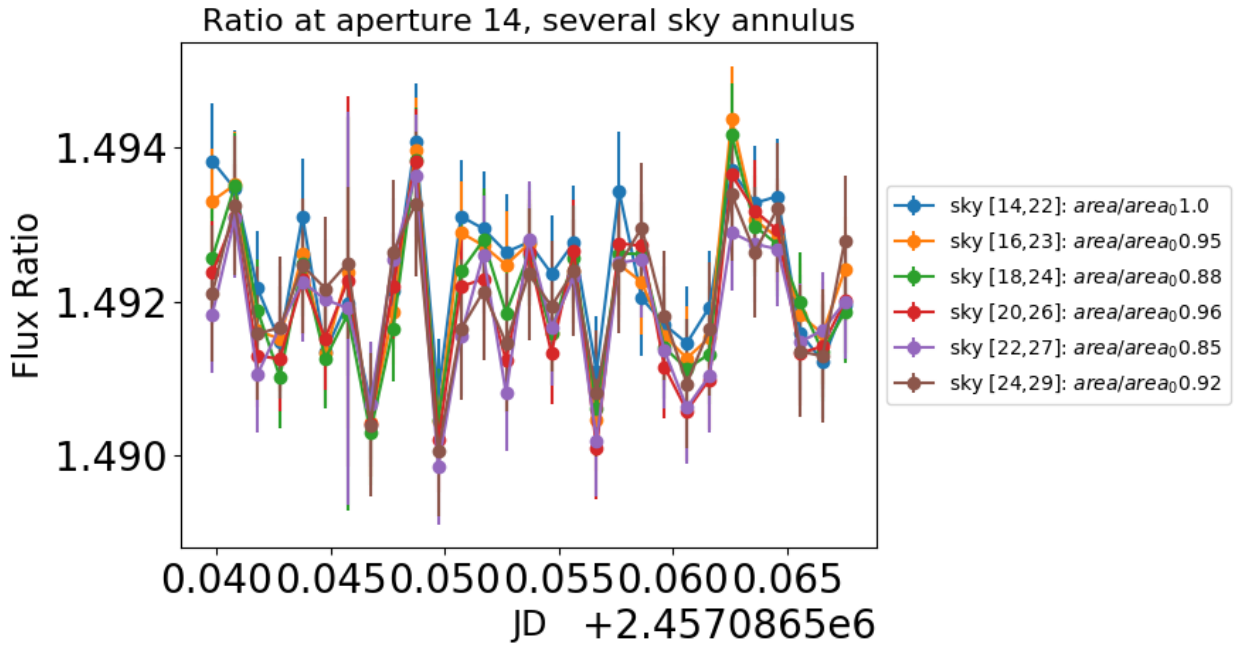


Figure 9: Plot of flux, outside the transit event, at different sky annulus keeping the same area.

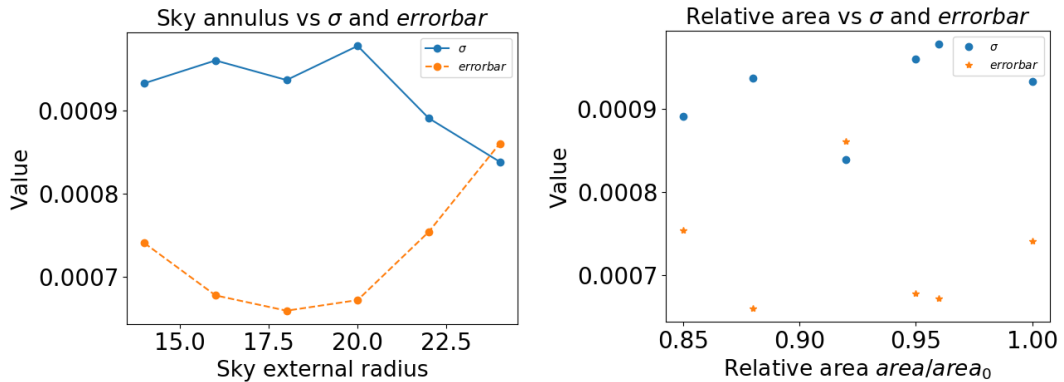


Figure 10: Plot of the sky (left) and relative area (right) versus standar deviation and mean error bar for several sky annulus in Fig. 9.

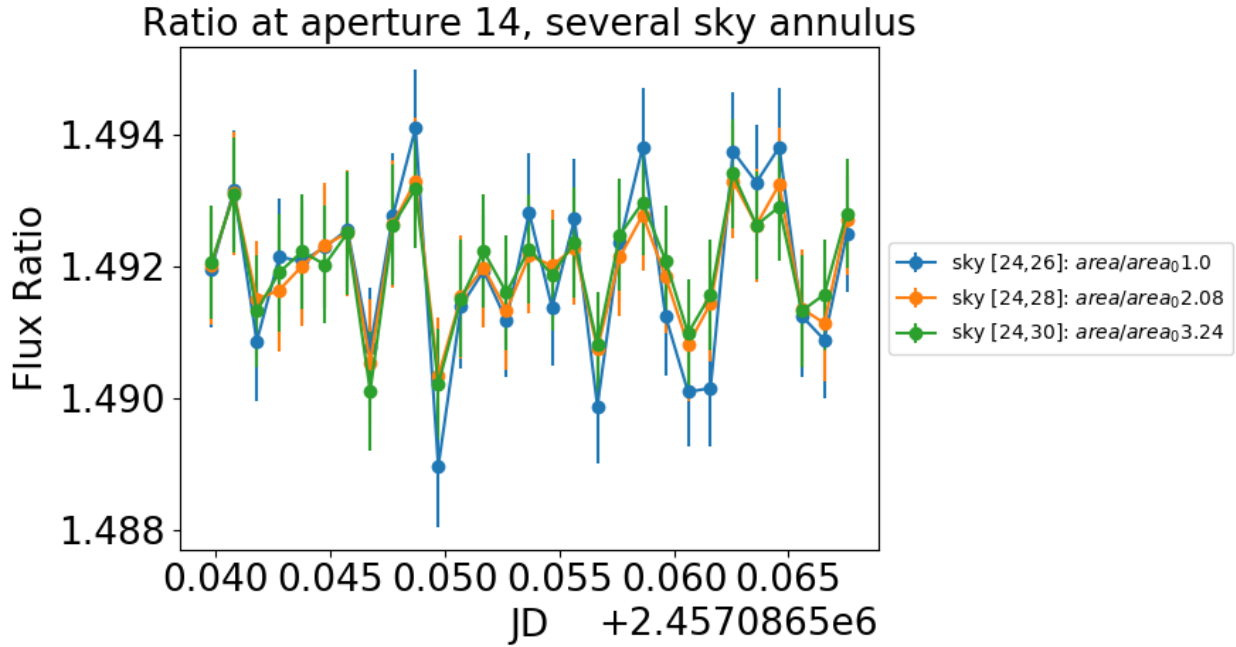


Figure 11: Flux out of transit for different sky external radius with the same internal radius (chosen in a arbitrary way).

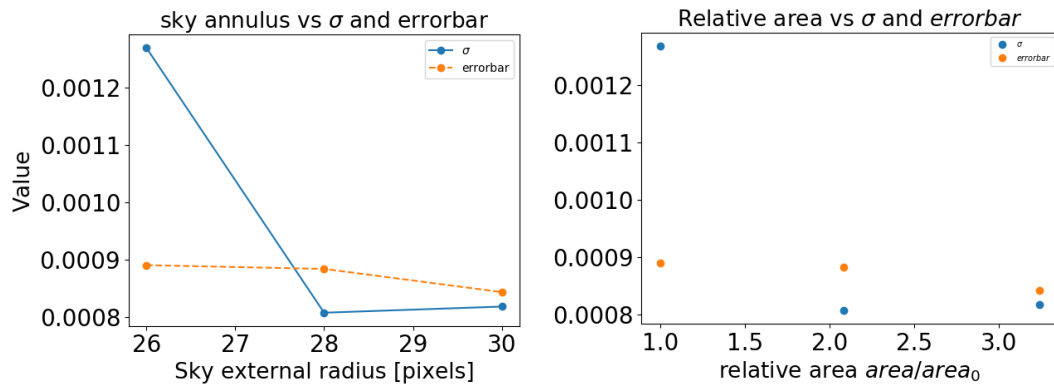


Figure 12: Plot sky (left) and area ratio (right) vs standard deviation and mean errorbar for the skys used in Fig. 11.

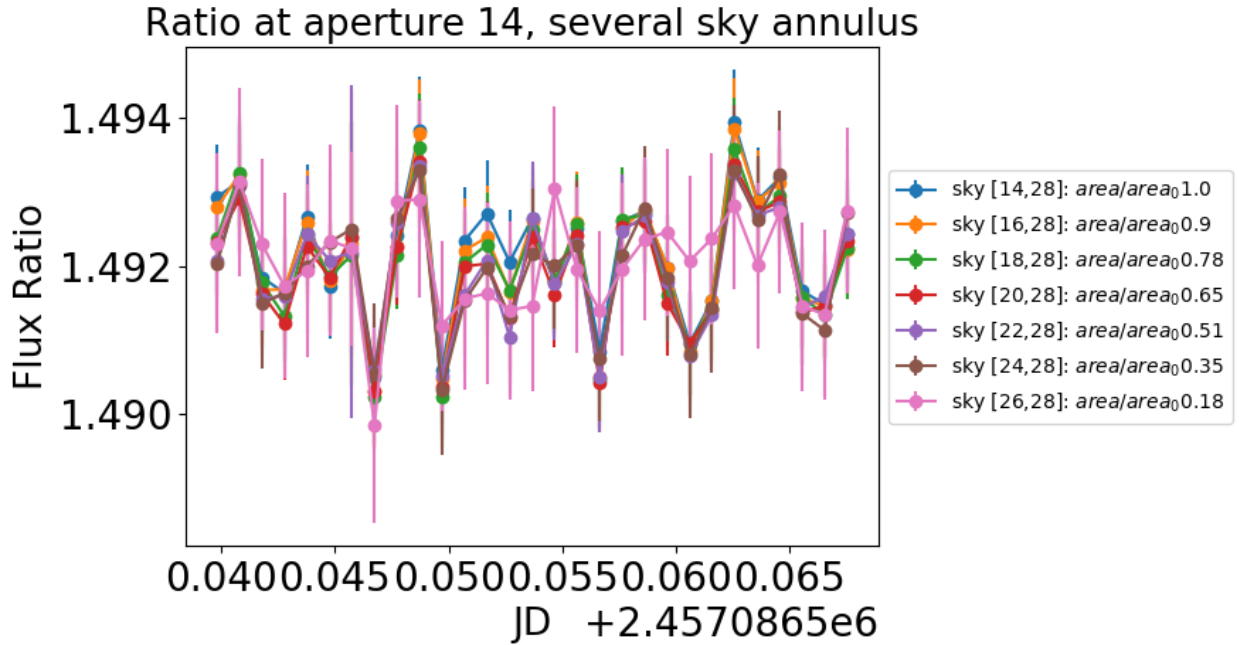


Figure 13: Flux out of transit for different sky internal radius with the same external radius (chosen from the minimum standard deviation in Fig. 12).

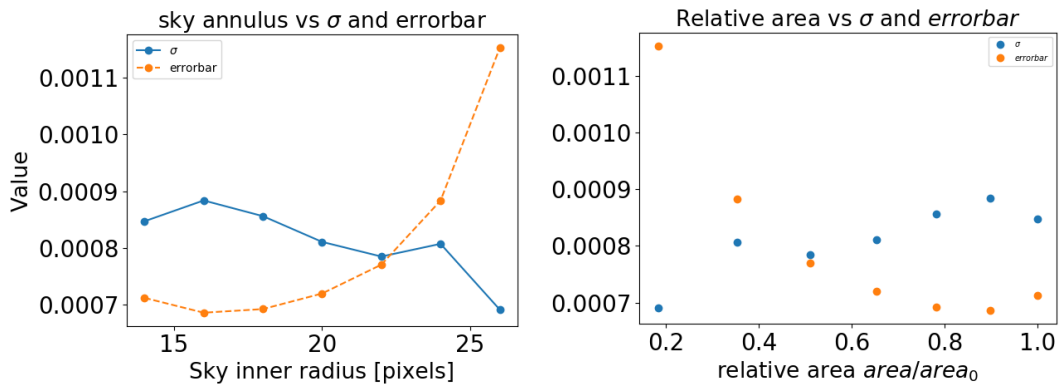


Figure 14: Plot sky (left) and area ratio (right) vs standard deviation and mean errorbar for the skys used in Fig. 13

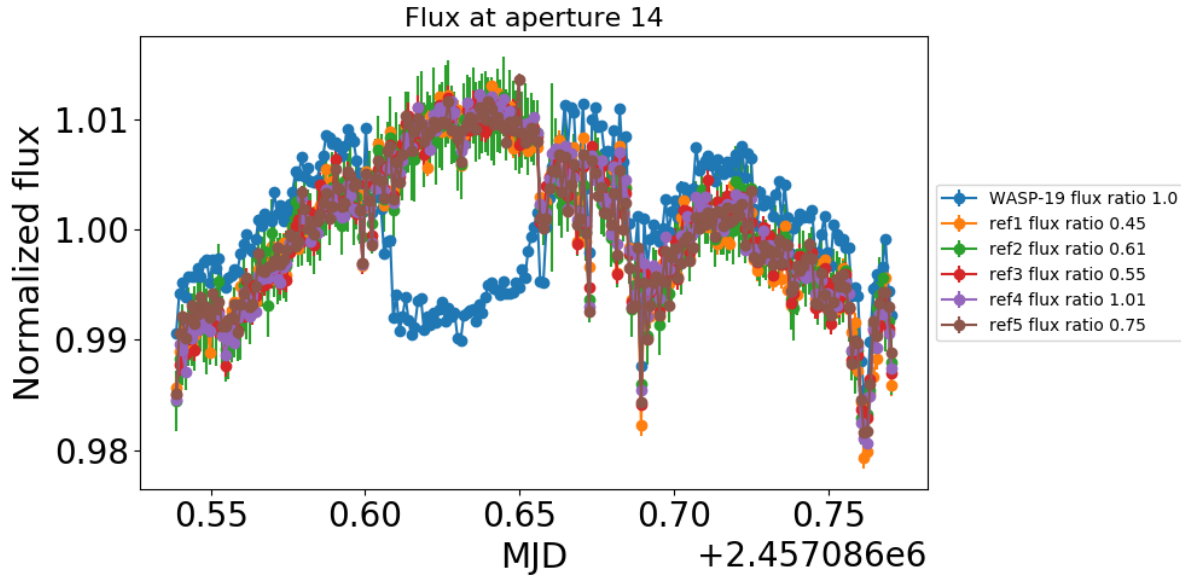


Figure 15: Normalized flux of the target and references at the chosen aperture (from the minimum standard deviation in Fig. 8) for the entire time series, the x-axis it is in Modified Julian Date.

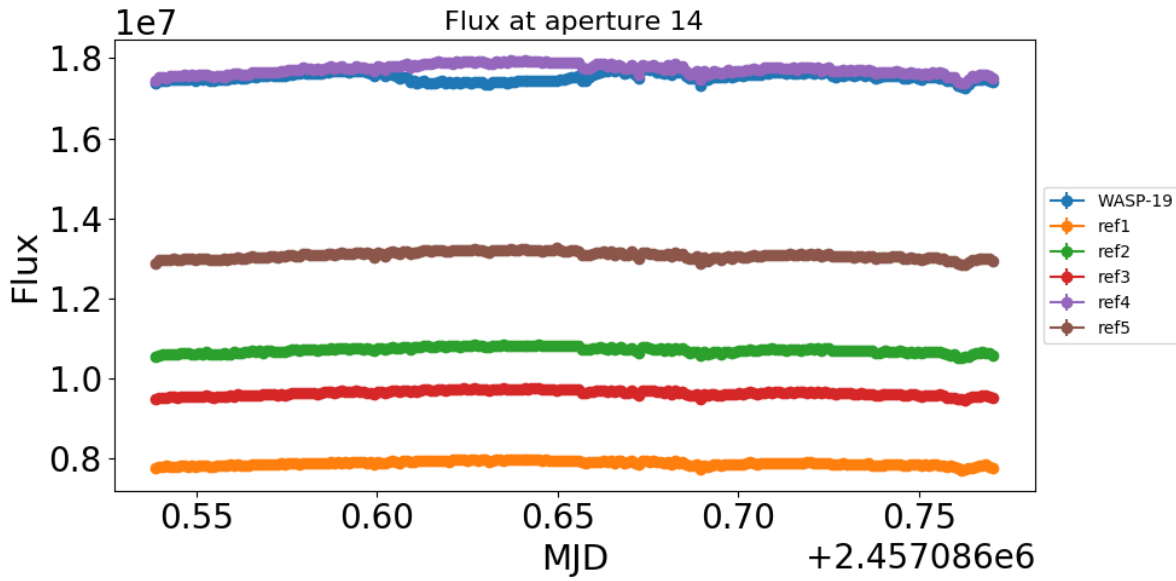


Figure 16: Flux of the target and references at the chosen aperture (from the minimum standard deviation in Fig. 8) for the entire time series, the x-axis it is in Modified Julian Date.

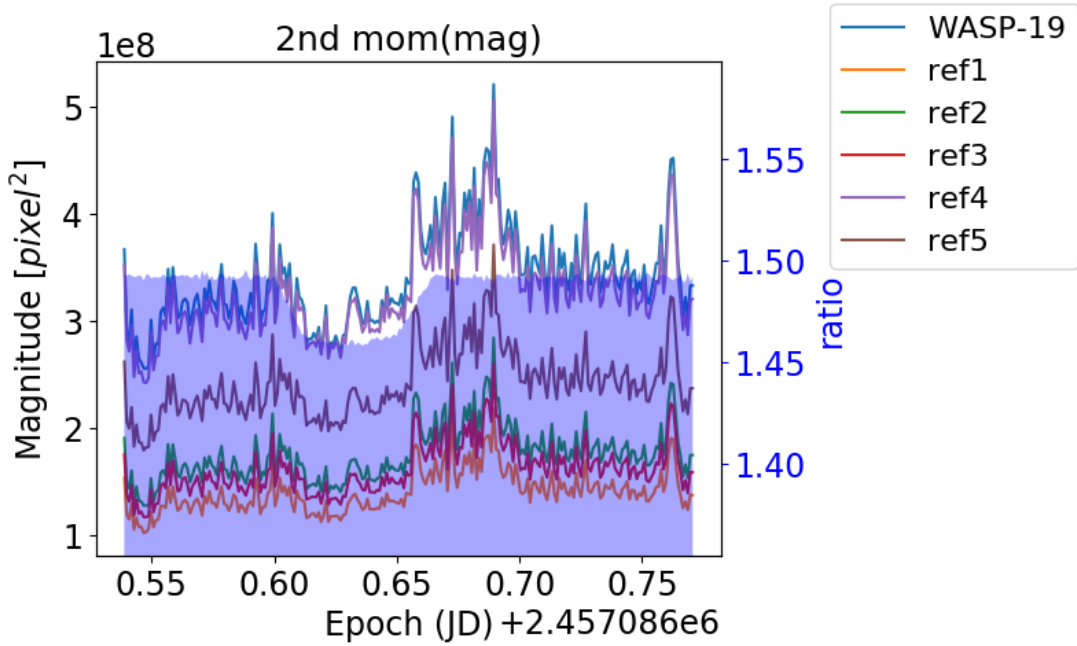


Figure 17: Magnitude of second momentum for target and references.

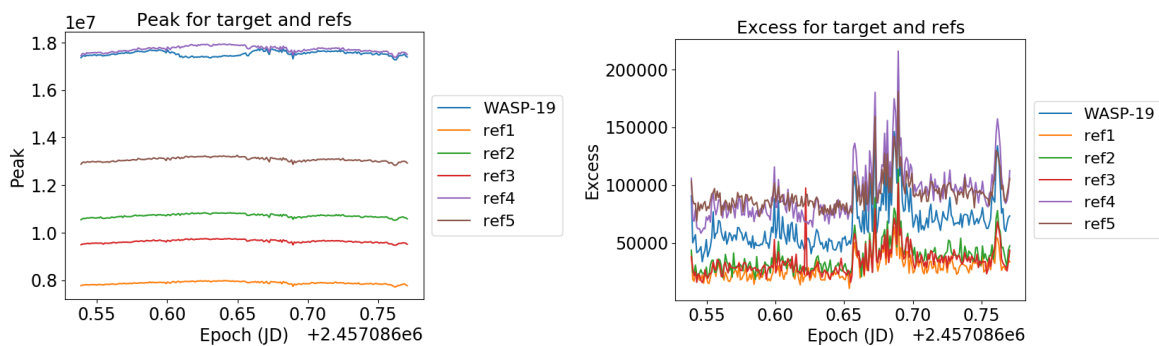


Figure 18: Plot of variations of the peak (left) and excess of pixels (right) relative to the chosen aperture (from the minimum standard deviation in Fig. 8).

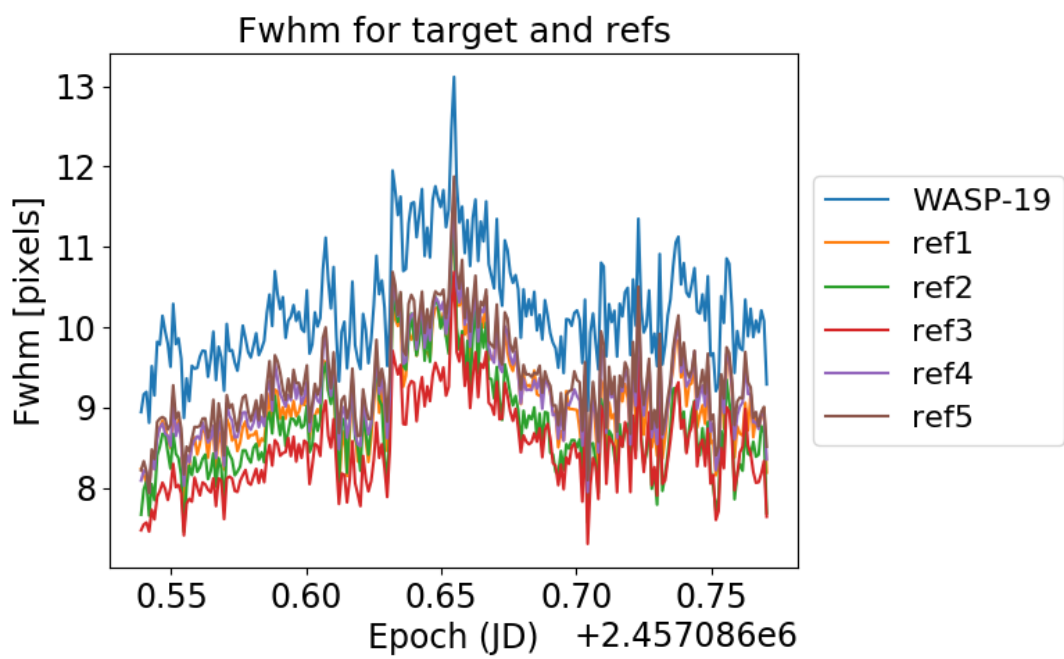


Figure 19: Variations of the full width half maximum across the time series for target and references.

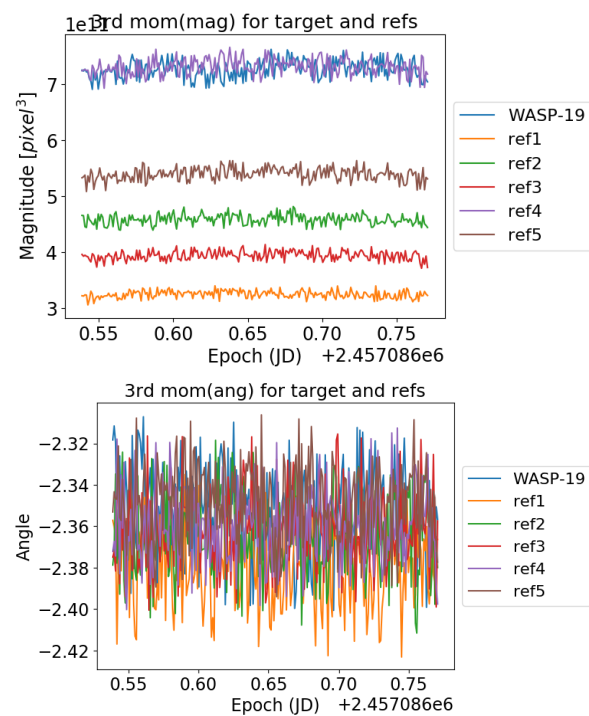


Figure 20: Variations of magnitude(left) and angle (right) of the third momentum for target and references.

Example of running the pipeline:

```
from tramos import pipeline as pl
import numpy as np
#labels = [ 'WASP-19' , 'ref1' , 'ref2' , 'ref3' , 'ref4' , 'ref5' ]
coords_xy = [[1074,967],[586,954],[1397,557],[1565,821],[1489,975],[1480,1201]]

ts , phot = pl.pipeline(files_path="raw/WASP19_*.fits" , calib_path="calib/*.fits" ,
                        coords_xy=coords_xy ,
                        object_in_hdr="WASP19" ,
                        target="WASP-19" ,
                        stamp_rad=30, recenter=True , brightest=4,
                        sector=[1,30] ,
                        labelsize=16,
                        filter_band="R" ,
                        ccd_lims_xy=[0,2148,0,2048] ,
                        max_counts = 600000, **pl.dk154.old)

flux , error , s , e = ts.get_ratio()
np.savetxt("data/WASP-19_20150304.txt" , np.array([phot.epoch , flux , error]).T, delimiter=" ")
#[ccd_lims_xy=[0,1019,0,1165]
#[[1015,1181],[1341,936],[692,971],[1320,650],[1565,895]
#target="WASP19",
```